Model membrane systems, membrane-active peptides and application possibilities

Inaugural-Dissertation

zur

Erlangung des Doktorgrades

der Mathematisch-Naturwissenschaftlichen Fakultät

der Universität zu Köln

vorgelegt von

Mareike Horn

aus Friedrichroda

Köln

2017

Berichterstatter: Prof. Dr. Ines Neundorf

Prof. Dr. Ulrich Baumann

Tag der mündlichen Prüfung: 19. Dezember 2017

Die im Rahmen der vorliegenden Arbeit durchgeführten Experimente und Untersuchungen wurden im Zeitraum von April 2014 bis August 2017 am Institut für Biochemie der Universität zu Köln unter der Anleitung von Frau Prof. Dr. Ines Neundorf durchgeführt.

Abstract

The ability of cell-penetrating peptides (CPPs) to translocate a variety of covalently or non-covalently linked cargoes, particularly therapeutics and imaging agents, across the plasma membrane of living cells renders them of broad interest in the medical field as well as in biotechnological development. Thus, the use of CPPs, e.g. in therapeutics, increases the necessity of understanding their mechanism of action, a subject still under debate.

For the first step of peptide internalization, the interaction between the positively charged amino acid side chains within the peptide sequence and the anionic constituents of the membrane bilayer is assumed. However, owing to the complexity of biological plasma membranes, studying the mode of action of CPPs on a molecular level is very difficult. With this in mind, model membrane systems, especially large and giant unilamellar vesicles and giant plasma membranes vesicles derived from live cells plasma membranes, were prepared and several techniques were established in order to monitor the initial step of cell entry – binding to and translocation through the cell membrane as well as identification of key components of the plasma membrane required for efficient uptake.

The first chapter focuses on the membrane interactions and perturbation mechanism of two structural modified variants of the well-described CPP sC18, a cyclized and a dimeric branched version, with artificial model membranes. Fluorescence analysis demonstrated the importance of negatively charged lipids for an efficient uptake of Arg-rich CPPs, supporting the assumption that electrostatic interactions are required for the initial stage of cell entry. In case of dimeric variants, the strong affinity was further accompanied by intense membrane destabilizing effects, presumably responsible for their lytic behavior as anticancer peptide. Moreover, the cyclization of the peptide backbone turned out to be a promising strategy as well to improve their cell-penetrating capability. Using CD spectroscopy, structural arrangements when in contact with neutral and anionic vesicles further revealed that a certain flexibility and thus the static arrangement of the guanidinium groups within the cycle seem to positively affect peptide-membrane interaction. In summary, these evidences suggest that the internalization of the peptide variants depends highly on the membrane composition of the target cell.

In the second chapter, the focus lay on the design and characterization of novel peptide conjugates, composing of a wound healing promoting peptide and sC18 as cell penetrating peptide, with the final goal to further enhance the wound healing activity. Besides, the new conjugate Tylotoin-sC18* exhibited further promising antimicrobial activity and moreover a certain selectivity towards cancer cells, suggesting that Tylotoin-sC18* is a good candidate for further studies and the possible development as a therapeutic agent for infected wounds.

Zusammenfassung

Die Fähigkeit zellpenetrierender Peptide (cell-penetrating peptides, CPPs) die Plasmamembran lebender Zellen passieren zu können und dabei kovalent und nicht-kovalent gebundene Moleküle, insbesondere therapeutisch aktive Wirkstoffe und Farbstoffe, zu transportieren, macht sie sowohl für die Medizin als auch für den Biotechnologiesektor besonders interessant. Für eine erfolgreiche therapeutische Anwendung zellpenetrierender Peptide ist die Erforschung derer genauen Wirkmechanismen essentiell. Als erster Schritt der Internalisierung wird dabei weithingehend die Interaktion der positiv geladenen Aminosäuren innerhalb der Peptidsequenz mit den negativ geladenen Komponenten der Membrandoppelschicht angenommen. Eine besondere Herausforderung der Forschung stellt jedoch die Komplexität biologischer Plasmamembranen dar, weswegen sich die Aufklärung der Wirkmechanismen zellpenetrierender Peptide auf molekularer Ebene als besonders schwierig erweist.

Vor diesem Hintergrund wurde sich für den Einsatz artifizieller Modell-Membran-Systeme, insbesondere unilamellare Liposomen (large and giant unilamellar vesicles, LUVs and GUVs) und Membranvesikel (ginat plasma membrane vesicles, GPMVs), die von lebenden Zellmembranen abstammen, entschieden. Darauf basierend wurden in dieser Arbeit verschiedene Techniken etabliert, welche die Untersuchung des ersten Schrittes der Internalisierung in die Zelle – die Anbindung, sowie die Translokation durch die Zellmembran – ermöglichen sollten. Weiterhin sollten die Schlüsselkomponenten, welche zur effizienten Aufnahme beitragen, identifiziert werden.

Das erste Kapitel widmet sich den Interaktions- und Destabilisierungsprozessen zweier strukturell modifizierten Varianten des bereits gut untersuchten zellpenetrierenden Peptides sC18, einer zyklisierten und einer verzweigten Version, unter Verwendung von artifiziellen Modellmembranen. Dabei stellten Fluoreszenzanalysen die Wichtigkeit negativ geladener Lipide für die effiziente Aufnahme Arg-reicher Peptide heraus. Dies unterstützt die Vermutung, dass elektrostatische Interaktionen in der ersten Phase der Zellpenetration eine zentrale Rolle spielen. Im Fall der verzweigten Varianten zeigte sich, dass deren starke Affinität von intensiven Destabilisierungseffekten der Membran begleitet wurde. Diese könnten für deren lytisches Verhalten als Zytostatika-Peptid verantwortlich sein. Weiterhin erwies sich die Zyklisierung des Peptid-Rückgrats als vielversprechende Strategie zur Verbesserung der Zellinternalisierung. CD-spektroskopische Analysen mit neutral und negativ geladenen Vesikeln zeigten, dass eine gewisse Flexibilität und damit die Anordnung der Guanidiniumgruppen innerhalb des Zyklus die Peptid-Membran-Interaktion positiv beeinflussen können. Zusammengefasst lassen die Ergebnisse darauf schließen, dass die

Internalisierung der Peptid-Varianten stark von der Membranzusammensetzung der Zielzelle abhängig ist, wodurch eine gewisse Selektivität vermutet wird.

Im zweiten Kapitel lag der Fokus auf dem Design und der Charakterisierung eines neuen Peptid-Konjugats, welches sich aus dem wundheilungsfördernden Peptid Tylotoin und dem zellpenetrierenden Peptid sC18 zusammensetzt, mit dem Ziel den Wundheilungsprozess noch weiter zu beschleunigen. Das neue Konjugat Tylotoin-sC18* zeigte darüber hinaus eine vielversprechende antimikrobielle Wirkung und eine gewisse Selektivität gegenüber einer getesteten Krebszelllinie. Diese Eigenschaften machen Tylotoin-sC18* zu einem aussichtsreichen Kandidaten für weitere Studien, um eine neue Klasse von therapeutischen Wirkstoffen zur Behandlung infizierter Wunden zu entwickeln.

Table of contents

1. Introduction

1.1 Biological and model membranes

1.1.1 Eukaryotic and bacterial membranes

Biological membranes play a crucial role in the cellular protection against the surrounding environment as well as in the control and the transport of nutrients. Particularly, cellular membranes are only permeable for compounds within a narrow range of size, net charge and polarity. Thereby, the membrane provides an efficient way for a cell to prevent uncontrolled influx or efflux of solutes and compounds, which could otherwise be harmful. [5]

In 1925, Gorter *et al.* first suggested the concept that biological membranes are composed of two opposite layers of lipids [65]. Almost 50 years later, Singer *et al.* proposed the advanced fluid mosaic model, in which the biological membrane is considered as a two-dimensional liquid where lipids and proteins diffuse more or less unhindered within the plane of the membrane [170].

Since then, many developments were brought to this model in terms of the membrane composition and molecular organization, e.g. the discovery of lateral microdomain structures [167], revealing the complex nature of the cell membrane structure (Figure 1) [137].

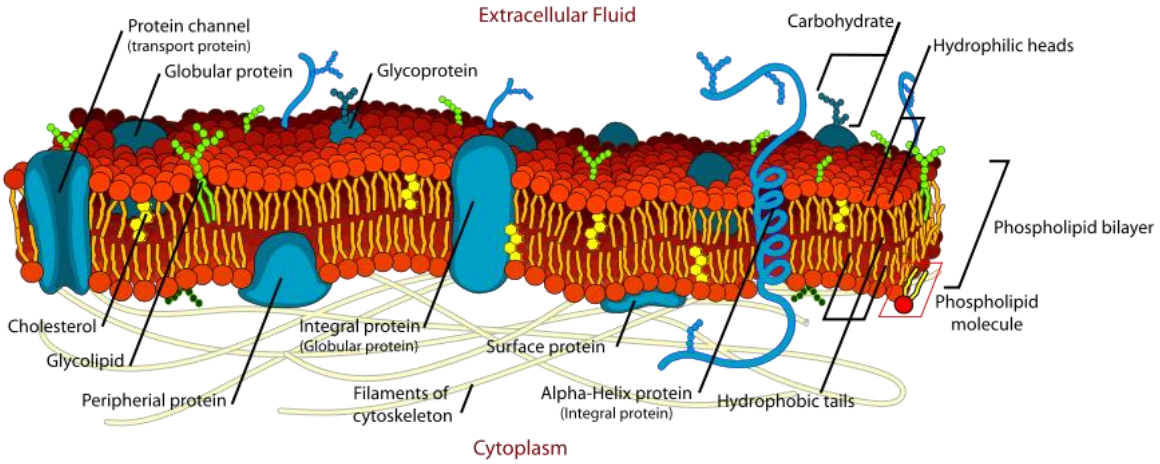

Figure 1. A schematic representation of the plasma membrane. (from Mariana Ruiz, 2007)

In general, the plasma membrane is composed of three categories of membrane lipids according to their chemical structure, namely glycerol-based lipids, ceramide-based sphingolipids and cholesterol (Figure 2) [137].

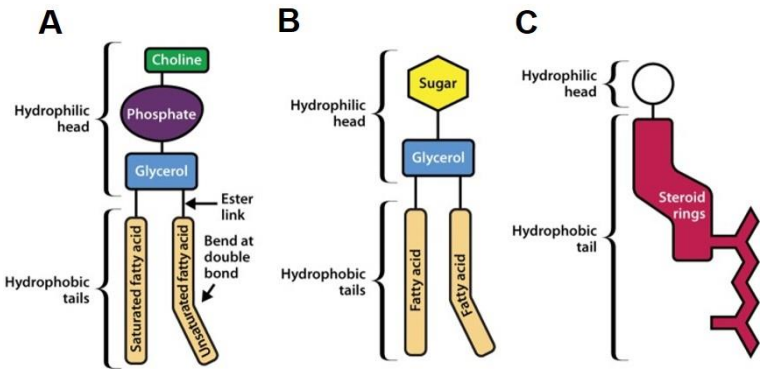

Figure 2. Schematic illustration of the three main membrane lipids. Phospholipids **(A)** Glycolipid **(B)** and Cholesterol **(C)**. (adapted from Watson, H., 2015 [197])

The glycerol-based lipids or phospholipids are the most abundant membrane lipids consisting of two fatty acid chains linked to glycerol and a phosphate group [197]. They are further classified into various subgroups based on their hydrophilic head groups which are then attached to the phosphate group [137]. The four major glycerol phospholipids are phosphatidylcholine (DOPC), phosphatidylethanolamine (DOPE), phosphatidylserine (DOPS) and phosphatidylinositol (PI) [204].

Sphingolipids, another important group of membrane lipids, are composed of a sphingosine, instead of the glycerol backbone, which is attached to a long unsaturated hydrocarbon chain [5]. Moreover, sphingomyelin, which is the major sphingolipid in mammalian cells, is believed to be involved in the formation of lateral microdomains, so called lipid rafts [26]. In addition, cholesterol is also enriched in these microdomains of tightly packed domains [49] as result of its favorable interaction with the glycosphingolipids [159]. Subsequently, cholesterols hydrophilic carboxyl group interacts with the hydrophilic head groups of glycosphingolipids and the bulky hydrocarbon rings interact with the hydrophobic acyl chains of membrane lipids [137].

The lipid compositions can be very different in various types of membranes, organisms and also between the two leaflets of the lipid bilayer [5, 60, 107]. Thus, several lipid species are distributed differentially in the two monolayers of biological membranes, resulting in asymmetric lipid distribution [107]. In mammalian cells, the outer leaflet of the plasma membrane contains predominantly phosphatidylcholine and sphingomyelin, whereas lipids with neutral or negatively charged head groups (e.g., phosphatidylethanolamine, phosphatidylserine, and phosphatidylinositol) are preferentially located in the inner leaflet [197]. However, cholesterol is present in both layers [203]. Furthermore, several studies revealed that the cell membrane composition changes in cancer cells, which is indicated by the overexpression of certain types of proteoglycans and the enrichment of negatively charged lipids, more precisely phosphatidylserine, in the outer leaflet [85, 120, 193]. Thus, phosphatidylserine is no longer restricted to the cytosolic leaflet of the plasma membrane

and is translocated to the outer leaflet by the action of an enzyme called scramblase [118, 197]. Therefore, the membrane of cancer cells become more anionic than those of healthy cells.

Moreover, the cell membranes of bacteria (gram-positive and gram-negative) differ in their composition significantly from mammalian cell membranes [60]. In particular, one of the major differences between bacterial and eukaryotic cell membranes is the presence of a large amount of cholesterol in eukaryotic cell membranes, while in bacterial cells, cholesterol is completely missing (Figure 3A) [23]. In addition, the membranes of bacteria are rich in negatively charged lipids, like phosphatidylglycerol and cardiolipin. Phosphatidylethanolamine is the most common neutral phospholipid in bacterial cell membranes (Figure 3A) [60, 63].

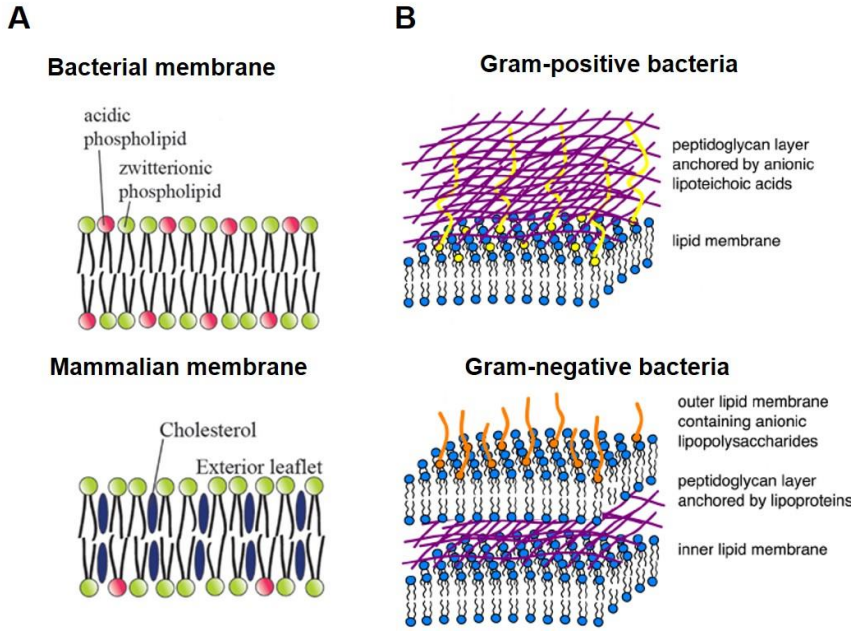

Figure 3. Bacterial *versus* mammalian membranes. Schematic representation of the key features of the bacterial and mammalian cell membrane compositions **(A)**. The membrane structure of gram-positive and gram-negative bacteria **(B)**. ((A) adapted and modified from Brender *et al.*, 2012 [23]; **(B)** adapted and modified from Chen and Bothun, 2014 [32])

Moreover, the outer membrane of gram-negative bacteria additionally comprises lipopolysaccharides as anionic components, whereas lipoteichoic acids are found in gram-positive bacteria (Figure 3B) [60].

1.1.2 Vesicles as artificial model membrane system

In general, model membrane systems are defined as artificial lipid bilayers in which the lipid compositions mimic the arrangement of those in biological cell membranes [137]. The interior of the spherical-shaped vesicles is characterized by aqueous solutions [164, 194]. Such liposomes are usually categorized, according to their size and lamellarity, into multilamellar vesicles (MLVs) and in small-, large- and giant unilamellar vesicles (SUVs,

LUVs and GUVs) [4]. Since MLVs are composed of multiple lipid bilayers, they are therefore not suitable and only rarely used as model membrane system [37].

Large and giant unilamellar vesicles

Large and giant unilamellar vesicles are the most studied and predominantly used model systems not only because of the more homogenous lipid distribution but also because of their suitable size. LUVs are characterized by diameters varying from 10 to 100 nm, while giant unilamellar vesicles have diameters above 10 µm and are therefore close to actual cell size [137].

Furthermore, they can be relatively easy prepared by several methods. The most common method for the preparation of large unilamellar vesicles is illustrated in Figure 4.

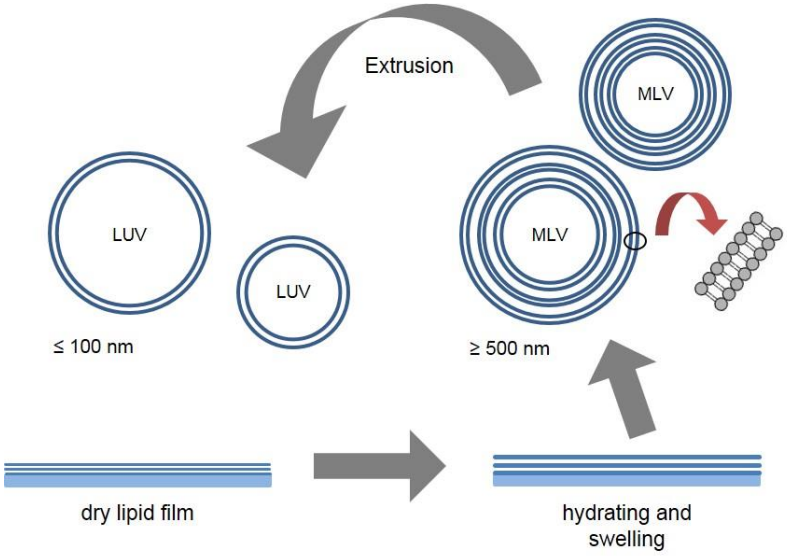

Figure 4. Formation of large unilamellar vesicles. Thin dried lipid films were hydrated and stacks of liquid crystalline bilayers become fluid and swell. Subsequently, hydrated lipid sheets self-close to form large, multilamellar vesicles (MLVs). To get LUVs, the size of the formed MLVs must be reduced by mechanical energy (extrusion). (modified after Lasic, A. D., 1988 [103])

Classically, LUVs are prepared by dissolving lipids of interest in organic solvents like chloroform, followed by *in vacuo* evaporation to form a thin dried lipid film [137]. Subsequently, the dried lipid film is hydrated in aqueous buffer and MLVs will be formed. In order to obtain large unilamellar vesicles, the MLV suspension is then disrupted by several freeze-thaw cycles, which results in homogenous size distribution in the final suspension [137]. Finally, this suspension is subjected to extrusion through polycarbonate filters to produce large unilamellar vesicles with diameters up to 200 nm, depending on the pore size of the polycarbonate filter.

GUVs are mostly prepared by electroformation [10], but this technique requires considerable technical effort. Whereas, the gentle hydration method, provided by Horger *et*

al., allows the preparation of giant unilamellar vesicles in a fast manner without the need of specialized equipment [76]. Going into detail, Horger and coworkers described the formation of giant unilamellar vesicles by hydration from a hybrid film of partially dried agarose and lipids [76]. In brief, a thin film of agarose will be prepared on a clean glass slide. Next, the lipid mixture, dissolved in chloroform, is applied on the dried agarose film resulting in the formation of a hybrid film of agarose and lipids. Finally, the last stage comprises the hydration of the hybrid film leading to the formation of GUVs within minutes.

Giant plasma membrane vesicles obtained from live cells

Giant plasma membrane vesicles are cell-derived vesicles and therefore provide a more natural system than large and giant unilamellar vesicles [162]. The attractiveness of GPMVs originates mostly from their complexity, since they maintain the lipid and protein diversity of cellular membranes, which they derived from [165]. GPMVs are released from cells upon chemical induction by either dithiothreitol (DTT) and formaldehyde (PFA) (Figure 5) or by N-ethylmaleimide (NEM) to avoid cross-linking-derived artifacts of lipids [14, 134, 165].

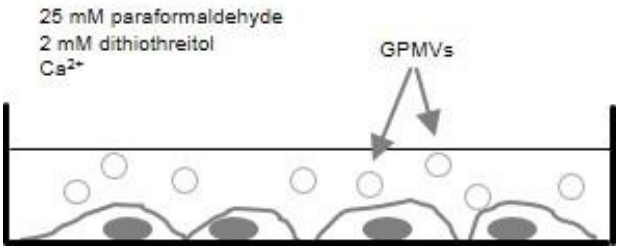

Figure 5. Principle of giant plasma membrane vesicle formation. (after Säälik *et al.*, 2011 [156])

Moreover, GPMVs phase-segregate easily into liquid-ordered (L_o) and -disordered (L_d) lipid domains [156] They showed spherical shapes and varied in size up to 15 µm and are therefore distinctly smaller than GUVs.

1.2 Cell-penetrating peptides

The cellular plasma membrane constitutes an effective semi-permeable barrier that primarily protects living cells form the surrounding environment [111, 206]. At the same time, the cell membrane represents a barrier to the intracellular delivery of large hydrophilic molecules, e.g. for therapeutic applications [69]. Thus, the successful transport of such macromolecules to target specific cells and tissues is a major hurdle for administering bioactive molecules [52], which results in the necessity to find strategies allowing the efficient delivery of therapeutics across the membrane [145].

In this regard, the ability of certain peptides, so called cell-penetrating peptides (CPPs), to cross the cellular membrane was simultaneously reported by Frankel and Pabo [57], and Green and Loewenstein [66] for the first time in the late 80s. Particularly, their research in

the field of AIDS revealed that the TAT peptide, derived from the human immunodeficiency virus (HIV), passes very efficiently through cell membranes of HeLa cells and promotes viral gene expression [57, 66].

In general, cell-penetrating peptides are relatively short peptides containing less than 40 amino acids, which are accompanied by an amphipathic or highly cationic character, usually rich in basic amino acids [36, 196]. Furthermore, CPPs are able to mediate the uptake of bioactive molecules into the cell, and thus transporting therapeutically active cargoes, including small molecules, plasmid DNA, siRNA, therapeutic proteins and imaging reagents [144, 145].

Thus, the discovery of CPPs almost 30 years ago has paved the way for the development of cell delivery approaches and so, CPPs have gained considerable interest in clinical applications.

1.2.1 Classification and uptake mechanisms

Cell-penetrating peptides can be classified into different subgroups according either to their origin or to their physical-chemical characteristics [111, 210]. Based on their origin, three main classes of CPPs can be distinguished, including protein-derived peptides, chimeric peptides that are formed by the combination of two natural sequences, and finally synthetic peptides, which are rational designed sequences [16, 111]. Classical examples of each class are depicted in the following table.

Table 1. Sequences and origins of well-studied CPPs.

Peptide	**Origin**	**Sequence**	**Ref.**
Protein-derived peptides			
Tat(48-60)	Protein Tat HIV-1	GRKKRRQRRRPPQ	[192]
Penetratin	Antennapedia homeodomain	RQIKIWFQNRRMKWKK	[40]
Chimeric peptides			
Transportan	Galanin/ mastoparan	GWTLNSAGYLLGKINLKALAALAKKIL	[139]
MAP	*de novo*	KLALKLALKALKAALKLA	[132]

Synthetic peptides			
Oligoarginines	Model peptide	R_n	[59, 125]
Pep-1	reverse transcriptase/T antigen	KETWWETWWTEWSQPKKKRKV	[42]

According to their structure, CPPs can be categorized as cationic CPPs with a high positive net charge, hydrophobic CPPs consisting mostly of nonpolar amino acid residues and as amphipathic peptides comprising both polar and nonpolar regions [121, 122, 210]. The class of amphipathic CPPs can be further subdivided into primary and secondary amphipathic CPPs [210].

The first class, the cationic or nonamphipathic CPPs, are defined as rather short peptides, like Tat(48-60) or nona-arginine (R9), having a high content of positively charged amino acids (Arg or Lys) [151]. Further, it was shown that cationic peptides bind electrostatically to negatively charged components of the plasma membrane of cells, leading to efficient translocation [97]. Primary amphipathic CPPs, such as Transportan, typically consist of more than 20 amino acid residues and their primary structure includes hydrophilic and hydrophobic domains [155]. The uptake mechanism of these peptides is proposed to occur by the insertion into the surface of the cellular membrane followed by pore forming events (direct translocation, Figure 6) [210, 211]. The last group comprises the secondary amphipathic peptides, e.g. penetratin, containing normally less than 20 amino acids in their sequence [111]. They reveal their amphipathic properties only through a change in their secondary structure upon the interaction with the lipid membrane [111, 151, 210]. The membrane binding affinity of these peptides increases with the negatively charged lipid content of the membrane [210].

Although, the exact mechanism used by CPPs to translocate across the cellular plasma membrane is not fully resolved, it is widely believed that the uptake mechanism varies for different classes of CPPs, and moreover, several mechanisms might even coexist depending on experimental conditions, such as the applied concentration, temperature, incubation time, the cell line used or the attached cargo [70, 111, 145, 151].

However, the two proposed major translocation mechanisms of cell-penetrating peptides include the energy-dependent endocytotic pathway and the direct translocation via energy-independent pathways [111, 206].

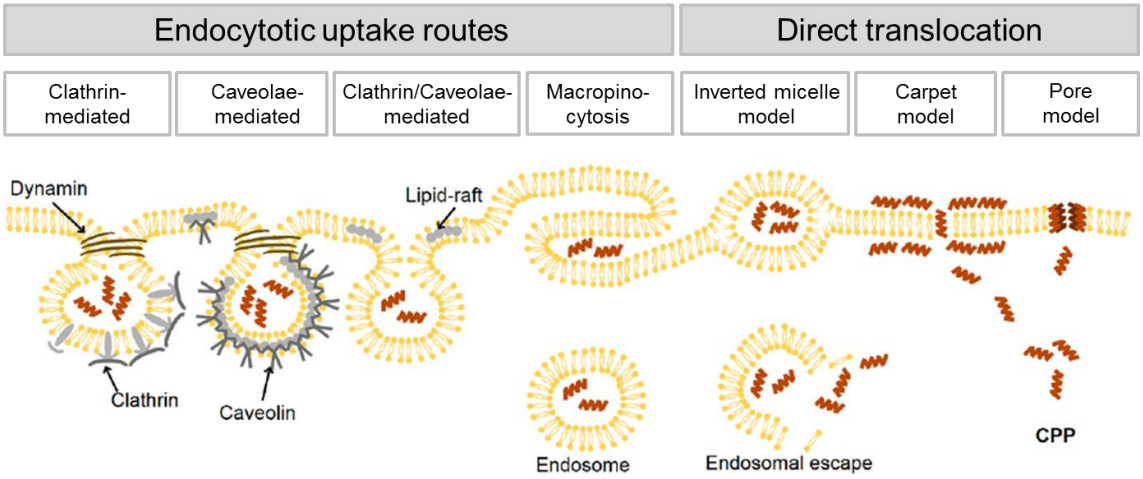

Figure 6. Scheme of different suggested uptake pathways for cell-penetrating peptides. (modified after Mickan *et al.*, 2014 [121])

Figure 6 summarizes the different uptake routes by which CPPs might penetrate the cell membrane. The endocytosis-mediated translocation mechanism, including clathrin-mediated endocytosis and caveolae/lipid raft-mediated endocytosis as well as macropinocytosis, which provides the main pathway utilized by most CPPs, especially when peptides are attached to large cargo molecules [145, 206]. These four morphologically distinct pinocytotic pathways differ in the size of the coat (if any) and in the size of the detached vesicles [99]. However, endocytosis generally consists of two steps: the endocytotic entry which is followed by the endosomal release, whereby the latter step is crucial in order to avoid lysosomal degradation and moreover to allow the peptide/cargo to reach its extracellular target site [16].

The uptake mechanism via direct translocation is most likely for primary amphipathic peptides at high CPP concentrations [111]. Three different energy-independent uptake pathways have been described: the inverted micelle model, the carpet model and the pore model, which is further divided into the toroidal pore and the barrel-stave model (Figure 6 and 7) [155].

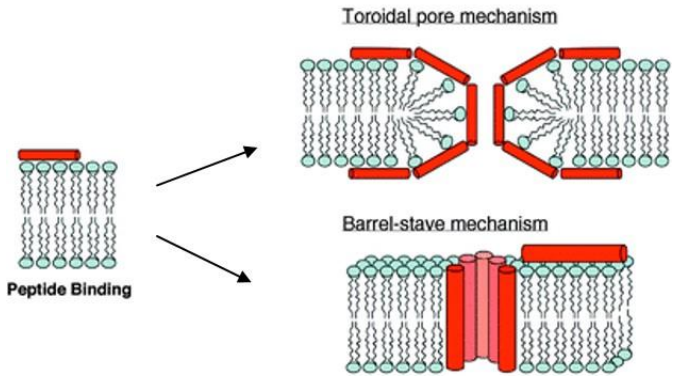

Figure 7. Pore-forming models proposed for the cellular entry via direct translocation. (modified after Sanderson, J. M., 2005 [159])

In general, these models are mainly based on the electrostatic interaction of positively charged CPPs with negatively charged components of the cellular membrane (e.g. glycosaminoglycan and phospholipids), leading to the temporary or permanent destabilization of the lipid bilayer caused by the CPPs inserted in the membrane [155, 196]. More precisely, the inverted micelle mechanism causes local disorder of the lipid bilayer, which leads to the formation of such inverted hexagonal structures containing CPPs. As these micelles cross the membrane, they invert, which results in the destabilization of these micelles and finally, the release of the CPPs into the cytosol [145, 155, 186]. According to the carpet model, the peptide aligns parallel to the lipid membrane and when a threshold concentration is reached, transient pores can be formed that enable the translocation of the CPP into the cells [145, 159]. The mechanisms involved in the formation of “toroidal” and “barrel-stave” pores presumed the existence of a well-defined secondary structure of the CPP [186]. In the toroidal pore mechanism, the peptides insert into the lipid bilayer and bend the lipid monolayer into the interior, forming a hydrophilic pore in the cell membrane (Figure 7) [155]. In the barrel-stave model, the hydrophobic regions of the peptides interact with the hydrophobic core of the cell membrane, while the hydrophilic regions of the peptide face the lumen of the pore (Figure 7) [155, 159].

In summary, the endocytotic pathway is supposed to be the dominant mechanism for the majority of CPPs, particularly when attached to large cargoes. However, it is essential to emphasize that the translocation pathway by which the cell-penetrating peptides enter into the cell depends on several parameters including (i) the nature and secondary structure of the CPP; (ii) its capability to interact with membrane components; (iii) the nature, type and concentration of the cargo; and (iv) the cell type and membrane composition [74].

1.2.2 Interactions of CPPs with membranes

As already mentioned earlier, the first step of peptide internalization requires the electrostatically interaction between the cationic cell-penetrating peptide and the negatively charged constituents of the cell membrane [196]. Thus, when translocating through the cellular membrane, the first potential partners that CPPs will encounter at the cell surface are the negatively charged glycosaminoglycans and anionic phospholipids [36, 196].

The role of proteoglycans

Proteoglycans are a heterogeneous group of proteins covalently attached with long, linear glycosaminoglycan (GAG) chains [6]. These chains are characterized by a high density of negatively charged sulfate and carboxylate groups [196]. Thus, proteoglycans are categorized according to the nature of the GAG chains [81]. Thereby, heparan sulfate (HS), chondroitin sulfate (CS) and dermatan sulfate (DS) are the most widespread GAGs in

proteoglycans [6]. As most CPPs contain positive charges, the peptide-GAG interaction is supposed to play a role in the internalization of peptides across the cell membrane, irrespective of the uptake mechanism [6, 140]. In this regard, taking into consideration that the most well-known CPPs are rich in Arg residues, the guanidium moieties of Arg could strongly interact with the sulfate and carboxylate groups of GAGs through bidentate hydrogen bonds (Figure 8A) [128, 196].

The role of phospholipids

Since the lipid composition of the plasma membrane, especially the anionic lipids, plays an essential role in the translocation pathway of CPPs, the negatively charged phospholipids of the cellular membrane represent the other main interaction partner of cell-penetrating peptides [6]. Despite lipids are not symmetrically distributed across the two leaflets of the cell membrane, anionic lipids are mainly found at the cytosolic site of the membrane and only a minor fraction is localized at the outer leaflet [36, 196]. Therefore, it is assumed that the peptides are able to recruit the anionic lipids in order to generate negatively charged nanodomains on the cell surface and thus allowing the critical internalization step [36, 196].

The role of Arg residues

Besides the evidence for the importance of anionic components in the cellular membrane and the cationic nature of CPPs, the type of the chemical hydrogen bond seems to be much more important [86].

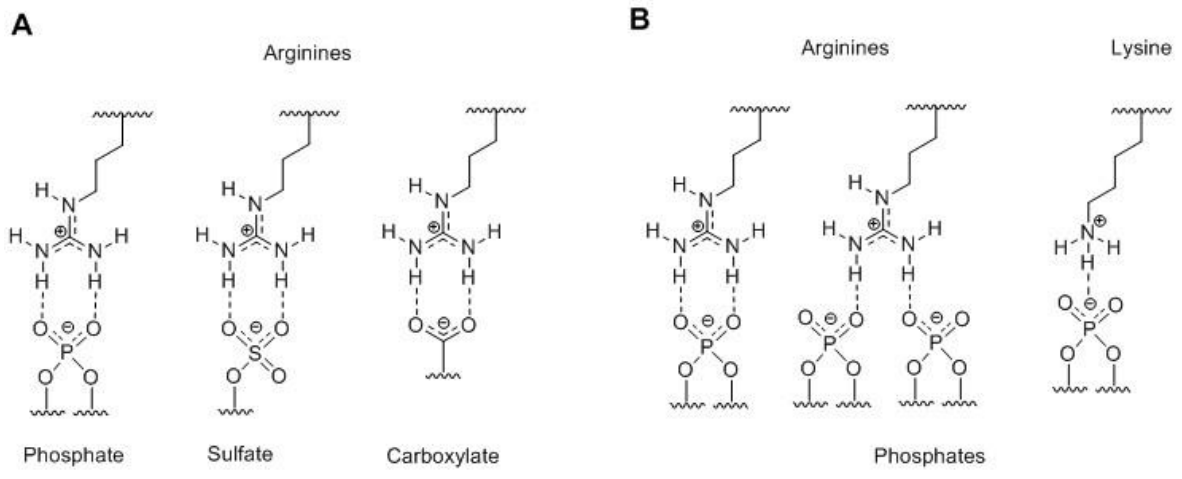

Figure 8. Interaction of arginine- and lysine rich peptides with negatively charged components of the plasma membrane. Favorable hydrogen bonding between guanidinium moieties of Arg-rich peptides and phosphate, sulfate and carboxylate groups of glycosaminoglycan **(A)**. Differences in phosphate binding mechanism of Arg and Lys residues **(B)**. (modified after Jobin *et al.*, 2014 [86])

Several studies have shown that Arg-rich peptides efficiently penetrate the cells, while Lys-rich CPPs do not, which is in accordance with the fact that the replacement of Arg by Lys

totally suppresses the cellular uptake of these CPPs [8, 86, 125]. In this context, Rothbard *et al.* revealed that Lys residues can only form monodentate interactions with the anionic cell surface which is not sufficient for the successful translocation of CPPs through the cell membrane, since Arg residues form bidentate hydrogen bonds (Figure 8B) [154].

1.3 Skin and wound healing

1.3.1 Skin as barrier

The skin is the largest organ of the human body and is known to cover an area of up to 2 m^2 and its weight consists of more than 10 wt.% of the total weight of an adult body [89]. The primary function of the skin is to serve as a protective barrier against external mechanical, chemical, microbial and physical influences [41] and further helps to regulate the body temperature and permits the sensations of touch, heat, or pain [89]. The cellular architecture of the skin is depicted in Figure 9.

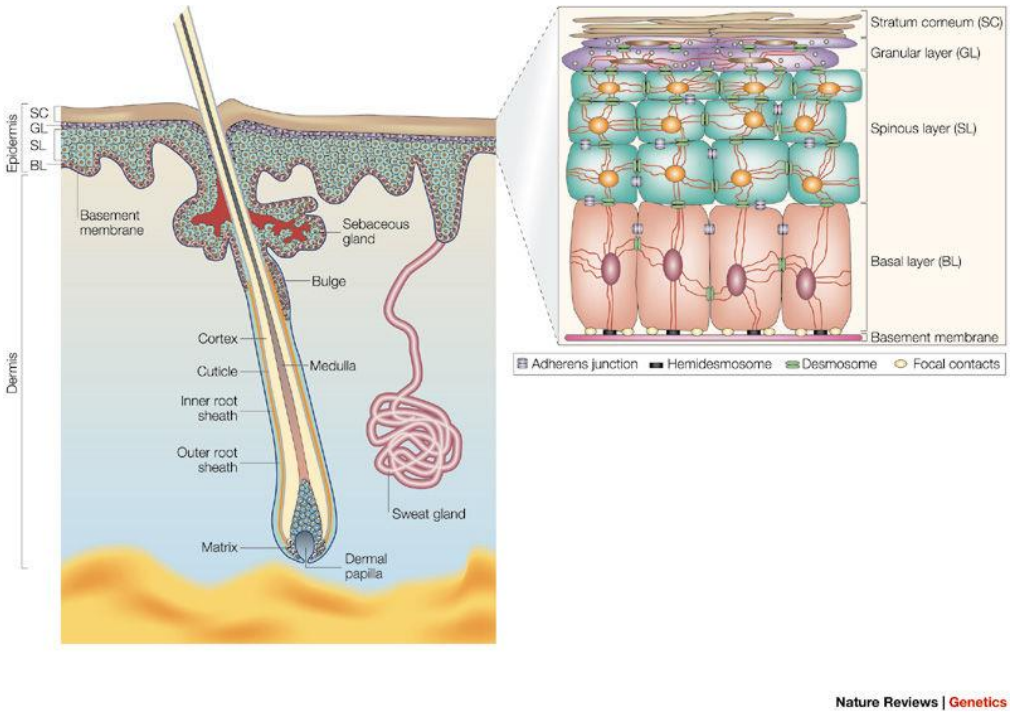

Figure 9. Mammalian skin. The skin consists of the epidermis, the outermost layer of the skin and the dermis, the layer beneath the epidermis. The stratified structure of the epidermis is shown in the right panel. (adapted from Fuchs and Raghavan, 2002 [58])

The skin consists of two main tissue layers, the epidermis and the underlying connective tissue, which comprises the dermis and the hypodermis [5]. The epidermis is a multilayered epithelium mainly composed of keratinocytes [5]. The stratum corneum (SC), the outermost layer of the epidermis, consists of a 10 – 15 µm thick matrix of dead keratinocytes (corneocytes), which are surrounded by highly ordered lipid layers serving as cover. Thus, the SC provides the foremost barrier protecting our body from the influx of external materials

into the skin [22, 41]. The SC is underlaid by the viable epidermis (50 – 100 µm thick), which is responsible for the generation of the SC. The viable epidermis is composed of the granular, spinous and basal cell layer (Figure 9), whereby each layer is characterized by position, shape, morphology and state of the differentiation of keratinocytes [21, 22]. Directly adjacent to the epidermis lies the dermis, approximately 1 – 2 mm thick, providing the mechanical support for the skin. The dermis and also the hypodermis are thus highly supplied with blood vessels and nerves [5, 21, 22]. The hypodermis layer is composed of subcutaneous fat tissues providing thermal isolation and mechanical protection to the body [89]. In addition to the main tissues, sweat glands and hair follicles are spread throughout the skin [58].

1.3.2 Wound healing and peptides

Since the skin serves as a protective barrier against the surrounding environment, any type of skin injury has to be mended in a rapid and efficient manner [119]. Wound healing is thus a critical process and starts normally immediately after the injury [169]. The cutaneous injury initiates a complex set of events comprising three overlapping phases: the inflammation, the proliferative process leading to tissue restoration and tissue remodeling (Figure 10) [109].

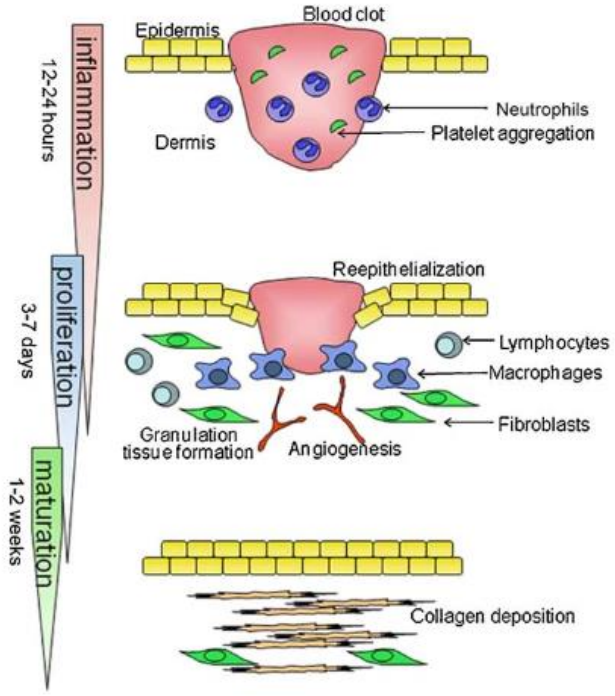

Figure 10. The three stages involved in skin wound healing. (adapted from Kondo and Ishida, 2010 [96])

Cutaneous wound healing typically begins with the inflammation response, which is characterized by erythema, heat, swelling and pain, which are the results of capillary vasodilation and increased permeability [13]. Neutrophils and macrophages (inflammatory

cells) further infiltrate the wound site and trigger the process of wound healing [94]. The proliferative phase comprises the migration and proliferation of endothelial cells, fibroblasts and keratinocytes leading to re-epithelialization [109]. Approximately 4 days after injury, the dermal reconstitution begins at the wound site, which is characterized by the formation of granulation tissue including angiogenesis and collagen formation [96, 109]. The final stage of wound healing is the remodeling of the wound and the surrounding tissue by fibroblasts, which are responsible for the development of new epithelium and the final scar tissue formation. This stage of wound repair begins 2 – 3 weeks after injury and may last for one year or even longer depending on specific and individual factors such as the age of the patient, diseases and medication as well as the size, depth and cause of the wound [39, 142, 191].

Efficient wound treatment remains one of the most prevalent healthcare issue, since thousands of patients suffered annually from different kinds of skin damage or burns by hot water, flames or accidents [33, 89]. Moreover, chronic wound patients, which suffer from diseases like type 2 diabetes, obesity, and wound infections account for increasing health care costs [163]. Therefore, much effort has been expended on wound care with an emphasis on new therapeutic approaches and the development of technologies for acute and chronic wound treatment [191].

Until now, a plethora of studies exists concerning the therapeutic potential of antimicrobial peptides (AMPs) derived from multiple sources, e.g. humans or amphibians, as efficient modulators of wound healing [116]. In general, antimicrobial peptides, composed of 10 – 50 amino acids, mostly exhibit an amphipathic character due to the prevalence of basic amino acid residues and a high content of hydrophobic amino acids [149]. AMPs, also known as host defense peptides, show a broad spectrum of antimicrobial activity against gram-positive and -negative bacteria, and play an essential role in the innate immune response as antimicrobial and immune-modulating agents [174].

Owing to their multiple functions, AMPs could act as effective agents in bacterial infected wounds, since the disruption of the skin barrier allows pathogens to attack the body and thus drastically increases the risk of infection.

Until now, pexiganan, a 22 amino acid long peptide analogue of the naturally occurring AMP, magainin 2, isolated from the skin of the African clawed frog, *Xenopus laevis* [61], is the first AMP evaluated for the treatment of infected human wounds, particularly for the treatment of diabetic foot ulcer [100]. Unfortunately, the use of pexiganan failed the Phase III clinical trial in 2016.

1.4 Peptides used within the thesis

1.4.1 The cationic cell-penetrating peptide sC18

The cell-penetrating peptide sC18 is a highly cationic fragment (amino acid residues 106 – 121) of the *C*-terminus of the 18 kDa cationic antimicrobial protein CAP18, and highlighted as a useful delivery vehicle for cytostatic compounds [62, 79, 130, 172]. Furthermore, sC18 was shown to efficiently internalize into cells which might be attributed to its amphipathic α-helical nature [130, 183]. The major uptake route of sC18 is proposed to follow the energy-dependent endocytotic pathway. However, previous studies demonstrated that structural modifications of sC18, particularly the cyclization of the peptide backbone and the dimerization of the peptide sequence resulting in a branched version, lead to an efficient and moreover increased cellular uptake showing somehow a certain selectively towards cancerous cells [68, 77, 78].

Furthermore, a study by Splith *et al.* showed the successful delivery of a novel designed sC18 conjugate composing of a nitroimidazole unit (NIA) as radiosensitizer, a radioactive label and sC18 as transporter, to target hypoxic tumor tissues [173]. Lately, Bergmann *et al.* improved this delivery vehicle by introducing $_{D}$-amino acids instead of $_{L}$-amino acids, leading to a proteolytically more stable peptide, since this system was hampered by fast degradation [18].

The following table represents an extract from sC18 variants, which were applied for various approaches.

Table 2. An extract from sC18 variants for diverse application approaches. B: L-propargylglycine, X: L-(Ɛ-azido)-lysine; ___: amino acids involved in cyclization; NIA: 2-(2-nitroimidazol-1-yl)acetic acid

Peptide	Sequence	Features	Ref.
sC18	GLRKRLRKFRNKIKEK	Transport tool for cytostatic drugs, e.g. metal complex and imaging probes	[130, 152, 172]
(sC18)$_2$	GLRKRLRKFRNKIKEK | GLRKRLRKFRNKIKEK	Drug delivery, tumor-selectivity	[68, 78]
cyc3	BLRKRLRKFRNX	Vehicle for gene delivery	[77]

DOTA-sC18(NIA)	DOTA-βA-GLRK(NIA)RLRKFRNKIKEK	Specific targeting of hypoxic tumor tissue	[173]
NODAGA-$_D$sC18(NIA)$_2$	NODAGA-βA-GLRK[(βA)$_2$-(NIA)]RLRKFRNK[(βA)$_2$-(NIA)]IKEK		[18]

Overall, the cationic sC18 peptide provides a highly attractive tool through which bioactive molecules can reach their intracellular target.

1.4.2 The naturally derived peptide Tylotoin

Tylotoin, a short peptide consisting of 12 amino acid residues, was recently identified and extracted from the skin of the salamander *Tylototriton verrucosus* [126]. The precursor of Tylotoin was found to belong to the family of cathelicidin, which is a conserved protein family among vertebrates [126]. More precisely, Tylotoin is derived from the *C*-terminal part, like other antimicrobial peptides, e.g. LL-37 [2] or sC18 [130] but in contrast to these peptides, Tylotoin exhibits no antimicrobial activity [126]. However, the main feature of Tylotoin is provided by its ability to significantly accelerate the healing of full-thickness wounds in mice indicating that topical application of Tylotoin has a potent healing effect on full-thickness skin wounds [126]. Thereby, the short peptide was shown to directly function in the migration and proliferation of fibroblasts, keratinocytes, and vascular endothelial cells, which are all important key cell types during the wound healing process [126, 169].

With this potent peptide in hand, another step towards the understanding of the cellular and molecular events underlying the rapid wound healing process in salamanders could be done, which might lead to the development of rapid wound healing therapies in the future.

2. Aims of the thesis

The primary goal of this thesis was to understand the initial step of cell-penetrating peptides cell entry in more detail on a molecular level. At the same time, model membrane systems have gained increased attractiveness and thus were used to establish different techniques that can be helpful to shed light on the action mechanism of CPPs. The second chapter focuses on the design, characterization and the application of cell-penetrating peptide conjugates in skin wound healing.

2.1 Establishment of diverse bilayer model systems and their applications in peptide-lipid interactions

In this chapter, different model membrane systems, more precisely large and giant unilamellar vesicles and membrane vesicles, which are exclusively derived from live cells plasma membranes, were employed to evaluate peptide-membrane interactions and their significance for the successful translocation across the cell membrane. For this purpose, various methodologies are described that have been established in our working group by myself, and which represent particularly great tools to assess the relationship between peptides and various membrane components to understand the molecular level of translocation of CPPs. More specifically, great attention is paid to aspects concerning peptides effect on membrane integrity, structural behavior of peptides in the presence of lipid bilayer systems and finally, the elucidation of the relevance of mammalian plasma membrane compositions. Thus, these newly acquired techniques were then applied using two different structural modified variants of the cationic cell-penetrating peptide sC18 to unravel how CPPs interact with live cells on a molecular level using artificial membrane systems.

2.2 CPPs and wound healing

So far, no study of which we are aware has been reported on the use of CPPs in the application field of human skin wound healing. Thus, for the first time, a cell-penetrating peptide was covalently conjugated to a wound healing promoting peptide with the main goal to accelerate the wound healing process. Herein, these novel conjugates were evaluated upon their cytotoxicity, cellular internalization behavior and moreover, the impact of peptides on *in vitro* wound healing was investigated.

3. Materials and methods

The chemicals, reagents and consumables used in this present thesis were obtained from the companies Merck (Darmstadt, Germany), Sarstedt (Nümbrecht, Germany), Sigma-Aldrich (Taufkirchen, Germany) and VWR (Darmstadt, Germany), unless otherwise specified. N_{α}-Fmoc protected amino acids were purchased from IRIS Biotech (Marktredwitz, Germany).

The following table depicts the applied equipment during the working time.

Table 3. An overview about the equipment used during the thesis.

Instrument	Producer
Balance	Analytical balance FA-210-4, Faust Laboratory balance SBA52, Scaltec
Blotting system	kuroGEL semi-dry-blotter, VWR
CD spectrometer	JASCO J-715 spectropolarimeter
Cell culture clean bench	Hera Safe
Centrifuges	Thermo Scientific; Heraeus Multifuge X1R Thermo Scientific; Heraeus Pico 17
CO_2-incubator	BINDER
Electrophoresis system	Mini-PROTEAN Tetra Vertical Electrophoresis System; Bio-Rad
ESI mass spectrometer	Bruker Esquire HCT
Flow cytometer	Guava® easyCyte flow cytometer, Merck, Darmstadt BD Accuri C6 flow cytometer, Heidelberg
Haemocytometer	Neubauer improved, superior Marienfeld
Heating block	Eppendorf – Thermomixer compact
HPLC (analytic)	Chromolith Performance column (RP-18, 130 Å, 2 µm, 100 × 4.60 mm, Merck
HPLC (preparative)	Elite Lachrom Hitachi Pump L-2130, Elite Lachrom Hitachi Autosampler L-2200, Elite

	Lachrom Hitachi Diode Array Detector L-2455, Teledyne ISCO Fraction Collector Foxy R1, Column: Phenomenex Jupiter, 4 µm Proteo 90 Å, 250 x 15 mm
LC-mass spectrometer	LC: Hewlett Packard Series 1100 MS: Finnigan MAT-LCQ
Lyophilizer	Lyovac GT2 with CertomaT SII Thermo Savant Refridgerated Vapor Trap RVT5105
Microscope	Inverted microscope (Motic AE31, Wetzlar) Confocal laser scanning system (Nikon D-Eclipse C1)
Mini-extruder	Avanti Polar Lipids Inc., Alabaster, USA
Multipette® plus	Eppendorf
PCR Thermal Cycler	FlexCycler, Analytik Jena, Jena, Germany
Pipettes	Eppendorf Research
Pipetting aid	NeoLab
Plate reader	Tecan infinite M200, Salzburg, Austria
Rotary evaporator	VWR
Rotary Shaker	KL-2, Edmund Bühler GmbH Certomat H/SII, Braun Biotech, Göttingen, Germany
Spectral photometer	Thermo Scientific Genesys 10S UV-Vis
Speed-Vac	Thermo Scientific Speedvac Concentrator Savant SC210A, RVT5105 Refrigerated Vapor Trap VLP80 Vacuum Pump
Synthesis roboter	MultiSynTech Syro I, Bochum, Germany
Thermomixer compact	Eppendorf
Vacuum pump	VWR
Vortex	Scientific Industries – Vortex Genie 2
Water bath	Julabo SW22
XcelVap™	Horizon Technology

3.1 Peptides and lipids

3.1.1 Peptides

All peptides used in this work and their sequences are listed in Table 4.

Table 4. Sequences and references of investigated peptides. All peptides are amidated at the *C*-terminus and *N*-terminally labeled with 5(6)-carboxyfluorescein B: L-propargylglycine, X: L-(Ɛ-azido)-lysine; ___: amino acids involved in cyclization.

Peptide	Sequence	Reference
sC18	GLRKRLRKFRNKIKEK	[68, 78, 130]
sC18*	GLRKRLRKFRNK	[77]
$(sC18)_2$	GLRKRLRKFRNKIKEK | GLRKRLRKFRNKIKEK	[68, 78]
lin$(sC18)_2$	GLRKRLRKFRNKIKEKGLRKRLRKFRNKIKEK	[129], this work
$(sC18^*)_2$	GLRKRLRKFRNK | GLRKRLRKFRNK	
lin$(sC18^*)_2$	GLRKRLRKFRNKGLRKRLRKFRNK	
cyc1	BLRXRLRKFRNK	[77]
cyc2	BLRKRLRXFRNK	[77]
cyc3	BLRKRLRKFRNX	[77]
Tylotoin	KCVRQNNKRVCK	[126]
rTylotoin	RNCVKKNCRVKQ	this work
Tylotoin-sC18	KCVRQNNKRVCKGLRKRLRKFRNKIKEK	
sC18-Tylotoin	GLRKRLRKFRNKIKEKKCVRQNNKRVCK	
Tylotoin-sC18*	KCVRQNNKRVCKGLRKRLRKFRNK	
sC18*-Tylotoin	GLRKRLRKFRNKKCVRQNNKRVCK	

3.1.2 Lipids

All lipids used in this study are depicted in Table 5.

Table 5. Lipids used in this study were obtained as chloroform solution (10 mg/ml).

Lipid	Company
1,2-dioleoyl-*sn*-glycero-3-[phospho-L-serine] (DOPS)	Avanti Polar Lipids, Inc. (Alabaster, USA)
1,2-dioleoyl-*sn*-glycero-3-[phospho-*rac*-(1-glycerol)] (DOPG)	Avanti Polar Lipids, Inc. (Alabaster, USA)
1,2-dioleoyl-*sn*-glycero-3-phophoethanolamine (DOPE)	Avanti Polar Lipids, Inc. (Alabaster, USA)
1,2-dioleoyl-*sn*-glycero-3-phosphocholine (DOPC)	Avanti Polar Lipids, Inc. (Alabaster, USA)
Atto550 labeled DOPE	Atto Tec (Siegen, Germany)
cholesterol (Chol)	Sigma-Aldrich (Taufkirchen, Germany)
L-α-phosphatidylinositol-4,5-bisphosphate (porcine brain, PIP_2)	Avanti Polar Lipids, Inc. (Alabaster, USA)
sphingomyelin (porcine brain, SM)	Jena Bioscience (Jena, Germany)

3.2 Solid phase peptide synthesis (SPPS)

The peptides used in this thesis were synthesized via automated solid phase peptide synthesis as described below.

3.2.1 Automated solid phase peptide synthesis

Automated solid phase peptide synthesis offers a suitable strategy to produce chemical engineered peptides simultaneously. The peptides used were synthesized on a multiple Syro I peptide synthesizer following the Fmoc/*t*-Bu strategy. The synthesis runs in open polypropylene reactor vessels (2 ml syringes) equipped with a fritted disc. The software SyroXP calculates the amounts of amino acids (0.4 mol/l) and solvents required for the complete synthesis run. In order to synthesize a peptide amide, Rink amide resin (NovaBiochem, Bad Soden, Germany) was used. The Fmoc-protected Rink amide resins

(30 mg, 0.5 mmol peptide per gram resin; 15 µmol ≙ 1 eq.) were first swollen in DMF, then the Fmoc protecting groups were cleaved with 40% piperidine in DMF and following another deprotection step/cleavage with 20% piperidine in DMF. After four washing steps using DMF, the N_α-Fmoc protected amino acids were introduced in 8-fold excess by using a double coupling procedure and *in situ* activation with Oxyma and DIC. In a last step, when the defaulted amino acid sequence of the peptides was completed, the *N*-terminal Fmoc-protecting group was removed under previously mentioned conditions and the resin was washed with DMF. A reaction scheme of the automated solid phase peptide synthesis is illustrated in Figure 11.

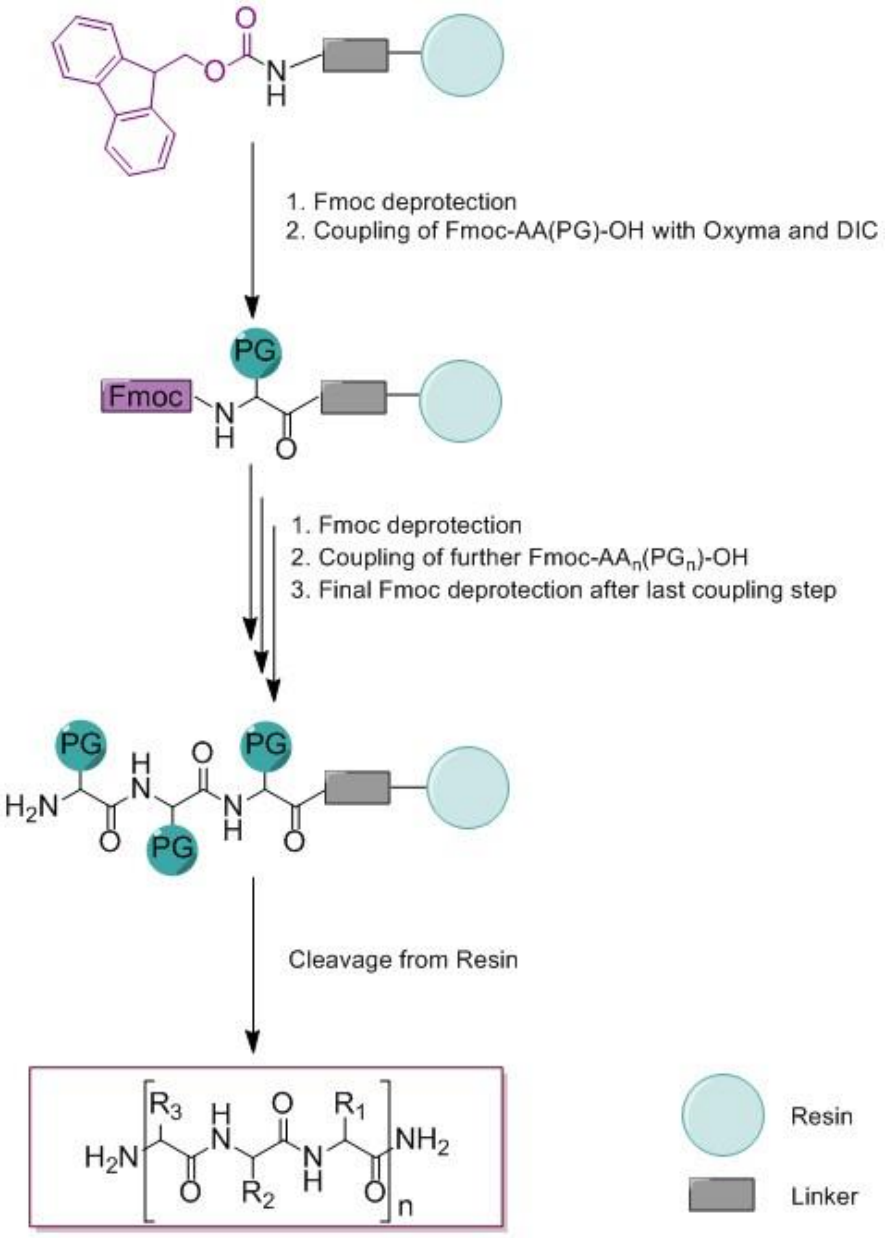

Figure 11. Schematic overview of general steps in solid phase peptide synthesis. R: different side-chains of amino acids. PG: protecting groups of amino acid side chains.

3.2.2 5(6)-carboxyfluorescein (CF) – labeling on resin

To allow microscopic and flow cytometric analysis, the peptides were *N*-terminally labeled with 5(6)-carboxyfluorescein. The labeling procedure was performed while the peptides were still bound to the resin with fully protected side chains. Thus, the resin was swollen in 1 ml DMF for at least 15 min. After the solvent was removed, 3 eq. of CF and HATU were dissolved in 300 µl DMF and added to the swollen resin. Subsequently, 3 eq. of DIPEA were added directly to the syringe and the reaction was carried out under vigorous shaking for 2 × 2 h at RT or overnight with 5 eq. of Oxyma and DIC. After the incubation time, the resin has been washed five times with DMF, CH_2Cl_2, MeOH and Et_2O and finally dried for 10 min in a Speed-Vac. To monitor whether the coupling was successful, a Kaiser test was performed. CF-polymers, which might have formed, were cleaved by treatment with 20% piperidine for 45 min.

3.2.3 Kaiser test [88]

In Fmoc solid phase peptide synthesis, monitoring the completeness of the coupling step is mandatory. Therefore, the Kaiser test is used to control the presence or absence of free amino groups based on the reaction of ninhydrin with amines. Therefore, a few resin beads were placed in a 1.5 ml reaction vessel and one drop of each solution (I, II and III; Table 6) was added consecutively. The samples were incubated at 95 °C for 5 min. A blue coloring of the resin beads and the solutions indicates free amino groups and hence an incomplete coupling, whereas a yellowish color represents no free amino groups and therefore a negative result. As a positive control the primary amine ethanolamine was chosen.

Table 6. Compositions of the solutions required for the Kaiser test.

Solution	Composition
Solution I	1.0 g ninhydrin in 20 ml EtOH
Solution II	80.0 g phenol in 20 ml EtOH
Solution III	0.4 ml KCN solution in 20 ml piperidine

3.2.4 Sample cleavage

To verify the success of the coupling reaction, it is advisable to perform a sample cleavage. Therefore, 2.5 µl of triisopropylsilane (TIS) and 2.5 µl of water, working as scavengers, were added to a small amount of resin beads. In the case of Tylotoin conjugates containing cysteine within the sequence, 7 µl of thioanisole and 3 µl of 1,2-ethandithiol (EDT) must be used as scavengers. Afterwards, the mixture was filled up to 100 µl with TFA and the reaction was carried out under shaking conditions for 3 h at RT. After the incubation time,

1 ml of ice-cold diethyl ether was added to the mixture to precipitate the peptide and was left for 20 min or overnight at -20 °C. Afterwards, the mixture was washed with 1 ml diethyl ether and centrifuged (4 °C, 4 min at 10,000 x g) for at least five times until no scavenger smell was perceived. The resulting pellet was finally dried for 10 min in the Speed-Vac and dissolved in 100 µl H_2O/*t*-BuOH (3:1, v/v). Finally, the sample was analyzed by HPLC-ESI-MS.

3.2.5 Full cleavage of peptide

The peptide amides were cleaved with a mixture of TFA/TIS/water (95:2.5:2.5, v/v/v) except for Tylotoin conjugates, which were cleaved by a mixture of TFA/thioanisole/EDT (90:7:3, v/v/v) within 3 h as previously described. The peptides were precipitated from cold diethyl ether (10 ml) at -20 °C and collected by six centrifugation steps (4 °C, 4 min at 5,000 x g) and lyophilized from water/*t*-BuOH (LyoVac GT2, Leybold, Germany). A sample of the peptide solution was analyzed by HPLC-ESI-MS.

3.3 Peptide analysis

3.3.1 Analytical HPLC-MS

A high-performance liquid chromatography electrospray ionization mass spectrometry (HPLC-ESI-MS) method was used to evaluate the purity and the identity of the peptides. Therefore, the peptide solution was diluted with a starting gradient of 10% ACN in water with 0.1% formic acid (FA). 10 µl of the solution was injected and separated by an ACN gradient which was raised from 10 to 60% by the HPLC. The flow rate was set to 0.6 ml/min. The analytics were performed on an Elite LaChrom VWR-Hitachi system using a Chromolith Performance column (RP-18, 130 Å, 2 µm, 100 × 4.60 mm, Merck). One part of the eluate was passed to the electrospray ionization source whereby ions were generated and their m/z ratio was determined.

3.3.2 Preparative RP-HPLC

Purification of the peptides was achieved by preparative RP-HPLC on a Phenomenex Jupiter column (Proteo, 90Å, 4 µm, 250 × 15.00 mm) using a linear gradient of 10 – 60% B in A (A = 0.1% TFA in water; B = 0.08% TFA in ACN) over 45 min and a flow rate of 6 ml/min. The peptides were detected at 220 nm and the fractions were collected separately. Afterwards, the peptide solution was removed from ACN using either the Speed-Vac or the XcelVap™ and then lyophilized overnight.

3.3.3 Circular dichroism (CD) spectroscopy

The CD spectra were recorded from 260 nm to 180 nm in 0.5 nm intervals at 20 °C using a JASCO J-715 spectropolarimeter in a N_2 atmosphere. Peptide solutions were dissolved in 10 mM potassium phosphate buffer (pH 7.0) containing either 0 or 50% (v/v) trifluoroethanol (TFE) to a final peptide concentration of 20 µM. The CD spectra were measured using a 1 mm quartz cell and each measurement was repeated three times. Instrument parameters were set as follows: sensitivity, 100 mdeg; scan mode, continuous; scan speed, 50 nm/min; response time, 2 s and bandwidth, 1.0 nm. All CD spectra were smoothed and corrected by subtraction of the CD spectrum form the respective buffer to eliminate potential measurement errors caused by the solvents. The ellipticity was expressed as molar ellipticity [Θ] in $\frac{deg \times cm^2}{dmol}$.

3.4 Peptide-lipid interactions

3.4.1 Preparation of large unilamellar vesicles (LUVs)

For the preparation of different composed LUVs, several lipids were required, which are dissolved in $CHCl_3$. To remove residual solvent, the lipid mixture was placed in a round-bottomed flask under vacuum at 37 °C for at least 1 h to remove residual solvent. The dried lipid film was either hydrated with HKS-glucose buffer (for flow cytometric studies and CF-release experiments) or with 25 mM phosphate buffer, pH 7.4 (for CD spectroscopic studies) at 45 °C for 5 min to form liposomes with a final concentration of 2 mM (CD spectroscopic analysis), 4 mM (flow cytometric studies) or 8 mM (CF-release experiments). To form LUVs, the resulting multilamellar vesicle (MLV) dispersion was subsequently run through 10 freeze/thawing cycles and passed 21 times through a mini-extruder equipped with a 0.4 µm polycarbonate track-etch membrane (Avanti Polar Lipids, Inc.). Liposome preparations were analyzed by dynamic light scattering indicating a range of 250 – 400 nm in diameter.

HKS-glucose buffer

HEPES	25 mM (pH 7.4)
KCl	150 mM
Sucrose	10%

Table 7. All lipid compositions used during the thesis. For peptide-induced CF-leakage, LUVs entrapping 100 mM CF were prepared. The vesicle membranes were labeled with 0.2 mol% Atto550-DOPE for flow cytometric studies.

LUV compositions	Lipids [mol%]				
	zwitterionic		anionic		
	DOPC	DOPE	DOPG	Sphingomyelin	Cholesterol
I	50	50	-	-	-
II	40	30	30	-	-
III	25	-	5	50	20
IV	37.5	37.5	5	-	20
V	22.5	22.5	5	50	-

3.4.2 Preparation of giant unilamellar vesicles (GUVs)

Giant unilamellar vesicles were generated as previously described [76, 148]. Briefly, super low melting agarose (1%, w/v) was coated on a clean glass slide and dried on a hot plate (~50 °C) for 30 min. Afterwards, 10 µl of the respective lipid solution was spread on the agarose film and dried *in vacuo* for at least 1 h to remove residual chloroform. To visualize the membranes, the lipid solution was prior doped with 0.2 mol% Atto550-DOPE. Then, a seal ring was placed onto the lipid coated areas on the slide to obtain two sealed chambers. For the preparation of GUVs encapsulating the blue dye Oyster 405 (Luminaris GmbH, Münster, Germany), dextran buffer containing additionally 5 µM of Oyster 405 (300 µl each) was added to the hybrid film. The glass slide was then left in the dark for 2 h to allow hydration and swelling of the lipids. To harvest the GUV suspension, the glass slide was gently tilted in all directions to detach the liposomes from the surface. The giant liposomes were then stored in LoBind tubes (1.5 ml, Eppendorf, Hamburg, Germany) at RT and were used within three days.

Dextran buffer

HEPES	10 mM (pH 7.4)
KCl	50 mM
NaCl	50 mM
Dextran	1 mg/ml (from *Leuconostoc spp.*, 6 kDa)

Table 8. All lipid compositions used during the thesis. The vesicle membranes were labeled with 0.2 mol% Atto550-DOPE or with 0.2 mol% DiI to visualize the loosely packed liquid-disordered lipid phase (L_d).

GUV compositions	Lipids [mol%]				
	zwitterionic		anionic		
	DOPC	DOPE	DOPG	Sphingomyelin	Cholesterol
I	50	50	-	-	-
II	40	30	30	-	-
III	25	-	5	50	20
IV	37.5	37.5	5	-	20
V	22.5	22.5	5	50	-

3.4.3 Preparation of giant plasma membrane vesicles (GPMVs)

Cells (HEK-293 800,000; MCF-7 250,000) were seeded in a 6-well culture plate (Sarstedt, Nümbrecht, Germany) and were grown to 70 – 80% confluency in appropriate growth medium supplemented with 4 mM L-glutamine and 10% fetal bovine serum (FBS). Giant plasma membrane vesicles (GMPVs) were prepared as described earlier by R. E. Scott, 1976 [162] with minor modifications. First, the cells were washed twice with GPMV buffer. To induce the formation of cell-free vesicles, 1 ml of freshly prepared GPMV buffer supplemented with paraformaldehyde (PFA) and dithiothreitol (DTT) at final concentrations of 25 mM and 2 mM respectively were added and the cells were incubated for 2 h at 37°C while slowly shaken (60 rpm, Certomat H/SII, Braun Biotech). After incubation, the GPMV-rich cellular supernatant was transferred into a 15 ml conical tube, where the GPMVs were allowed to settle down on ice for 30 min. Afterwards, 20 – 50% of the total volume were transferred from the bottom of the conical tube into a 1.5 ml Eppendorf tube. For microscopic studies, 0.5 µg/ml DiI stain (final concentration, in EtOH) was added and incubated for 15 min at 37 °C. After isolation, GPMVs were stored at 4 °C for 1 – 2 days without visible degradation.

GPMV buffer

HEPES	10 mM (pH 7.4)
NaCl	150 mM
$CaCl_2$	2 mM

3.4.4 Secondary structure via CD spectroscopy

In the presence of LUVs, the peptide to lipid molar ratio in the cuvette was set to 1/50 and the instrument settings were chosen as described in section 3.3.3. All CD spectra were averaged over three scans, smoothed and the background was subtracted from the signal, respectively. The ellipticity was expressed as molar ellipticity [Θ] in $\frac{deg \times cm^2}{dmol}$.

3.4.5 Peptide-induced CF-release

CF-containing LUVs were prepared by hydrating a dried lipid film (8 mM) of desired compositions with HKS-glucose buffer containing 100 mM CF. The fluorescence intensity in the presence of 100 mM CF is low due to self-quenching but increases upon dilution. Free CF outside the LUVs was separated by size exclusion chromatography using a PD10 column (GE Healthcare). Then, peptides were added to LUVs and the release of CF from vesicles was monitored by measuring the increase in fluorescence intensity using the Tecan infinite M200 plate reader. At the end of each experiment, Triton X-100 (0.4% (w/v) final concentration) was applied to measure the maximum of dequenching that will be used to normalize data. The percentage of CF release was determined by the following equation

$$\%\ CF\ release = \frac{F_{(t)} - F_0}{F_f - F_0} * 100$$

where $F_{(t)}$ is the fluorescence intensity at time t, F_0 is the fluorescence intensity before peptide addition and F_f is the fluorescence intensity after the final addition of Triton X-100.

3.4.6 Flow cytometric binding studies

Various compositions of LUVs (4 mM) were applied to flow cytometry analysis as recently described by the Nickel group [180]. CF-labeled peptides were added to 25 µl solutions of LUVs and incubated at 25 °C for 2 h while mild shaking (450 rpm, Thermomixer compact, Eppendorf, Hamburg, Germany). After incubation, the peptide/liposome solutions were washed with 1 ml buffer (150 mM KCl, 25 mM HEPES, pH 7.4) and centrifuged at 15,000 x g for 10 min at 4 °C. The supernatants were carefully removed and the pellets resuspended in 400 µl buffer solution. Afterwards, the peptide/lipid interactions were analyzed with a fluorescence-activated cell sorter (FACS) instrument (BD Accuri C6 flow cytometer).

3.4.7 Confocal laser scanning microscopy

Microscopic studies with GUVs were performed as recently described by our working group [148]. Briefly, GUVs loaded with the membrane-impermeant fluorophore Oyster 405 were prepared as described in section 3.4.2. To remove untrapped Oyster 405, liposomes were centrifuged two times at 14,000 x g for 10 min at RT. A 40 µl aliquot of the GUV solution was diluted in 50 µl of the respective buffer without Oyster 405 and was then transferred

into a tissue culture vessel (FlexiPERM slide, 8 wells, Sarstedt, Germany). CF-labeled peptides diluted in Dextran buffer were added to the outer solution of GUVs at a final concentration of either 10 or 20 µM. The GUV−peptide interaction was analyzed using a confocal laser scanning system (Nikon D-Eclipse C1) consisting of an inverted microscope (Nikon Eclipse Ti) equipped with a 20× objective (NA 0.45, Plan Fluor; Nikon). Microscope pictures were recorded in 16-bit grayscale, pseudocolored in red (channel 1), green (channel 2), and blue (channel 3) followed by processing with ImageJ.

GPMVs were analyzed by CLSM as described by the Pooga group with minor modifications [10]. Concisely, after labeling the vesicles with the fluorescence stain DiI, the CF-labeled peptides at 1 µM concentrations were immediately added to GPMV suspension and incubated at RT for 1 h. Then, 20 µl of the peptide/membrane solution were deposited onto a µ-slide 8-well (Ibidi) plate and covered with glass cover slips (ø 9 mm, round, No 1). The GPMVs were investigated using a Nikon Eclipse Ti confocal laser scanning microscope equipped with a 60× oil-immersion objective. Images were recorded with Nikon EZ-C1 software and adjusted equally with ImageJ software.

3.5 *In vitro* studies

3.5.1 Microorganisms and media

The strain numbers and sources of the bacteria used in this thesis are *Micrococcus luteus* (DSM 20030) and *Salmonella typhimurium* (TA 100).

For both bacterial strains, Mueller Hinton broth agar plates were used for maintenance und broth medium was used to carry out antimicrobial activity studies.

Mueller Hinton Broth

Acid casein peptone	17.5 g/l
Beef infusion	2.0 g/l
Corn starch	2.5 g/l

For Mueller-Hinton Broth agar plates, 15 g/l of bacteriologic agar was additionally supplemented.

3.5.2 Antimicrobial activity

The determination of the antimicrobial activity of peptides against gram-positive and gram-negative bacteria was conducted using the *p*-iodonitrotetrazolium-chloride (INT) violet assay. INT is a tetrazolium based reagent which is converted to a pink formazan dye in the presence of metabolically active bacteria.

Therefore, *M. luteus* and *S. typhimurium* were cultured in Mueller Hinton broth overnight at 37 °C while mild shaking (180 rpm). Overnight-cultured bacteria were added into fresh medium, grown to an optical density at 600 nm of 0.7, and 10 µl bacterial solution were added in triplicate to wells of a 96-well plate (BD Falcon, USA). The peptides used at variable concentrations (0.25 – 25 µM) and 180 µl of Mueller Hinton medium were added to each corresponding well and incubated for 6 h at 37 °C. 70% EtOH served as positive control and H_20 was used as negative control. After the incubation time, 10 µl of the freshly prepared INT solution (1 mg/mL in DMSO) were added to each well and incubated for further 30 min at 37 °C. The viability of bacteria relative to untreated control was determined by measuring the absorption at 540 nm on a Tecan infinite M200 plate reader.

3.5.3 Cell lines and culture conditions

The cell lines used in this thesis included: HaCaT (Human adult low Calcium high Temperature keratinocytes), HEK-293 (human embryonic kidney cells), HeLa (human cervix carcinoma cells) and MCF-7 (human breast adenocarcinoma cells). Cells were cultivated in sterile 10 cm petri dishes (100 x 200 mm, BD Flacon) at 37 °C and 5% CO_2 in a humidified atmosphere. HaCaT cells were cultured in Dulbecco's modified Eagle medium (DMEMg) complemented with 4500 mg/l glucose, 10% FBS and 2 mM L-glutamine. For HEK-293 cells, complete DMEM media supplemented with 15% FBS and 4 mM L-glutamine was used. HeLa and MCF-7 cells were grown in complete RPMI 1640 medium containing additionally 10% FBS and 4 mM L-glutamine.

3.5.4 Maintenance and seeding cells

All cell culture work was done under sterile conditions with autoclaved materials under a clean bench, equipped with a hood. Once a year, all cell lines were tested for mycoplasma contaminations according to manufactures protocol (PCR Mycoplasma Test Kit II, Applichem, Darmstadt).

To cultivate the cell lines, they were split normally twice a week. Therefore, the medium was discarded and the cell layer was washed twice with PBS. Then, 1 ml of porcine trypsin solution (0.5 mg/ml in Hank´s balanced salt solution) was added to the culture dish and incubated at 37 °C till the cells have rounded up and begun to detach. Subsequently, the cells were resuspended in 9 ml of the appropriate FBS-containing culture media to block trypsin activity, transferred to new culture dishes and mixed with fresh medium depending on the certain split ratio. HEK-293 cells were not cultivated above the 30^{th} passage; MCF-7 and HeLa cells not over 40^{th}.

3.5.5 Freezing and thawing cells

To store cells for future studies, cryopreservation provides a great tool. Therefore, confluent cells were trypsinized and then centrifuged for 5 min at 300 x g. The cell pellet was resuspended in 1.5 ml appropriate medium containing FBS and additionally 10% of sterile-filtered DMSO. Afterwards, the cells were transferred to cryogenic vials and cooled down to 4 °C for 15 min and then kept at -20 °C for further 2 h. Next, the cells were incubated overnight at -80 °C and finally stored in liquid nitrogen.

To thaw cryopreserved cells, the frozen cells were defrosted rapidly in a 37 °C water bath and directly transferred to a culture dish containing the required pre-warmed medium with FBS. In case of HaCaT cells, the cells were first transferred to a 15 ml tube containing complete growth media, centrifuged for 5 min at 300 x g and finally moved to a 25 cm^2 flask. The cells were incubated for 24 h at 37 °C in a humidified atmosphere of 5% CO_2. The next day, the cells were washed twice with PBS to get rid of remaining DMSO and dead cells and finally maintained in appropriate complete growth media.

3.5.6 Cell viability assays

In order to examine possible cytotoxic effects of peptides on the cell viability, the following assays were applied.

Resazurin-based Assay

For a resazurin-based cell viability assay, 35,000 HeLa cells were seeded in triplicate onto a 96-well plate, grown to 70 – 80% confluency and incubated with various concentrations of peptides in appropriate growth medium without serum for 24 h under standard growth conditions. For the positive control, cells were treated with 70% ethanol for 10 min. After washing with PBS, resazurin stock solution (5% resazurin in PBS) was diluted with appropriate serum-free medium (1:10, v/v) and 100 µl of this solution was incubated with the cells for further 1 h at 37 °C. Subsequently, the cell viability was determined relative to untreated cells by measurement of the resorufin product at 595 nm (λ_{ex} = 550nm) on a Tecan infinite M200 plate reader.

Tetrazolium-based Assay

The toxic effect of peptides on HaCaT cells was evaluated using the 3(4,5-dimethylthiazol-2yl)2,5-diphenyltetrazolium bromide (MTT) colorimetric method. MTT is a tetrazolium salt which is reduced to a purple colored formazan product by mitochondrial reductases, present only in metabolically active cells. The intensity of the color is directly proportional to the number of metabolically-active cells. Keratinocytes were seeded in triplicate onto a 96-well plate at a density of 80,000 cells per well in DMEMg supplemented with 2 mM L-glutamine and 2% FBS. After overnight incubation at 37 °C and 5% CO_2 atmosphere, the medium was

replaced with 100 µl fresh serum-free media containing the peptides at different concentrations. After 24 h of incubation, 10 µl of MTT (0.45 mg/ml final, in PBS) were added to each well. After 4 h of incubation, the supernatants were removed and the formazan crystals were dissolved by adding 100 µl of dimethyl sulfoxide (DMSO). As positive control, cells were treated with 70% EtOH for 10 min. The absorption was measured at 570 nm and at a reference wavelength of 630 nm using a plate reader (Tecan infinite M200). Cell viability was expressed as percentage of viability in control cells (cells not treated with peptide).

3.5.7 Internalization studies

Confocal microscopic uptake studies

Cells were seeded in a µ-slide 8-well (Ibidi) plate (HaCaT 90,000; HEK-293 100,000; HeLa 45,000 and MCF-7 50,000) and grown to 70 – 80% confluency. Then, the cells were incubated with CF-labeled peptides in serum-free medium for the requested time at either 4°C or 37 °C as indicated. The nuclei were stained for 10 min with 0.6 µl Hoechst 33342 nuclear dye (bisbenzimide H33342, 1 mg/mL in H_2O, sterile filtered) prior to the end of peptide incubation. Finally, the solution was removed and the cells were treated for 30 s with 150 µl trypan blue (150 µM in 0.1 M acetate buffer, pH 4.15) for quenching the external fluorescence. After washing twice with PBS, 300 µl of FBS-containing cell culture medium were added to each well. Images were taken by using a Nikon Eclipse Ti confocal laser scanning microscope equipped with a 60x oil-immersion objective (N.A. 1.4, Plan APO VC, Nikon). Images were recorded with Nikon EZ-C1 software and adjusted equally with ImageJ software.

For cholesterol depletion, 300 µl of a 10 mM freshly prepared methyl-β-cyclodextrin (MβCD) solution dissolved in appropriate serum-free medium were added to the cells and incubated for 1h at 37 °C. Subsequently, the cells were washed once with PBS and then treated as described above.

For treatment with endocytosis inhibitor, 80 µM of dynasore (in serum-free medium, 297 µl) was added to the cells. After 1 h of incubation at 37 °C, 3 µl of a 1 mM CF-labeled peptide solution was added and incubated for further 30 min. Afterwards, the cells were handled as described above.

For specific cell organelle trafficking, cells were incubated with 10 µM of CF-labeled Tylotoin-sC18* together with either 1 µM MitoTracker Red FM dye (1mM stock solution in DMSO, Molecular Probes) or 75 nM Lyso-Tracker (1 mM stock solution in DMSO, LysoTracker Red, Molecular Probes) for 120 min at 37 °C and continued as mentioned above. In case of staining the endoplasmic reticulum, 1 µM of ER-Tracker (1 mM stock

solution in DMSO, ER-Tracker Red BODIPY, Molecular Probes) were added 15 min prior to the end of peptide incubation.

Flow cytometric uptake studies

Cells were seeded in triplicate in a 24-well plate (HaCaT 400,000; HEK-293 400,000; HeLa 170,000; MCF-7 200,000) and grown to 70 – 80% confluency under normal growth conditions. After incubation at 37 °C for 30 min with CF-labeled peptides in serum-free medium, the cells were washed twice with PBS, trypsinized and resuspended in indicator-free medium. Analyses were performed on a Guava® easyCyte flow cytometer (Merck, Darmstadt, Germany). Cellular autofluorescence was subtracted.

For cholesterol depletion, 400 µl of a 10 mM freshly prepared MβCD solution dissolved in appropriate serum-free medium were added to the cells and incubated for 1h at 37 °C. Subsequently, the cells were washed once with PBS and then treated as described above.

3.5.8 *In vitro* scratch assay

The ability of peptides to promote the migration of keratinocytes was studied using an *in vitro* wound healing migration assay. Briefly, HaCaT cells suspended in DMEMg containing 10% FBS were seeded in 12-well plates and grown until they reached confluence. Next, cells were starved in serum-free media for 16 h at 37 °C in a humidified atmosphere of 5% CO_2. For inhibitor studies, mitomycin C (20 µM final, in serum-free medium) to prevent cell proliferation were added 90 min prior to scratch generation. After this, an artificial wound was created across cell monolayers by performing a vertical scratch with a sterile 200 µl pipette tip resulting in a cell-free area of approximately 100 - 200 µm. After washing twice with PBS to remove cell debris, the cells were treated with 13.5 µM peptides in serum containing medium. Untreated cells served as negative control and the human epidermal growth factor hEGF (5 ng/ml final, in serum-free medium) as positive control. Scratches were photographed immediately after peptide treatment and 7, 25 and 30 h after peptide addition using an inverted microscope at 10x magnification (N.A. 0.3, Plan Fluor, Nikon). Same image fields were captured and the cell-covered areas and migration speed were estimated by Wimasis Image Analysis. The experiments were repeated several times and representative pictures are shown.

3.5.9 Western blot analysis

For the detection of EGFR and p-EGFR, western blotting was performed. After reaching a confluence of 90 – 100%, HaCaT cells were split up into a 6-well plate and cultivated to 70 – 80% confluency at 37 °C in an atmosphere with 5% CO_2. In the following, cells were serum-starved for 16 h and then stimulated with Tylotoin-sC18* for 5, 15 and 25 min for detection of phospho-EGFR as indicated. The hEGF (100 ng/ml final, in serum-free

medium) served as positive control. For EGFR inhibition, cells were pretreated with 0.2 µM AG1478 for 10 min and subsequently treated with hEGF for 5 min. Afterwards, cells were harvested on ice in 1x cell lysis buffer (Cell Signaling Technology, Beverly, USA) supplemented with 1 mM phenylmethylsulfonyl fluoride (PMSF), collected by centrifugation at 4 °C and 10,000 x g for 10 min and protein concentration was determined via Bradford protein assay. Next, 20 µg samples were mixed with 1x Laemmli buffer and boiled at 95 °C for 5 min to denaturate the secondary and tertiary structures. Subsequently, the probes were separated on 10% SDS-PAGE (TGX™ FastCast™ acrylamide starter kit, 10%, Bio-Rad, München, Germany) and transferred to a polyvinylidene difluoride membrane (Amersham™ Hybond™ P 0.45 µm, GE Healthcare, Solingen, Germany). Membranes were blocked with 5% skim milk in 1x TBS for 1 h while constant shaking. After three washing steps with 1x TBS, membranes were incubated with antibodies specific to EGFR and phosphor-EGFR (EGF Receptor (D38B1) XP Rabbit mAb; phospho-EGFR (Tyr1068) (D7A5) XP Rabbit mAb; (1:1000), Cell Signaling) overnight at 4 °C while gentle shaking and then treated with anti-rabbit horseradish-peroxidase (HRP)-conjugated secondary antibody (1:300, Cell Signaling) for 1 h. Then, blots were developed with SignalFire ECL reagent (Cell Signaling) and visualized by ChemiDoc MP imaging system (Bio-Rad).

1x Laemmli buffer

2-Mercaptoethanol	0.1%
Bromophenol blue	0.0005%
Glycerol	10%
Sodium dodecyl sulfate	2%
Tris-HCl	63 mM (pH 6.8)

10x SDS buffer

Tris-HCl	250 mM (pH 6.8)
Glycine	1.92 M
Sodium dodecyl sulfate	1%

10x TBS buffer

Tris-HCl	0.2 M (pH 7.6)
NaCl	1.5 M

10x Transfer buffer

Tris-HCl	20 mM (pH 8.3)
Glycine	192 mM
Methanol	20%

4. Results and discussion

4.1 Investigating CPP-lipid membrane interactions

The first part of the thesis deals with the investigation of CPP-lipid membrane interactions that govern the initial step and subsequently the internalization of CPPs into cells. For this purpose, different assay systems had to be primarily established in our working group. In the first chapter, the several experimental approaches, which were employed in the thesis, are introduced and described in greater detail. In the second chapter, these novel established techniques were applied to gain knowledge of the mechanism of action of structural modified variants of the sC18 peptide.

4.1.1 Experimental approaches on CPP-lipid membrane interactions

Regardless of the many studies that were performed on cell-penetrating peptides, the mechanism of their cellular uptake is still not fully understood [111]. Therefore, there is an urgent need to unveil the mechanism of cellular translocation in greater detail to enable the development of effective transport vehicles, allowing the delivery of therapeutic compounds across the cell membrane [47]. However, the delivery of drugs through the membrane underlays complex biological processes, often difficult to understand due to their dynamic nature. In this regard, the use of model membrane systems has provided a great tool to recognize the role of lipids as well as membrane constituents within cellular interactions [137]. Thus, lipid membrane systems have become increasingly relevant in recent years [137].

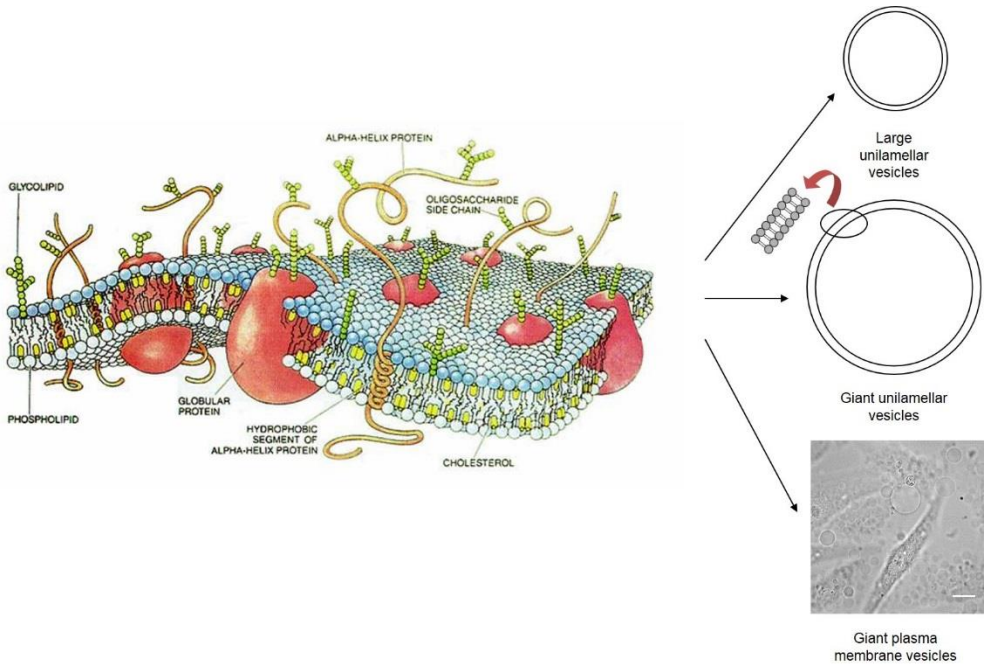

Figure 12. Scheme of cell membranes architecture [24] and model membrane systems. LUVs and GUVs mimic the arrangement of lipids in a cell membrane while GPMVs are deriving directly from the cells plasma membrane due to chemical induction.

Accordingly, Figure 12 illustrates different vesicle models used within the thesis as artificial mimetic systems for biological membranes to investigate peptide-lipid membrane interactions. As mentioned earlier, model membranes, in particular liposomes, are among the most important simplified systems in peptide-lipid interaction studies [137]. As indicated in Figure 12, unilamellar vesicles are ranging in size resulting in large unilamellar vesicles (LUVs) and giant unilamellar vesicles (GUVs). One of the major advantage of these vesicles is the possibility to choose a specific lipid composition of interest and thus selective investigations on peptide-membrane interactions to specific membrane components [51]. Moreover, giant plasma membrane vesicles (GPMVs) also provide a highly attractive system, since their membranes retain the molecular richness with lipids, proteins and extracellular matrix constituents of the cell membrane which they derived from [156]. Thus, using this system, it is possible to assess the peptide-membrane interactions in a biologically complex and highly relevant environment [134].

However, to unravel the factors which are mandatory for efficient cellular translocation and moreover drug delivery, it is important to study and characterize the interplay of CPPs and membrane components in detail. Therefore, several approaches were necessary and needed to be addressed, such as secondary structure, the influence of specific lipids as well as the binding affinity and membrane integrity. For this purpose, different biophysical methods, model systems and experiments were required owing to the fact that one single method is not sufficient in creating an overall picture about the elementary processes involved in the translocation of CPPs across lipid membranes.

Herein, the focus lied on different experimental approaches using artificial model membrane systems to assess in detail the interactions of CPPs, developed in our working group, with several lipid compositions, as well as the impact on membrane integrity. Moreover, structural changes of CPPs in a membrane mimetic environment became another subject of interest.

Therefore, several methodological techniques were established, which will be examined more precisely in the following.

Studying peptide-membrane interactions

The interaction of cell-penetrating peptides with model lipid membranes has been studied using fluorescence approaches including confocal laser scanning microscopy (CLSM) and flow cytometric analysis.

Giant unilamellar vesicles were used for microscopic analysis due to their large size facilitating microscopic observation, in contrary, large unilamellar vesicles were employed for flow cytometric binding studies. The phospholipids, sterols and sphingomyelin chosen

for the lipid compositions mimic those components of mammalian plasma membranes. At the same time, the system was tried to keep as simple as possible allowing to find specific answers concerning the elementary principles of peptide-membrane interactions and thus translocation mechanism.

So far, a large body of literature exists that already reported on the use of giant unilamellar vesicles to investigate peptide-lipid interactions using CLSM [83, 91, 200]. Herein, GUVs were prepared by gentle hydration method provided by Horger *et al.*, which includes the formation hybrid film of partially dried agarose and lipids (Figure 13) [76].

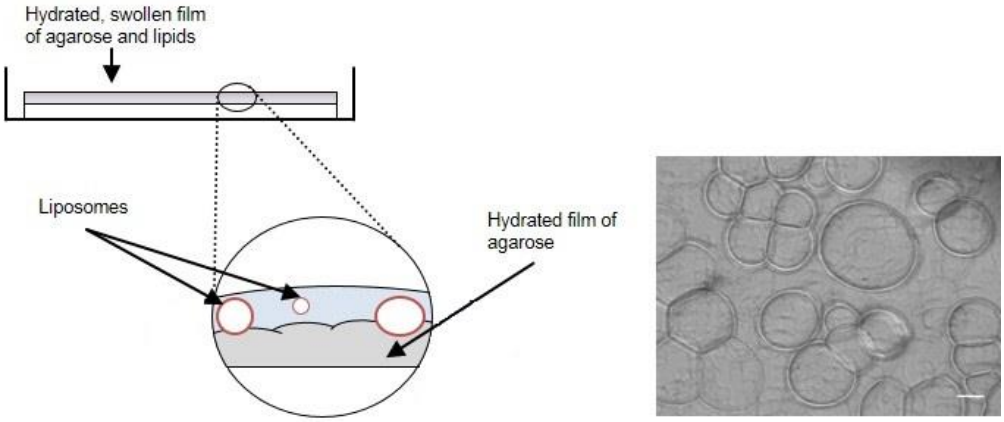

Figure 13. Formation of giant unilamellar vesicles by using the method of Horger *et al.*, 2009. GUVs containing different lipid compositions were generated (see figure right). (modified after Horger *et al.*, 2009 [76])

Hydrating the films of agarose and lipids under ionic conditions close to physical ones resulted in swelling and partial dissolution of the hybrid films and subsequently in rapid formation of giant unilamellar vesicles in high yield and large size (up to 100 µm) [76]. The great advantage over conventional procedures is the fact that this method did not require the presence of an electric field [10], a separate prehydration step [147] or specific lipids [3].

To allow the observation of peptide-GUVs membrane interactions with fluorescence techniques, lipid compositions were doped with a fluorescent probe prior to vesicle formation and 5(6)-carboxyfluorescein labeling was used to detect peptides (Figure 14B and C). Moreover, GUVs can be prepared featuring coexisting liquid-disordered (L_d) and -ordered (L_o) lipid phases using specific lipids and markers to visualize the phase separation (Figure 14A).

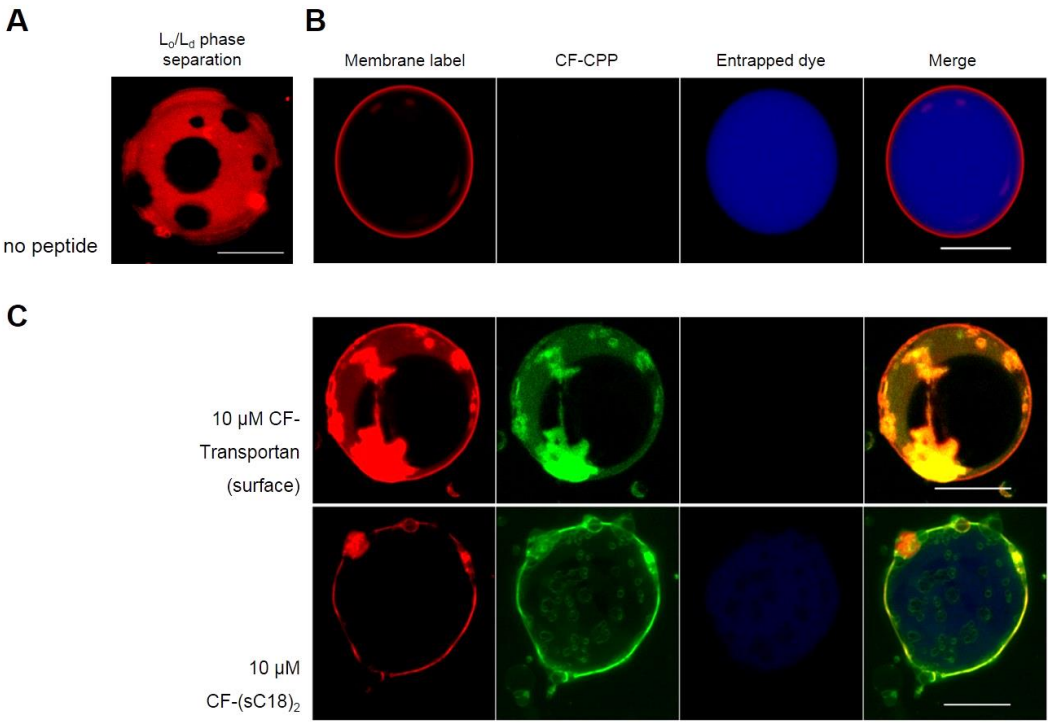

Figure 14. Fluorescence microscopic images of giant unilamellar vesicles (GUVs). GUVs composed of DOPC/DOPG/SM/Chol doped with DiI in order to visualize the L_d phases **(A)**. The microscopic image in **(B)** shows in red the labeled vesicle membrane with Atto550-DOPE and in blue the entrapped dye allowing to investigate membrane destabilizing effects of peptides. CLSM analysis of GUVs treated with CF-labeled Transportan and $(sC18)_2$ **(C)**. Scale bars, 30 µm.

In general, the experimental set-up enables us to gather selective information about the interaction loci of CPPs at the membrane of GUVs and specific membrane components required for an efficient interaction. Moreover, the direct visualization and quantitative analysis of pore forming events in model membranes will be possible [194]. For example, the upper microscopic image in Figure 14C shows the preferential accumulation of CF-labeled well-described CPP Transportan on the L_d phase of GUVs featuring L_o and L_d (red membrane label) domains. The lower image displays the strong accumulation of the dimeric sC18 peptide on negatively charged GUV membranes which is accompanied by a nearly complete release of the blue dye (Oyster 405). These results show that both cell-penetrating peptides bind with a strong affinity to the vesicle membranes which leads to noticeable membrane perturbations. Thus, experimental conditions, such as peptide concentration, membrane lipid composition, and charge of the lipids, are important factors which have to be considered [111].

Recently, a new flow cytometric assay was developed to quantify interactions between proteins and membrane lipids [180]. In particular, this system offers the opportunity to quantify the binding affinity of peptides to membrane lipids reconstituted in large unilamellar vesicles and moreover peptide-induced changes in membrane curvature and tethering in a rapid and efficient manner [180]. Furthermore, only small amounts of peptide and lipids are needed, making this method attractive. However, to detect peptide-lipid membrane

interactions using this technique, LUVs and peptides have to be labeled with a fluorescent marker [180]. Nevertheless, with this potent flow cytometric based assay in hand, essential binding affinities can be detected and quantified in an effective way (as mentioned in Section 4.1.2). Figure 15 illustrates the simplified work flow of such an experiment, also used in this thesis, in order to obtain more quantitative data about the accumulation of fluorescent labeled CPPs in vesicle membranes.

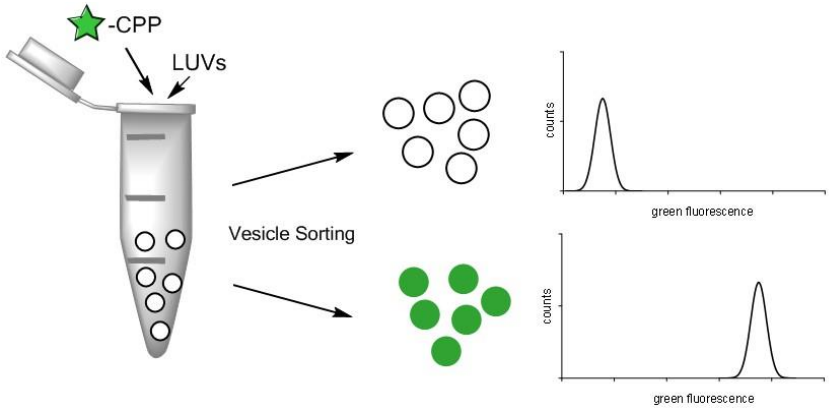

Figure 15. Schematic overview of the binding and penetration affinity of CPPs towards large unilamellar vesicles (LUVs). Both, LUVs and CF-CPPs are added to a 1.5 ml tube and incubated for 2 h while slowly shaken. The quantification of CF-labeled CPPs into LUVs is then determined by flow cytometry.

Lately, the use of giant plasma membrane vesicles as model membranes has received more attention to investigate interactions of peptides with components of membranes [7, 106, 156, 162]. Furthermore, the study by Säälik *et al.* revealed that the membranes of GPMVs segregate into liquid-ordered and liquid-disordered phases and could further demonstrate by confocal laser scanning microscopy that amphipathic CPPs (such as Transportan) preferentially interact with L_d membrane domains [156]. The experimental set-up and results of such an experiment are depicted in Figure 16.

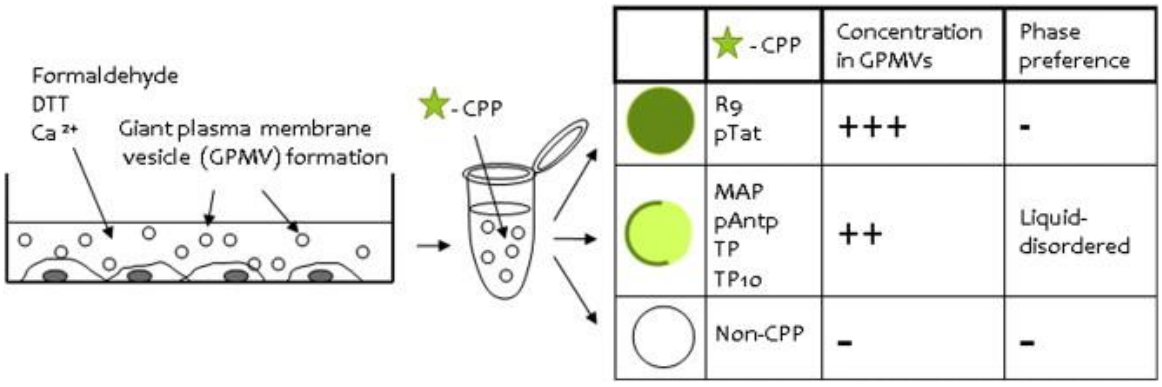

Figure 16. Illustrative overview ranging from the preparation of giant plasma membrane vesicles, the experimental set-up, as well as the interpretation of the results. (adapted from Säälik *et al.*, 2014 [156])

This kind of model membrane allows to identify other membrane components of plasma membranes, which are required for an efficient uptake. Moreover, using giant plasma-

derived vesicles, Amand *et al.* could demonstrate a linear correlation between GPMV binding and cellular internalization suggesting that internalization can be directly linked to the amount of peptide bound to the cell surface [7]. In this study, this technique was applied too.

Studying peptide-induced membrane destabilization effects

The ability to cause membrane perturbation seems to be a prerequisite for CPPs that are able to directly translocate across the cell membrane in an energy-independent manner. Thus, membrane destabilization effects appeared to play an important role in efficient uptake [51].

A common way to quantify the extent of membrane destabilization caused by peptides is via its capability to induce leakage of vesicle-entrapped fluorescent probes [48]. Within this work, 5(6)-carboxyfluorescein (CF) was included into large unilamellar vesicles. However, also the inclusion of calcein is often reported and both fluorophores are then used at a concentration that causes self-quenching [113]. Upon disruption of the membrane caused by peptides, the self-quenched fluorophore is released from the LUVs and generates strong fluorescence signals, which can be monitored using a plate reader [113]. Figure 17 represents a schematic overview of such a CPP-induced CF-leakage experiment that was established during this work.

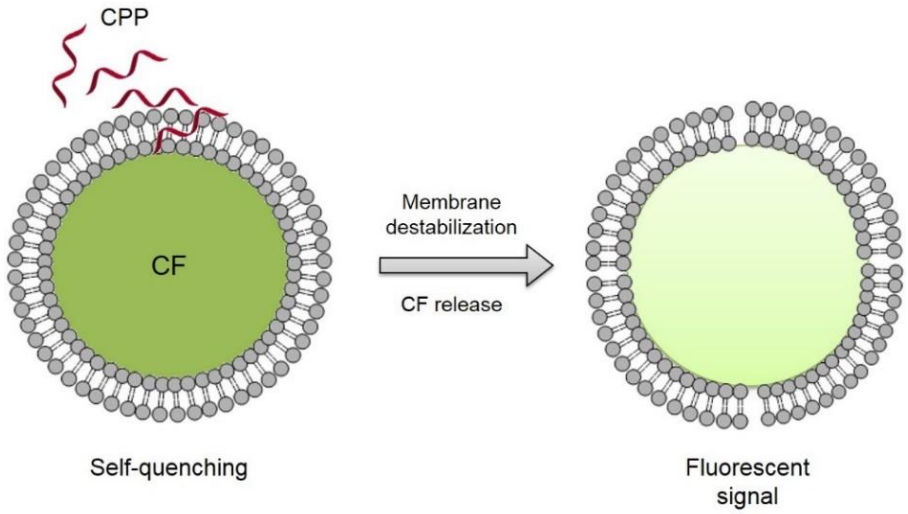

Figure 17. Schematic sketch of CPP-induced CF-release experiment. Cell-penetrating peptide was added to LUVs encapsulating high concentration of membrane-impermeant fluorophore CF. The fluorescence intensity in the presence of 100 mM CF is low due to self-quenching but increases upon CF release and therefore dilution in the outside medium.

The application of such dye releasing experiments can provide insight into possible pore forming events and thus into the mode of action [68]. Moreover, increased membrane permeability is also often related to toxicity of peptides [51, 157].

Studying secondary structure of CPPs upon membrane binding

Circular dichroism (CD) spectroscopy is often used to investigate peptide conformational changes upon association with model lipid membranes. For this purpose, large unilamellar vesicles (LUVs) are appropriate due to their size and smaller curvature [51]. In general, CD spectroscopy relies on the fact that optically active molecules (e.g. peptides) have different absorption of right- and left-polarized light [51, 113]. Thus, CD spectra of peptides, which are typically recorded in the far-UV region (250 – 180 nm) corresponding to peptide bond absorption, can be analyzed for the different secondary structural types, such as α-helix and β-sheet [92].

So far, several studies exist that have investigated the secondary structure of peptides in presence of model membranes to identify whether their tendency to adopt a secondary structure in a membrane mimetic environment correlates to their internalization capacities [87, 114]. However, for the first time, such experiments were performed for sC18 variants.

4.1.2 Impact of branched and cyclic CPPs on model membranes

In this chapter, the interactions of two structurally modified variants of the sC18 peptide with several bilayer models were studied, with the goal to contribute to the mechanistic understanding of peptide-membrane interactions as a step towards cellular internalization. Moreover, one aim was to identify components of the plasma membrane that govern the initial step of cell entry. Therefore, the four methodological approaches, as mentioned above, were employed to shed light on urgent features, which are necessary to identify CPPs as superior delivery vehicles.

Lately, the cell-penetrating peptide sC18, the cationic *C*-terminal fragment of the antimicrobial protein CAP18, was structurally modified by our working group to improve its efficiency as cell-penetrating peptide. Consequently, two strategies have been exploited, including the dimerization of sC18 resulting in a branched peptide structure [78], and the cyclization of the peptide backbone by click chemistry [77] in order to improve cellular uptake and drug delivery.

Table 9 summarizes in detail some characteristic facts about the branched and cyclic variants of the sC18 peptide used in this chapter.

Table 9. Names, sequences and analytical data of peptides. All peptides are amidated at the *C*-terminus and additionally labeled with 5(6)-carboxyfluorescein.

Peptide	Sequence	$MW_{calc.}$ [Da]	$MW_{exp.}$ [Da]	Yield [%]	Net charge
sC18	GLRKRLRKFRNKIKEK	2069.60	2070.47	36	+9
sC18*	GLRKRLRKFRNK	1570.96	1571.44	29	+8
$(sC18)_2$[a]	GLRKRLRKFRNKIKEK | GLRKRLRKFRNKIKEK	4122.16	4122.44	22	+17
lin$(sC18)_2$[a]	GLRKRLRKFRNKIKEKGLRKRLRKFRNKIKEK	4122.16	4122.05	38	+17
$(sC18^*)_2$[b]	GLRKRLRKFRNK | GLRKRLRKFRNK	3124.91	3125.04	43	+15
lin$(sC18^*)_2$[a]	GLRKRLRKFRNKGLRKRLRKFRNK	3124.91	3126.15	44	+15
cyc1[c]	BLRXRLRKFRNK	1635.01	1634.78	26	+7
cyc2[c]	BLRKRLRXFRNK	1635.01	1634.89	30	+7
cyc3[c]	BLRKRLRKFRNX	1635.01	1634.66	30	+7

B: L-propargylglycine, X: L-(ε-azido)-lysine; ___: amino acids involved in cyclization; [a] provided by Gronewold, A.; [b] provided by Natividad-Tietz, S.; [c] provided by Reichart, F.

Branched peptides

Peptide-membrane interactions play an essential role in the selective targeting of peptides to specific types of cells and tissues, since the membrane composition of both several organisms and cell compartments can be very different [60].

Hence, mammalian cell membranes are composed mostly of glycerol-based phospholipids, like phosphatidylcholine and phosphatidylethanolamine as zwitterionic lipids and phosphatidylserine and phosphatidylinositol as anionic lipids, sphingolipids and cholesterol [37, 204]. Beyond that, anionic phospholipids are usually only present in the inner leaflets of plasma membranes [37]. However, several studies have reported on a change in tumor cells membrane composition, which resulted in more anionic nature due to the enrichment of negatively charged lipids (like phosphatidylserine) in the outer leaflet of the plasma membrane [85, 188].

Previously, a study by Hoyer *et al.* demonstrated that the dimerization of sC18, namely $(sC18)_2$, led to an enhancement of the cellular uptake efficiency, which was particularly accompanied by a certain selectivity towards tumoral cells [78]. These results are in close agreement with those obtained recently by Gronewold *et al.* based on further intense cell selectivity studies [68], and moreover unveiled $(sC18)_2$ as promising carrier of the anticancer drug actinomycin D over its linear monomeric counterpart sC18 [68].

Herein, the main focus was laid on understanding the relevance of membrane compositions with respect to membrane interaction and integrity of the dimeric CPP $(sC18)_2$ in presence of membrane mimetic systems. Moreover, the influence of branching was further investigated, and therefore, several versions of the cell-penetrating peptide sC18 were designed and synthesized by our working group summarized in Table 9. Besides sC18, a truncated version of sC18, namely sC18*, missing four amino acids form the *C*-terminal part (inclusive glutamic acid) was chosen that still showed sufficient cell-penetrating properties [77]. Besides, the corresponding helical wheel plot highlighted the segregation of two distinct hydrophilic and hydrophobic faces resulting in a balanced ratio which was assumed to be essential for optimal peptide-membrane interactions [77]. Furthermore, to investigate the importance of branching for CPPs activity, both the branched dimeric versions of sC18 and sC18* and their linear counterparts, lin$(sC18)_2$ and lin$(sC18^*)_2$, were selected.

So far, it was already shown that the internalization efficiency in several cell lines of the branched dimeric peptide $(sC18)_2$ is vastly superior compared to the monomeric version sC18 [68, 78]. In particular, $(sC18)_2$ internalized to a much higher extent into the cancer cell line MCF-7 than into the non-cancer cell line HEK-293, which was further investigated by an extensive uptake screening on various cell lines supporting the idea of tumor cell selectivity [68]. Moreover, the mechanism of cell entry was shown to be energy-dependent

in HEK-293 cells, whereas $(sC18)_2$ was evenly distributed throughout the cytosol and in the nucleus in MCF-7 cells, clearly indicating that a large fraction of $(sC18)_2$ was internalized via direct penetration and by endocytosis followed by improved endosomal escape [68].

Additionally, the influence of branching on internalization efficiency and cytotoxicity was investigated using the linear version of $(sC18)_2$, revealing a strong internalization capacity similar to $(sC18)_2$ but also a tendency to a slightly higher cytotoxic profile [68]. However, regardless of branched or linear, the reason for the improved uptake efficacy of the dimeric sC18 conjugates is obviously attributed to the enhancement of the positive charges within in the peptide sequence resulting in increased peptide-membrane interactions essential for efficient uptake [68, 78]. In this context, initial insights on the relevance of membrane compositions were already obtained using large and giant unilamellar vesicles concerning the monomeric version and the branched dimer $(sC18)_2$. However, within this part, the focus will be on the branched and linear dimeric sC18 variants.

The influence of an anionic lipid on peptide-membrane interactions

First, the membrane interaction and destabilization activity of the peptide conjugates were investigated using neutral (DOPC/DOPE) and negatively charged lipid (DOPC/DOPE/DOPG) model systems as representatives of non-cancer and cancer cells, respectively. To allow microscopic analysis, membranes of giant unilamellar vesicles (GUVs) were prior doped with 0.2 mol% Atto550-DOPE (red fluorescent dye). In addition, to evaluate the peptide effect on membrane perturbation, GUVs encapsulating a membrane-impermeant blue fluorescent dye Oyster 405 were prepared.

Subsequently, the interaction of CF-labeled peptides with both giant unilamellar vesicle compositions were studied by confocal laser scanning microscopy (CLSM) depicted in Figure 18.

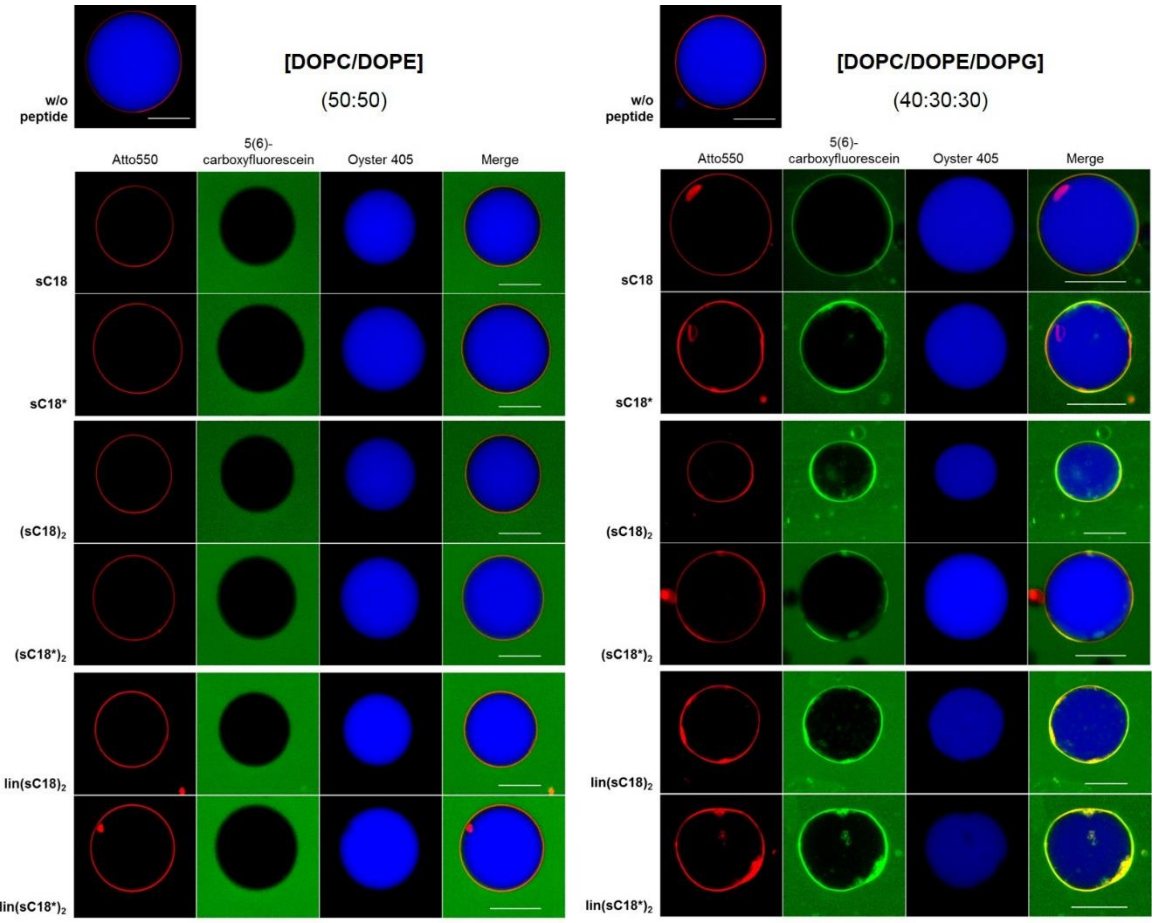

Figure 18. The influence of the negatively charged lipid phosphatidylglycerol (DOPG) on the interaction with model membranes. Microscopic analysis of GUVs composed of DOPC/DOPE (50:50) and DOPC/DOPE/DOPG (40:30:30) treated with various sC18 conjugates (10 µM) for 30 min and analyzed by CLSM. All GUVs contain 0.2 mol% Atto550-DOPE as lipid marker and were additionally loaded with 5 µM of the blue fluorescent dye Oyster 405. Scale bars, 30 µm.

As shown in the left panels of Figure 18, no significant accumulation of CF-labeled peptide conjugates was observed on the membranes of neutral GUVs when incubating them with 10 µM peptide solution for 30 min. In contrast, in the presence of anionic lipids (DOPG), peptide treatment resulted in strong green fluorescent signals on the membranes (right panels, Figure 18), which is not surprising since the preferential accumulation of Arg-rich peptides on negatively charged membranes was previously described by several studies [35, 181, 210]. Moreover, these results are in close consistency with former findings for sC18 and $(sC18)_2$ obtained by Gronewold *et al.* [68].

To gain a deeper insight into the membrane accumulation of peptide conjugates with giant unilamellar vesicles, GUVs were loaded with a fluorescent dye as mentioned above and the efflux of dye was assessed by fluorescence microscopy. The quantitative evaluation is represented in Figure 19A. Additionally, 5(6)-carboxyfluorescein leakage experiments were performed using large unilamellar vesicles (LUVs) of the same lipid compositions as GUVs and loaded with CF to investigate whether peptides perturbed vesicle membrane integrity (e.g. via pore formation) shown in Figure 19B.

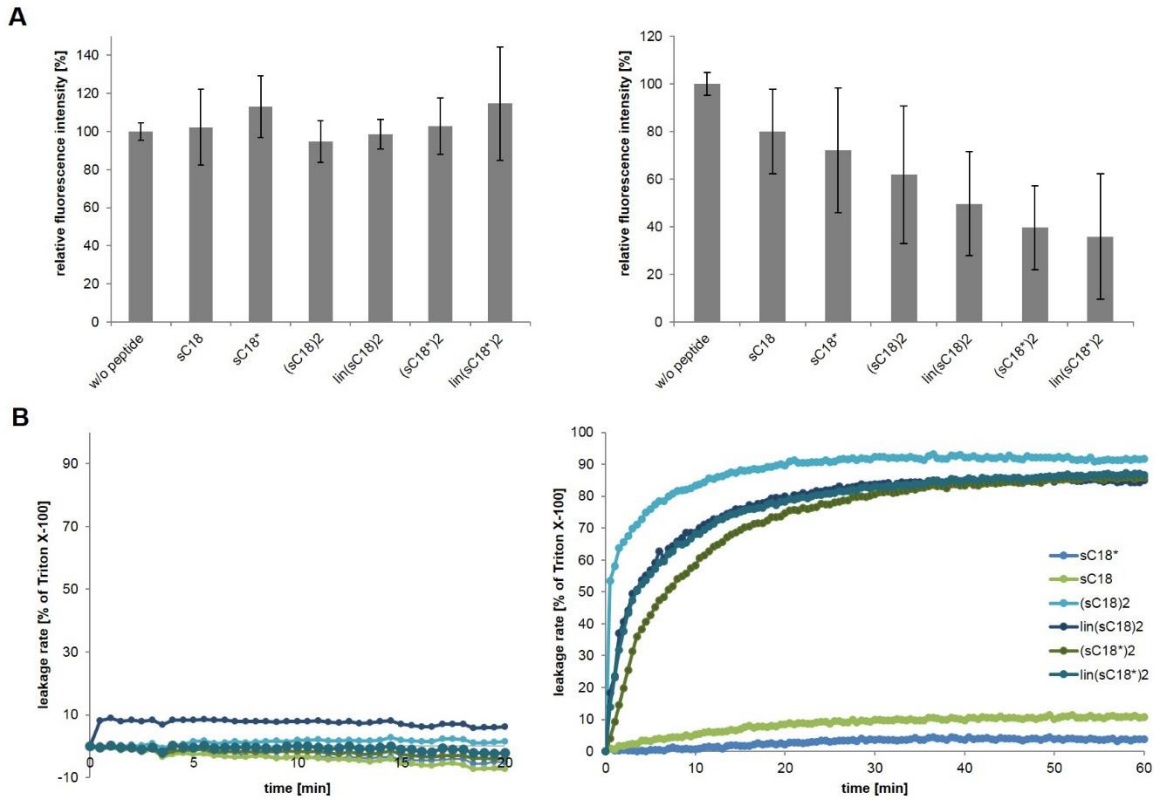

Figure 19. Peptide-induced leakage from DOPC/DOPE (50:50) and DOPC/DOPE/DOPG (40:30:30) model membranes treated with sC18 conjugates. The relative fluorescence intensities of the enclosed Oyster 405 dye in DOPC/DOPE (50:50) and DOPC/DOPE/DOPG (40:30:30) GUVs after incubation with 10 µM CF-labeled sC18 variants for 30 min **(A)**. As control, untreated GUVs were used. Means ± standard deviation (s. d.) of more than 10 GUVs are shown. CF release from neutral and anionic LUVs over time after peptide addition (1 µM) **(B)**. The results of CF-release experiments are representative of three independent preparations of LUVs. Experiments were conducted in duplicate with *n = 2*.

Judged from microscopical observation, no noticeable decrease in Oyster 405 signal was observed using neutral vesicles which could be further confirmed by CF-leakage experiments revealing no peptide-induced CF release (left panels, Figure 19A and B). Meaning that the membrane integrity was not affected by addition of peptide conjugates. However, in case of negatively charged model membranes, the effect of both linear and branched dimeric sC18 conjugates was remarkable compared to the parent monomeric versions (right panels, Figure 19A and B). Thus, the leakage rate was strikingly higher which was more obvious for CF-release experiments (right panel, Figure 19B). Here, the peptides led to a very fast leakage of CF that occurred in a matter of few minutes and saturated after about 1 h, indicating strong interactions with anionic membranes, which presumably triggered pore formation events. Meanwhile, the monomeric control peptides caused only negligible (below 10%) CF release, although the peptides bound to anionic membranes.

However, these results suggest that the dimeric peptides significantly perturbed the membrane integrity in the presence of anionic lipids (DOPG) accompanied by strong membrane accumulations, which agree with microscopic observations and moreover with the literature [68, 77, 86]. Furthermore, since the peptide conjugates were not able to

interact with neutral model membranes, our data corroborates further the importance of negatively charged components at the outer leaflet of plasma membranes.

The impact of membrane fluidity on peptide-membrane interactions

In a next step, sphingomyelin (SM) and cholesterol (Chol) were introduced to a negatively charged lipid composition (DOPC/DOPG). This was done not only because mammalian plasma membranes consist of these, but also to elucidate the effect of membrane fluidity on peptides interaction loci within the membrane, since the addition of SM and Chol resulted in a more tightly packed, cholesterol and sphingomyelin-rich liquid-ordered phase (L_o), also referred to as lipid rafts [49].

Therefore, DOPC/DOPG/SM/Chol (20:20:40:20) GUVs containing Oyster 405 were prepared and treated with 10 µM CF-labeled peptide conjugates for 30 min followed by the assessment of peptide accumulation using fluorescence microscopy. To visualize the effect of phase separation on peptide-membrane interaction, 0.2 mol% DiI, a dye that has been reported to distribute preferentially into the loosely packed, more dynamic liquid-disordered (L_d) lipid phase [15], was incorporated.

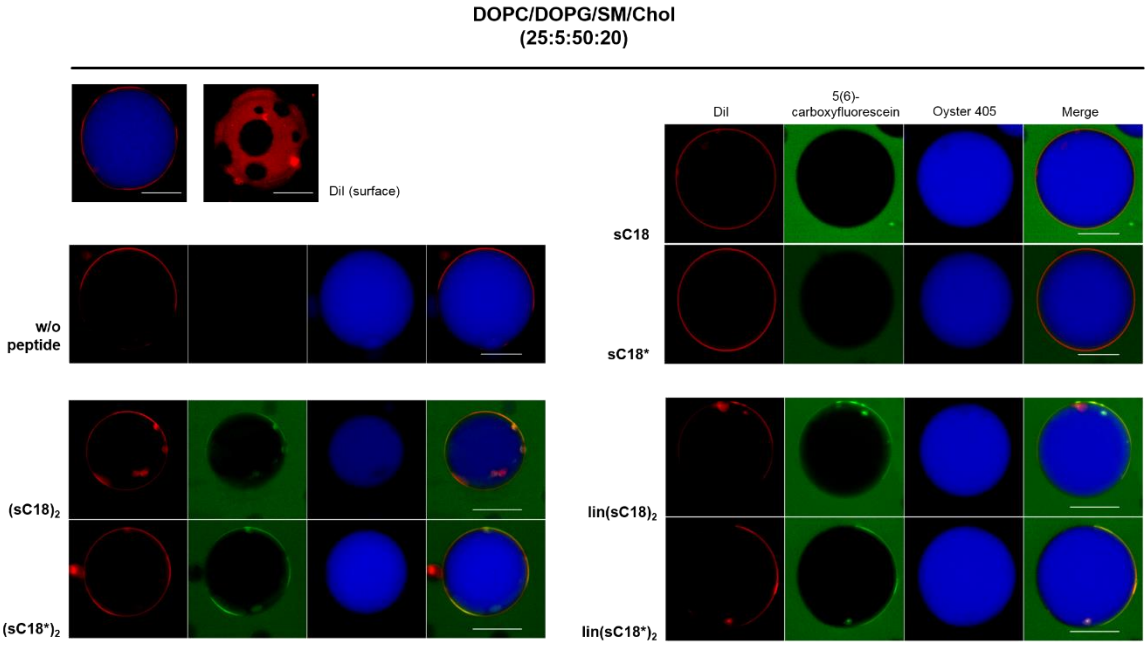

Figure 20. CLSM analysis of GUVs composed of DOPC/DOPG/SM/Chol (25:5:50:20) treated with sC18 conjugates. GUVs loaded with Oyster 405 were incubated with 5(6)-carboxyfluorescein labeled sC18 conjugates (10 µM) for 30 min and analyzed by fluorescence microscopy. 5(6)-carboxyfluorescein labeled peptide (green) and Oyster405 dye (blue). All GUVs contain 0.2 mol% DiI as L_d phase marker (red), which was also regarded as lipid marker in this experiment. Scale bars, 30 µm.

As shown in red channels of Figure 20, DOPC/DOPG/SM/Chol vesicles revealed distinct phase separations, which become more evident focusing on the GUV surface. Thus, the black areas within the membrane represent the more tightly packed, cholesterol and

sphingomyelin-rich liquid-ordered phase, while the more dynamic L_d phase is labeled by incorporation of the DiI dye (red areas in Figure 20).

Interestingly, under the conditions used in this experiment, the monomeric peptides did not accumulate on the membranes, while the addition of dimeric versions resulted in strong peptide signals, which were not homogenously distributed along the membranes. In particular, the green fluorescence of the linear dimers seemed to co-localize well with those of the DiI dye suggesting that these peptides preferentially interact with membrane domains of a more dynamic and less densely packed nature. These results are indeed in line with previous reports revealing the preference for membrane-affine CPPs with liquid-disordered phases [156, 209]. However, for $(sC18)_2$ and $(sC18^*)_2$, no obvious phase preference could be found. Instead, the peptide signal was unevenly distributed on both L_o- and L_d phases. Nevertheless, the overall higher membrane affinity of the dimeric conjugates might be related, on the one hand, to the enhanced amphipathic properties of dimeric conjugates compared to the monomeric ones [210]. The linear dimers in particular adopt a nearly perfect α-helical structure separating charged and non-charged residues into an amphipathic structure, which might be accountable for the increased membrane affinity [68]. On the other hand, several studies have suggested that the presence of at least six arginine residues in the structure is necessary for efficient cellular uptake [59, 133, 198].

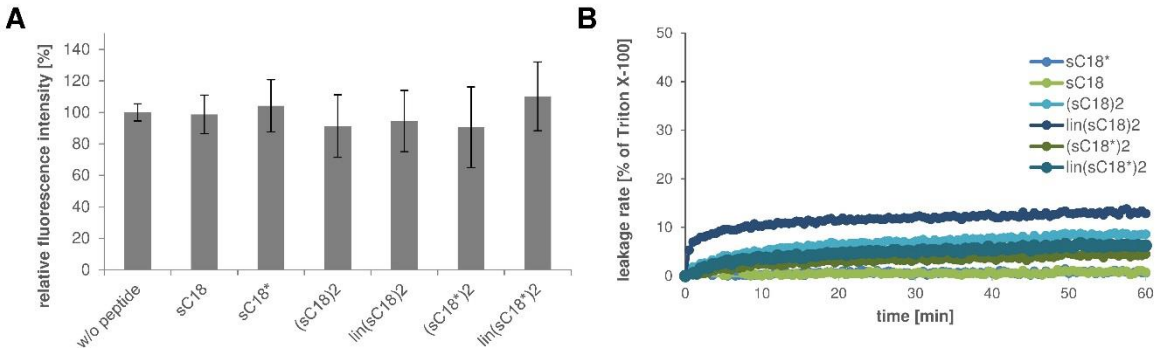

Figure 21. Peptide-induced leakage from DOPC/DOPG/SM/Chol (25:5:50:20) model membranes treated with sC18 conjugates. The relative fluorescence intensities of the enclosed Oyster 405 dye in DOPC/DOPG/SM/Chol (25:5:20:20) GUVs after incubation of 30 min with 10 µM CF-labeled sC18 variants **(A)**. As control, untreated GUVs were used. Means ± standard deviation (s. d.) of more than 10 GUVs are shown. CF release from LUVs mimicking mammalian plasma membrane over time after peptide addition (1 µM) **(B)**. The results of CF-release experiments are representative of three independent preparations of LUVs. Experiments were conducted in duplicate with *n = 2*.

Focused further on the encapsulated fluorescent dye within the GUVs (Figure 21A), no dramatic decrease in Oyster 405 signal was observed for all peptides, despite peptide binding. Similar results were obtained when CF-entrapped LUVs were treated with peptide conjugates for 60 min indicating that in the presence of SM and Chol, the membrane destabilization effect of peptides, as observed for anionic model systems, was significantly impaired. In this context, a previous study by Katayama *et al.* demonstrated that the addition

of cholesterol in GUV membranes prevented the leakage of an encapsulated fluorescent dye [91]. Moreover, Säälik *et al.* reported on an increase in penetration efficiency of CPPs of different subclasses into cholesterol-depleted giant plasma membrane vesicles. This provoked the assumption that since Chol has been demonstrated to be crucial for the formation of the L_o phase [49, 168], it could indeed hinder the internalization of CPPs and therefore the efflux of an entrapped dye [156]. Thus, this could be an explanation that no significant release of the GUV and LUV-encapsulated fluorescent dye could be observed (Figure 21).

However, as a result of this observation, it was questioned whether Chol is indeed responsible for the impaired leakage rate or whether the presence of the so-called lipid raft domain in general is accountable. Therefore, this purpose was researched in greater detail by preparing GUVs and LUVs composed of DOPC/DOPE/DOPG, which were additionally supplemented either with Chol or SM, and the membrane interaction and integrity was assessed by fluorescence microscopy (Figure 22) and spectroscopy (Figure 23).

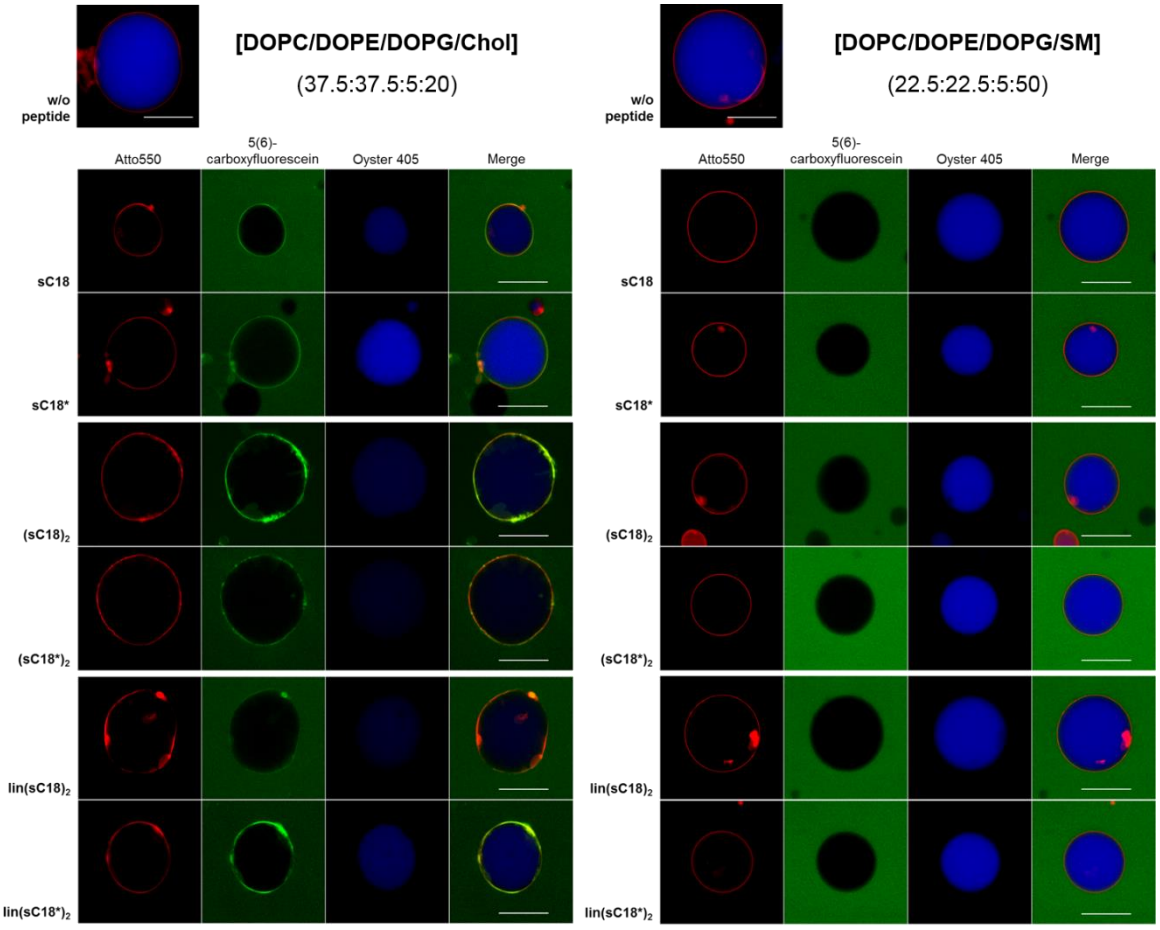

Figure 22. The influence of cholesterol and sphingomyelin on the interaction with model membranes. Microscopic analysis of GUVs composed of DOPC/DOPE/DOPG/Chol (37.5:37.5:5:20) and DOPC/DOPE/DOPG/SM (22.5:22.5:5:50) treated with various sC18 conjugates (10 µM) for 30 min and analyzed by CLSM. All GUVs contain 0.2 mol% Atto550-DOPE as lipid marker and were additionally loaded with 5 µM of the blue fluorescent dye Oyster 405. Scale bars, 30 µm.

As shown in the left panels of Figure 22, all peptides bound with a strong affinity to GUV membranes supplemented with Chol which was surprising, since these observations differ from that reported by others [91, 156]. Furthermore, only minor Oyster 405 signals remained inside the GUVs after 30 min of peptide incubation indicating remarkable impacts of peptide conjugates on the membrane integrity, presumably through pore forming events. As comparison, while adding SM to DOPC/DOPE/DOPG vesicles, no accumulation along the membrane could be revealed which was accompanied by no Oyster 405 escape (right panels in Figure 22).

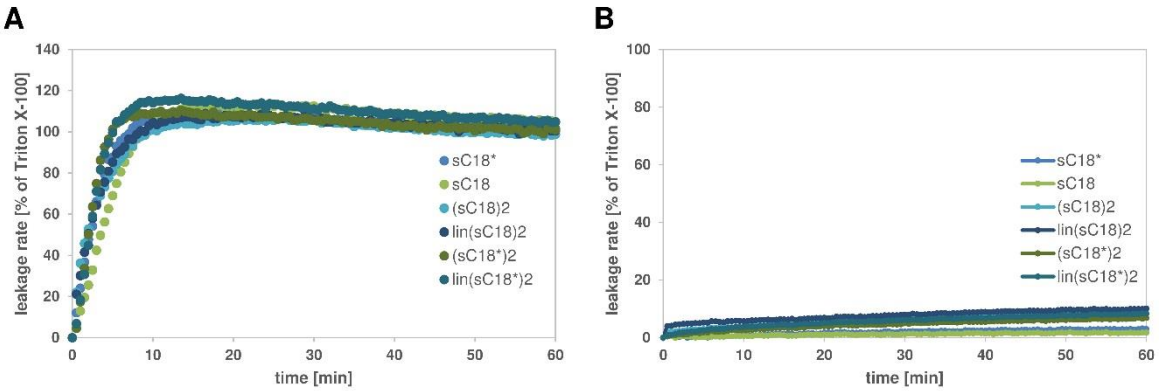

Figure 23. The impact of cholesterol and sphingomyelin on the membrane perturbation activity of sC18 conjugates. CF-leakage experiments from LUVs composed of DOPC/DOPE/DOPG/Chol (37.5:37.5:5:20) **(A)** and DOPC/DOPE/DOPG/SM (22.5:22.5:5:50) **(B)**. Peptides (1 µM) were added to LUVs and the release of CF from vesicles was monitored by measuring the increase in fluorescence intensity. At the end of each experiment, Triton X-100 (0.4% (w/v) final concentration) was applied to measure the maximum of dequenching that was used to normalize data. Experiments were conducted in duplicate with *n = 2*.

Furthermore, a detailed analysis of the influence of Chol and SM on the membrane perturbation activity of these peptides revealed a rapid and complete CF release when Chol LUVs were treated with 1 µM peptide conjugate over a time of 60 min (Figure 23A). While the peptides could not disrupt the membrane in the presence of SM and thus, no CF release from the vesicles could be observed (Figure 23B).

However, the anionic phospholipid DOPG was added only in small amounts (5 mol%) and therefore cannot be responsible for the strong membrane affinity in DOPC/DOPE/DOPG/Chol GUVs and LUVs. Rather, it is assumed that the presence of Chol in the membrane of liposomes contributes to the increased membrane affinity which is accompanied by lytic membrane activity. Interestingly, the presence of SM alone had no impact on membrane interaction and integrity which is in consistence with a previous study by Wallbrecher *et al.* Here, it was reported that the translocation of the well-known CPPs R9 (nona-agrinine) and penetratin into POPC/POPG/Chol GUVs either supplemented with SM or not were not dependent on the presence of SM [195]. Nevertheless, the data let

conclude that in the presence of both membrane components in the vesicles, peptides membrane disruption activity is hampered.

However, considering Chols importance in the formation of L_o domains and in endocytosis and the fact that endocytotic pathway was found to play a dominant role in sC18 and $(sC18)_2$ uptake in HEK-293 cells and to some extent in MCF-7 cells, the next experiments focused on the effect of cholesterol on translocation.

Cholesterol and its effect on peptides cellular uptake efficacy

We looked into the role of L_o domains on CPP internalization in living cells by abolish the formation of lipid rafts. A simple method to avoid these L_o phases is provided by the removal of cholesterol using methyl-β-cyclodextrin (MβCD) [17, 72]. Thus, cholesterol depletion assays were performed, monitored by fluorescence microscopy and finally quantified by flow cytometry (Figure 24).

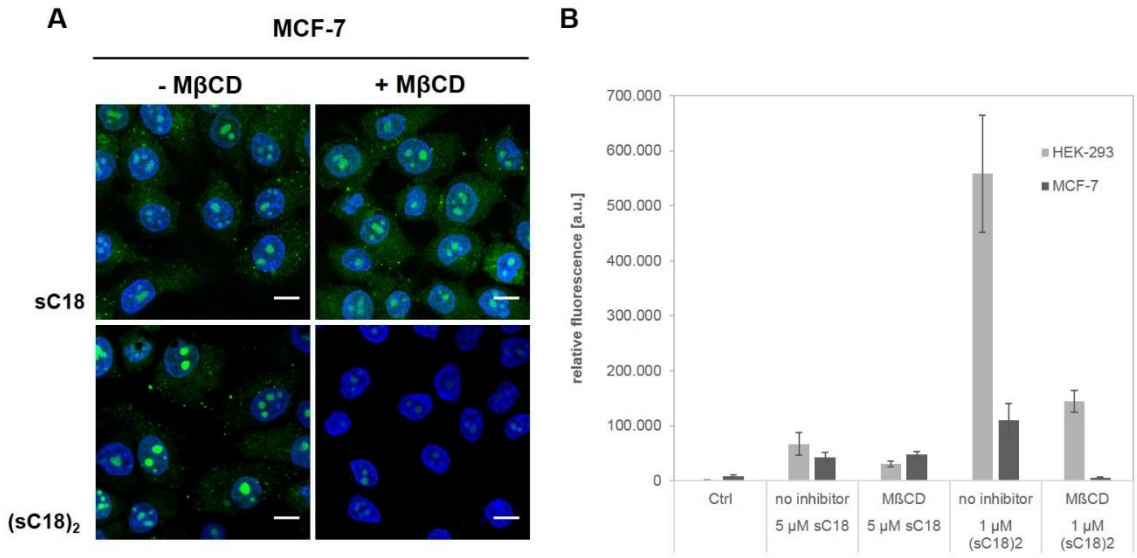

Figure 24. The influence of cholesterol extraction by cyclodextrin treatment on internalization efficiency. MCF-7 and HEK-293 cells were treated with 10 mM methyl-β-cyclodextrin (MβCD) for 1 h and subsequently incubated with 5 µM CF-sC18 or 1 µM CF-(sC18)2 for 30 min at 37 °C. Microscopic analysis of peptide internalization is shown in **(A)**. The peptide is labeled in green and the cell nuclei stained in blue. Scale bars, 10 µm. Quantification by flow cytometry is presented in **(B)**. Experiments were performed in triplicate with *n = 3*.

Herein, the main emphasis is on the branched dimeric version $(sC18)_2$ and the monomeric sC18 control peptide using HEK-293 and MCF-7 cells, respectively. Unfortunately, the experimental set-up for microscopic analysis of HEK-293 cells failed. Consequently, we obtained data only from the quantitative evaluation by flow cytometry.

However, a significant effect of cholesterol extraction on the internalization of sC18 could not be revealed in both the non-cancer cell line and cancer cell line (Figure 24A and B), indicating that cellular uptake and subcellular distribution was not affected. These results

are a bit controversial, since strong membrane interactions with GUVS and LUVs composed of DOPC/DOPE/DOPG/Chol could be observed which were accompanied by peptide-induced CF-leakage. In contrast, MβCD treatment in both HEK-293 and MCF-7 cells reduced the internalization capability of $(sC18)_2$ dramatically and moreover the cytoplasmic fluorescence. As shown in Figure 24A, the peptide was still marginal localized within the nucleus, while no peptide signal was found in the cytosol of MCF-7 cells. From these findings, it was suggested that the uptake of $(sC18)_2$ may also involve the lipid raft-dependent endocytosis, besides direct translocation, since cholesterol depletion is also a method to inhibit this type of endocytotic uptake [16]. Accordingly, the exact pathway of endocytosis used by sC18 could not be identified.

However, the interplay of all these results might indicate that efficient translocation of these cationic peptide conjugates relies on the presence of anionic lipids, such as DOPG, and moreover on the presence of membrane domains with high fluidity, which also appears mandatory for the uptake to occur. Furthermore, in case of the parent control peptide, Chol depletion by MβCD treatment revealed no impact on its internalization capability, while the uptake of the branched dimer $(sC18)_2$ was significantly hampered which lets one assume that the dimeric peptide translocates across the membrane via lipid raft-dependent endocytosis. Since peptide signals in the nucleus were still observed (Figure 24A), which indicates a pathway via direct translocation, these results suggest that the $(sC18)_2$ peptide is internalized by more than one mechanism depending on the composition of the target cell membrane.

The role of other membrane constituents in peptide-membrane interactions

So far, some insights into the interplay of membrane composition and peptide-lipid interactions of branched and linear versions of the cell-penetrating peptide sC18 were provided. However, to go further into detail giant plasma membrane vesicles (GPMVs) were used, which provide a more natural membrane system than LUVs and GUVs, since their membrane composition resembles that of living cells [156, 162].

Therefore, the role of other membrane lipids or proteins in the translocation ability of the peptides was further explored. Here, I established a method of preparing GPMVs from biological cells, in particular from HEK-293 and MCF-7 cells, by chemically induced plasma membrane vesiculation, as already described by Scott, R.E. [162]. To monitor peptides interactions with GMPVs, DiI was selected to label the membranes, while 5(6)-carboxyfluorescein was used to mark peptides as already mentioned. Then, GPMVs were incubated with all sC18 conjugates at 1 µM concentration for 1 h at RT followed by visualization through fluorescence microscopy illustrated in Figure 25.

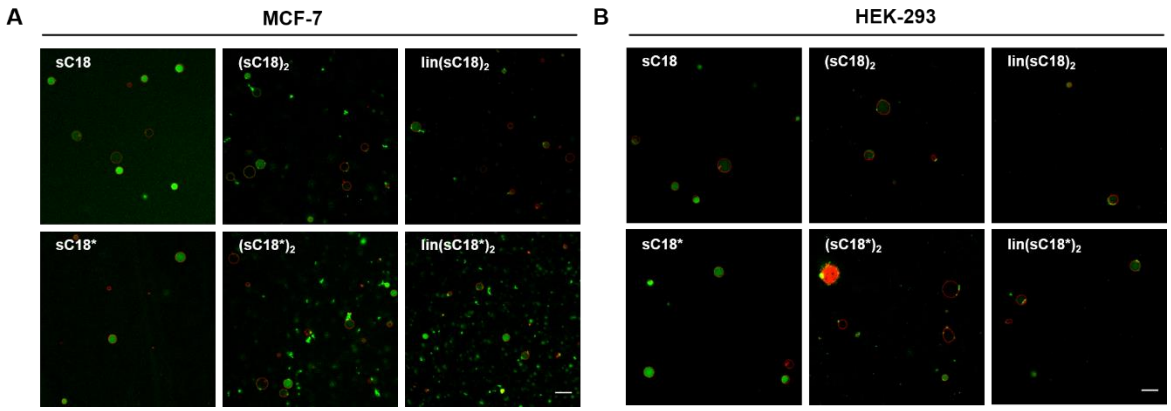

Figure 25. Accumulation of CF-labeled sC18 conjugates into giant plasma membrane vesicles (GPMVs) prepared from both MCF-7 and HEK-293 cells by DTT/formaldehyde treatment. GPMVs were incubated with CF-labeled peptides (green) at 1 µM concentration for 1 h at RT. Membranes were labeled with DiI (red). Scale bars,10 µm.

All peptides were found to internalize and accumulate into GPMVs irrespective of the cell line used. Especially, the branched and linear dimeric sC18* versions strongly interacted with the membrane of MCF-7 derived GPMVs, resulting in vesicle debris depicted in the lower panels of Figure 25A.

However, the strong accumulation of the CF-labeled peptides into the lumen of GMPVs obtained from both MCF-7 and HEK-293 cells compared to GUVs might suggest that some membrane proteins embedded within the vesicle membrane could specifically increase the peptide uptake across the cell membrane, but this requires further investigations.

Nonetheless, this data shed new lights on the relevance of membrane compositions for the internalization mechanism of these peptides and moreover allowed us to identify some membrane properties, which are mandatory for efficient translocation.

Cyclic peptides

By now, many publications exist demonstrating that structural modifications of cell-penetrating peptides contributed positively to their cellular penetration features [115, 185, 198]. In particular, the use of cyclized peptides becomes increasingly attractive as promising delivery vectors, since backbone rigidification of CPPs leads to improved cellular uptake and proteolytic stability over its linear and more flexible counterpart [77, 104, 133].

Indeed, we showed recently that cyclization of the truncated version sC18*, which resulted in three cyclic peptide derivatives varying in ring size and thus in the number of arginines included, leads to improved cell-penetrating properties, concerning proteolytic stability and translocation activity (for sequences refer to Table 9 and Figure 26) [77]. In more detail, we assumed that the enhanced distance between the guanidinium groups in the large cycle (cyc3) through cyclization of the peptide backbone and further introduction of a triazole

bridge leads to the enhanced cellular uptake over the smaller cycles and the linear counterpart.

Thus, our data are consistent with previous studies, which reported that increased rigidity and the static display of guanidinium groups enhances the membrane contact and thus cellular penetration [77, 104, 185, 199]. Moreover, a study by Traboulsi *et al.* suggests that higher uptake rates of cyclic peptides are correlated with the increasing number of arginine residues within the cycle [185]. Consequently, it is supposed that the arginine residues are crucial for efficient cellular uptake due to the role attributed to their ability to interact with negatively charged components of the plasma membrane, e.g. the polar headgroups of phospholipids or the sulfate groups of glycosaminoglycans [30, 53].

Hence, since the uptake of CPPs has been attributed to the ability to engage in electrostatic interactions with the negatively charged constituents of the plasma membrane, artificial membrane systems lacking energy-driven processes were employed to shed light on the molecular level of cyclic peptides cell entry.

Therefore, based on the truncated version sC18*, three cyclic peptides (cyc1 – cyc3), that varied in ring size and thus in the number of arginine residues included, were designed and finally synthesized by our working group (Table 9 and Figure 26). To allow selective side-chain cyclization via copper (I) mediated alkyne-azide click (CuAAC) chemistry, glycine and lysine were substituted by propargylglycine and aziodlysine, respectively. Furthermore, to address the impact of cyclization on peptide-membrane interactions, the corresponding linear counterpart sC18* was synthesized as control.

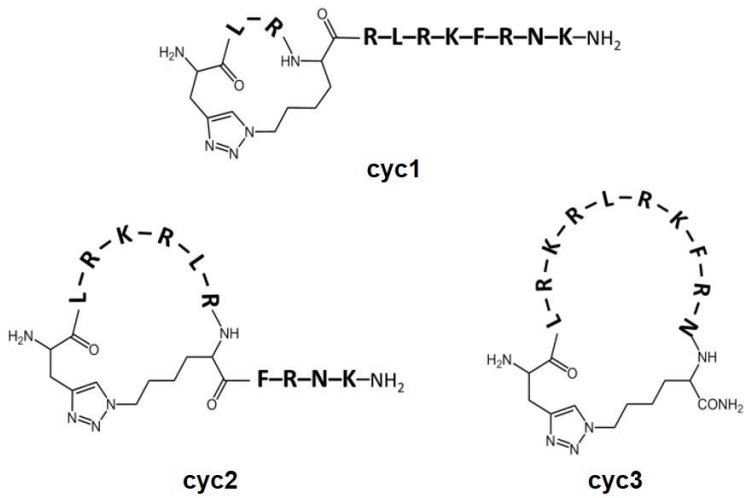

Figure 26. Structures of cyclized peptides. Cyclization was achieved by the CuAAC reaction connecting residues 1 + 4 **(cyc1)**, 1 + 8 **(cyc2)** and 1 + 12 **(cyc3)** of the linear peptide (^{1}GLRKRLRKFRNK^{12}).

So far, the uptake mechanism of these cyclic peptides was found to be energy-independent in cancer cells (MCF-7), while endocytosis was confirmed as main entry pathway in the non-cancer cell line HEK-293, since the cellular efficiency was significantly diminished at 4 °C

[77]. Moreover, first insights into peptide/lipid interactions were already gathered using giant unilamellar vesicles (GUVs) as artificial membrane system. Our findings highlighted a considerably strong accumulation of the different sized cycles on anionic GUV membranes, which is interesting considering that the outer leaflet of cancer cells have been shown to be primary anionic [85].

However, the secondary structure formation of CPPs might play a major role in stabilizing their interactions with membranes and thus promoting cellular uptake [50, 77]. Therefore, the ability of these peptides to adopt an ordered secondary structure, at least in a membrane mimetic environment, is indispensable.

Structural characterization of cyclic peptides in the presence of vesicles

For this purpose, circular dichroism spectroscopy was used to analyze the structural state of the cyclized peptides in the presence of neutral and negatively charged large unilamellar vesicles (LUVs).

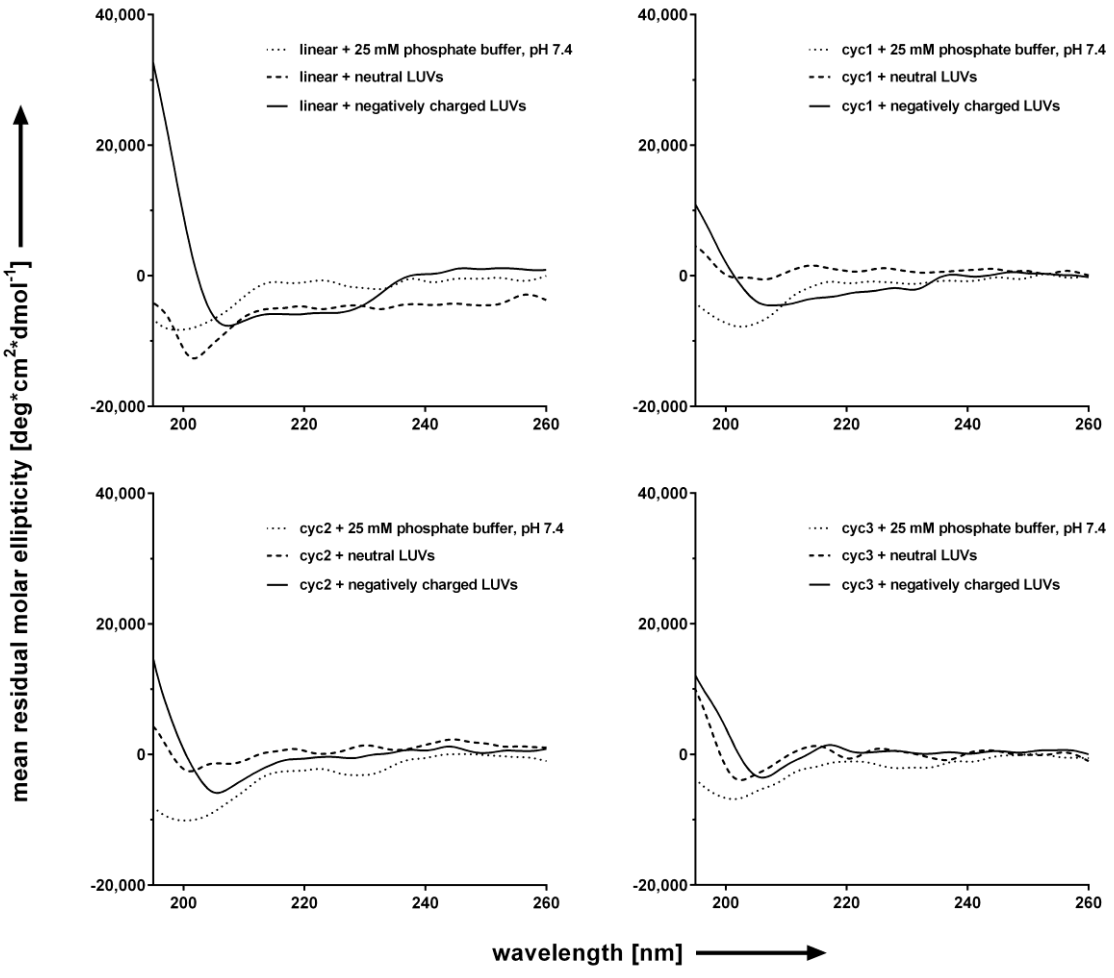

Figure 27. Circular dichroism spectra of 20 µM 5(6)-carboxyfluorescein labeled cyclic peptides (cyc1 – cyc3) and linear precursor peptide sC18* in 25 mM phosphate buffer, pH 7.4 and in presence of neutral and anionic LUVs at a P/L ratio of 1/50.

As shown in Figure 27, all peptides revealed an unstructured conformation in phosphate buffer. Despite it has been reported that cyclic peptides might be conformationally stabilized by a 1,4 disubstituted 1,2,3-triazole bridge [28, 77], the present observations did not match with any secondary structure motif. Nevertheless, similar results were obtained in the presence of neutral vesicles and thus, the secondary structures did not change noticeably. However, in the presence of anionic lipids, the peptides became more structured; particularly the small-sized cycle cyc1 and the linear version might be highly influenced when incubated with negatively charged LUVs. Therefore, our data suggest that only cyc1 and the linear version underwent a conformational transition from a random coil to a well-defined secondary structure. This is not surprising since the *C*-terminal linear part of cyc2 consists of only four amino acids which are indeed not able to form an appropriate secondary structure and cyc3 consists of no linear part.

However, since strong interactions of cyc3 with anionic GUV membranes were observed, but no secondary structural motif, it was assumed that at least the guanidinium groups are forced into maximally distant positions leading to a stabilizing effect and thus a better peptide-membrane interplay, which might help to improve membrane integration and finally penetration.

Membrane binding affinity and perturbation activity of cyclic peptides in the presence of vesicles

Therefore, taking a closer look, the membrane binding affinity and the membrane perturbation effect of the peptides were investigated using neutral and anionic large unilamellar vesicles (LUVs) shown in Figure 28.

First, the focus was on the membrane binding affinity of CF-labeled cyclic peptides as well as sC18* examined by flow cytometric analysis (Figure 28A).

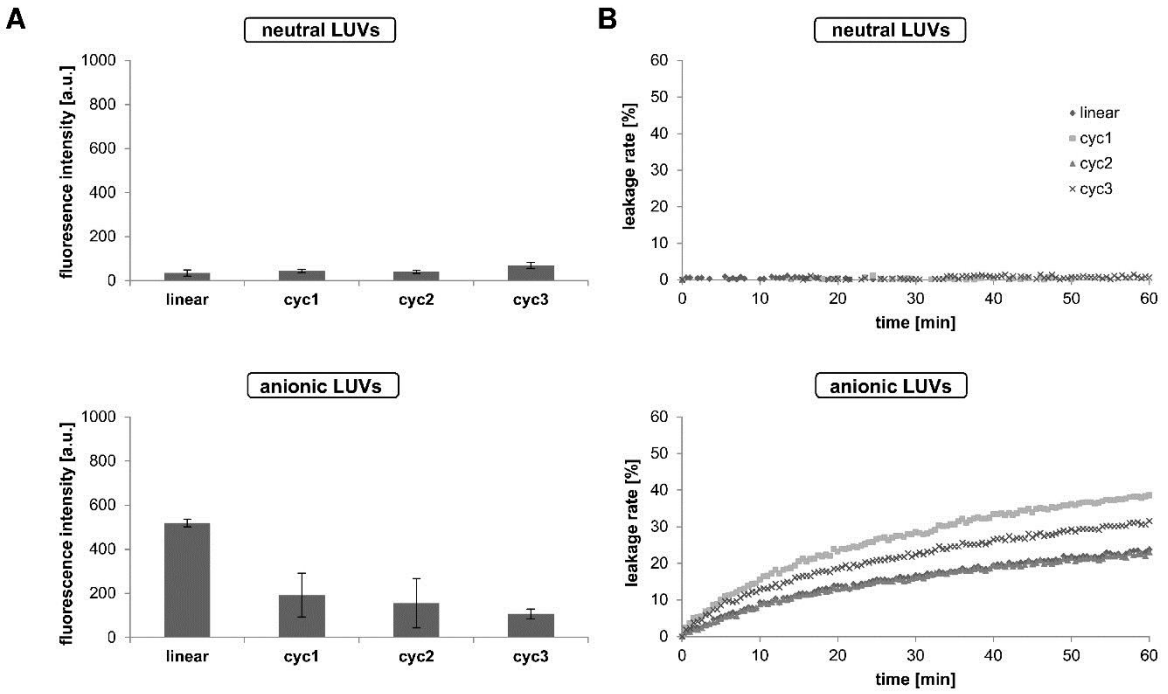

Figure 28. Binding affinities and peptides effect on membrane destabilization using neutral and anionic LUVs. Flow cytometric binding studies of CF-labeled peptides (10 µM) with neutral and anionic LUVs after 2 h of incubation **(A)**. Experiments were conducted in duplicate with *n = 3*. Error bars represent the standard deviation. Time course of peptide-induced (20 µM) CF release from neutral and anionic LUVs **(B)**. The results of CF-release experiments are representative of three independent preparations of LUVs.

Obviously, an overall stronger accumulation was detected when peptides were incubated with negatively charged LUVs contrary to neutral LUVs (Figure 28A), which correlates well with our findings on giant unilamellar vesicles. However, the overall measured fluorescence of the cyclic peptides was only moderate when compared to the linear version.

To investigate the possibility whether the peptide/lipid interaction causes alterations of the membrane integrity, 5(6)-carboxyfluorescein release experiments were performed as shown in Figure 28B. Therefore, LUVs composed of DOPC, DOPE (1:1) and DOPC, DOPE and DOPG (4:3:3) were employed and incubated with peptides at a P/L ratio of 1/50. The extent of CF-leakage from the vesicles induced by peptides was assessed over 60 min by monitoring increased fluorescence from the released fluorophore. As indicated in Figure 28B, none of the peptides caused release of the entrapped fluorophore from neutral LUVs which is consistent with their inability to interact with zwitterionic membranes as determined by flow cytometric binding studies (Figure 28A). Consequently, these data let conclude that interactions of the cationic peptides with neutral LUVs are weakened due to repulsion between the cationic peptides and positively charged head groups of DOPC and DOPE. This assumption is in accordance with Gopal *et al.*, who reported on weakened interactions of positively charged peptides with vesicles mimicking eukaryotic membranes due to repulsion [64]. However, in presence of anionic lipids, all peptides caused fast and efficient

release of up to 40% of total CF after 60 min of incubation. Strikingly, even though the binding affinity of the linear peptide towards the negatively charged LUV membranes was dramatically increased, the membrane activity of cyc1 and cyc3 was still significantly higher compared to the linear counterpart, which might suggest different modes of actions or different behavior during the translocation process. Therefore, it is quite possible that the mechanism of non-endocytotic entry, as observed for cyclic peptides in cancer cells, is related to the ability to cause localized destabilization of the plasma membrane since the membrane perturbation effect of cyc1 and cyc3 was remarkable.

The impact of PI(4,5)P_2 on peptide binding

Further mechanistic investigation was conducted to determine the influence of the negatively charged phosphatidylinositol-(4,5)-bisphosphate (PI(4,5)P_2) on peptide binding. Although, PI(4,5)P_2 is only a minor component of the plasma membrane, localized on the cytoplasmic leaflet, it plays a major role as crucial regulator of various cellular processes including cell signaling, cytoskeleton organization as well as protein and membrane trafficking [161, 179]. Since PI(4,5)P_2 is also known to be essential for a number of steps along the endocytotic pathway [38, 177], it was further interesting to shed light on the mechanistic process of endocytosis considering that this mechanism was supposed to be the main pathway of cyclized peptides in non-cancer cells.

Thus, LUVs composed of DOPC as neutral lipid additionally supplemented with different mol% of PI(4,5)P_2, kindly provided by Marcel Zeitler (group member of working group of Prof. Dr. Walter Nickel, BZH Heidelberg), were employed to assess the binding affinity of cyclic conjugates using flow cytometric technique (Figure 29A). Furthermore, LUVs loaded with CF were used in order to address whether the cyclic CPPs could disrupt the membrane and thus causing the release of CF from the vesicles (Figure 29B).

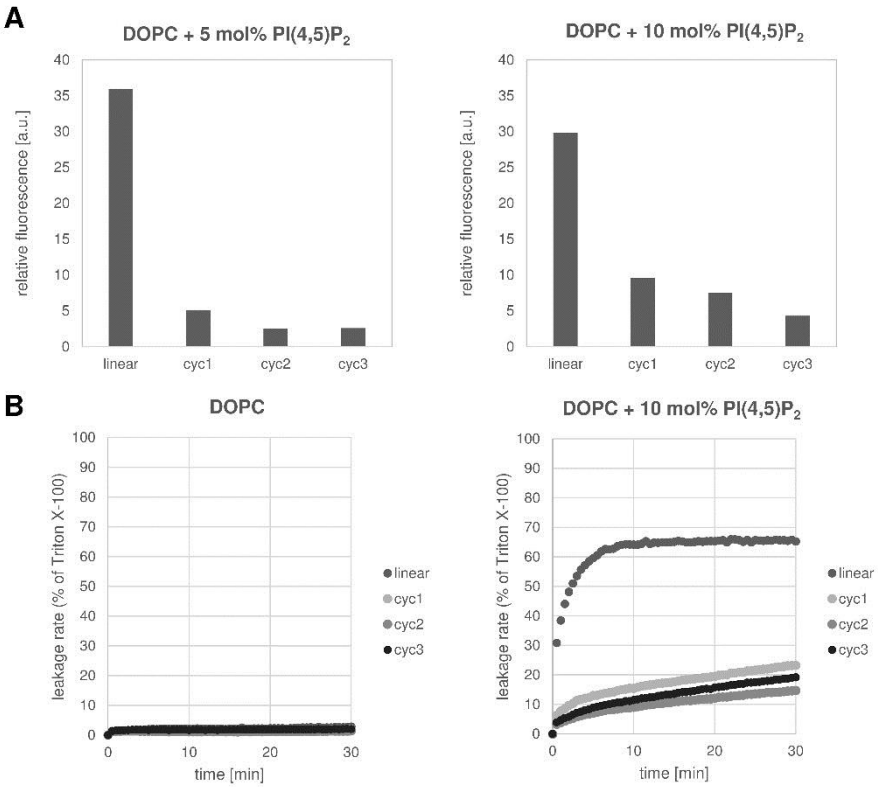

Figure 29. The influence of PI(4,5)P_2 on binding affinities and membrane destabilizing activity using large unilamellar vesicles. Flow cytometric binding studies of CF-labeled peptides (2.5 µM) after 2 h of incubation with neutral LUVs supplemented with 5 mol% and 10 mol% PI(4,5)P_2, respectively. **(A)**. Experiments were conducted in triplicate with *n = 1*. Time course of peptide-induced (1 µM) CF release from neutral LUVs and DOPC vesicles supplemented with 10 mol% PI(4,5)P_2 **(B)**. These experiments were performed in cooperation with working group of Prof. Dr. Walter Nickel, BZH Heidelberg.

As shown in Figure 29A, especially the linear peptide demonstrated high binding affinity to LUV membranes composed of phosphatidylcholine (DOPC) and 5, or 10 mol% PI(4,5)P_2, whereas cyc1-3 showed decreased levels of accumulation depending on their ring size small < large. Moreover, the membrane destabilizing effect of the linear counterpart was also more evident and thus, sC18* was able to induce a significant dye release from LUVs supplemented with 10 mol% PI(4,5)P_2, which is in consistent with the strong membrane binding affinity (Figure 29A). On the contrary, the incubation with cyclic peptides resulted in 15 – 25% CF release over a 30 min time period (Figure 29B). However, not one of the peptides caused a sufficient dye release in neutral LUVs, which is in good agreement with the results obtained with LUVs composed of DOPC and DOPE (Figure 28B).

These results strongly suggest that the linear peptide binds tightly to PI(4,5)P_2 which was accompanied by membrane perturbation, while the binding affinity of cyclic peptides is not that pronounced. However, since it is known that peptides behavior depends highly on the peptide concentration as well [111], the low peptide concentration used during the experiments should be taken into account. Nevertheless, all these observations further

provide evidence for different lipid/peptide interactions and peptide membrane integration depending on lipid composition and peptide used.

Moreover, these findings might provide an indication that the linear peptide can escape from endosomes more efficient, since the binding affinity towards $PI(4,5)P_2$ was shown to be noticeable. In contrast, the weak binding of cyclic peptides might be related to the preferential uptake route via direct translocation and therefore, the binding affinity towards $PI(4,5)P_2$ was not that strong. However, to better understand the peptide structure-membrane-binding relationship, further investigations are necessary.

The influence of further membrane constituents on peptide-membrane interactions

In a last experiment, further mechanistic studies using giant plasma membrane vesicles, representing a more natural membrane model, were performed to elucidate in more detail how cells plasma membrane constituents affect peptides cell entry in conditions lacking endocytosis.

Therefore, giant plasma membrane vesicles made of HEK-293 and MCF-7 cells were investigated in presence of fluorescently labeled peptide variants using fluorescence microscopy (Figure 30).

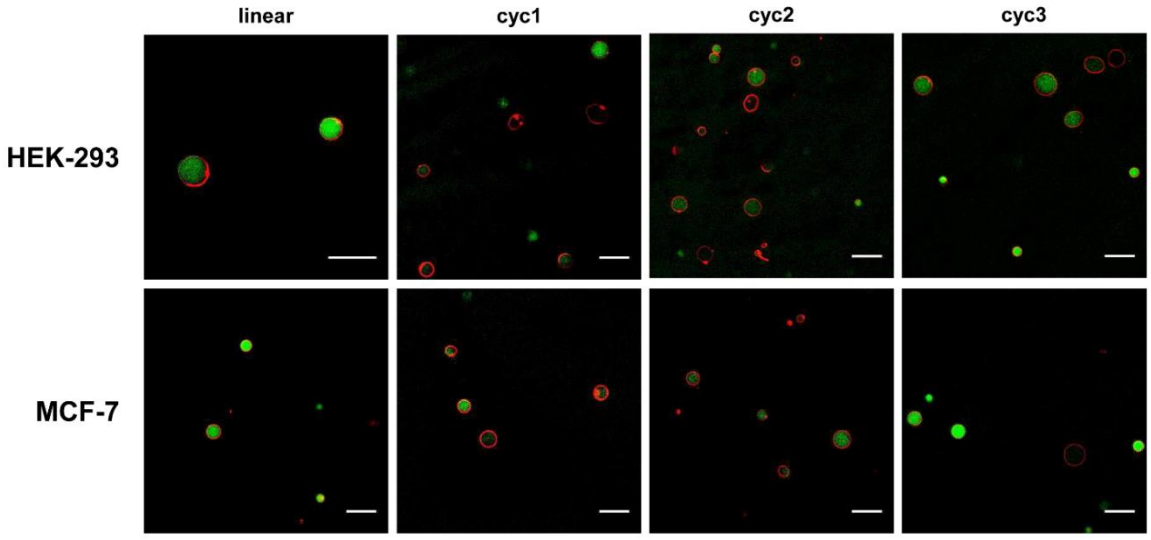

Figure 30. Accumulation of CF-labeled peptides into giant plasma membrane vesicles (GPMVs) prepared from both HEK-293 and MCF-7 cells by DTT/formaldehyde treatment. GPMVs were incubated with CF-labeled peptides (green) at 1 µM concentration for 1 h at RT. Membranes were labeled with DiI (red). Scale bars, 10 µm.

As shown in Figure 30, all peptides were found to efficiently interact with GPMV membranes and translocate into GPMVs. The intensity of the internalization activity increases in the order cyc1 < cyc2 < cyc3 = linear. However, no differences in the uptake profile could be observed when incubating the peptides with GPMVs obtained from either HEK-293 or MCF- 7 cells. Though, considering that an endocytic uptake route for cyclic peptides in

HEK-293 cells was proposed, these findings might provide an indication that other direct translocation pathways are used when intact machinery responsible for endocytosis is not working properly, since strong signals within the vesicles were detected.

Finally, our results obtained from model membrane studies confirm on the one hand that the presence of negatively charged lipids such as DOPG or PI(4,5)P_2 are indeed essential to trigger the peptide-membrane interaction of cationic CPPs [35, 181]. On the other hand, it has been suggested that the presence of the larger dipole moment provided by the triazole bridge positively influenced the membrane integrity of cyclic peptide and thus related to the stronger membrane activity observed in anionic LUVs. However, the different modes of lipid interaction of the peptides might further indicate different uptake mechanisms, which should be further investigated.

Nevertheless, the great uptake efficiencies, accompanied by superior serum stability over the linear counterpart, non-cytotoxicity, and synthetic accessibility, renders particularly the large-sized cycle as a useful transporter for e.g. plasmid DNA [77].

4.2 Cell-penetrating peptide conjugate with wound healing promoting activity

4.2.1 Design of peptides and peptide synthesis

The aim of this part of the thesis was to synthesize chimeric peptide conjugates consisting of a wound healing promoting peptide sequence, namely Tylotoin, and a cell-penetrating peptide followed by elucidation of their structural characteristics and biological activity (Figure 31).

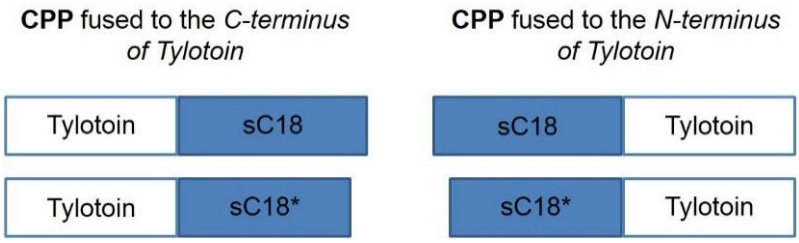

Figure 31. Design of chimeric peptide conjugates. The cell-penetrating peptide sC18/sC18* is either conjugated to the *C*-terminus or the *N*-terminus of Tylotoin.

The cell-penetrating peptides used in this part were the sC18 peptide, derived from the *C*-terminal domain of the cationic antimicrobial peptide CAP18 [130] and a truncated version lacking four amino acids from the *C*-terminal part [77], namely sC18* still showing cell-penetrating properties. The CPP was then either fused to the *C*-terminus or *N*-terminus of Tylotoin, a short peptide identified from salamander skin of *Tylototriton verrucosus* (Figure 31) [126].

Recently, this peptide was found by Mu *et al.* [126] to exert the ability to promote wound healing similar to the epidermal growth factor (EGF), a polypeptide playing an essential role in mammalian wound healing [67, 73]. Tylotoin has the capability to enhance both the migration and proliferation of fibroblasts, keratinocytes and vascular endothelial cells, resulting in accelerated re-epithelialization and granulation tissue formation in the wound site [126]. Moreover, Mu *et al.* showed that Tylotoin also promotes the release of transforming growth factor β1 and interleukin 6 (IL-6), which are essential key regulators in the wound healing process [126].

The goal of this chapter was to combine both peptides and thus create a more efficient peptide conjugate with improved wound healing efficacy and uptake efficiency that can be easily synthesized by solid phase peptide synthesis techniques and might be in future used as potent topical agent in wound treatment.

Table 10. Names, sequences and analytical data of peptides. All peptides are amidated at the *C*-terminus and *N*-terminally labeled with 5(6)-carboxyfluorescein.

Peptide	Sequence	Origin	$MW_{calc.}$ [Da]	$MW_{exp.}$ [Da]	Yield [%]	Net charge
sC18	GLRKRLRKFRNKIKEK	Rabbit cathelicidin	2069.6	2070.47	36	+9
sC18*	GLRKRLRKFRNK	Rabbit cathelicidin	1570.96	1571.44	29	+8
Tylotoin	KCVRQNNKRVCK	Skin of salamanders	1474.81	1474.55	66	+6
rTylotoin	RNCVKKNCRVKQ	-	1474.81	1474.88	76	+6
Tylotoin-sC18	KCVRQNNKRVCKGLRKRLRKFRNKIKEK	synthetic	3527.33	3527.57	74	+14
Tylotoin-sC18*	KCVRQNNKRVCKGLRKRLRKFRNK	synthetic	3028.71	3028.80	23	+13
sC18-Tylotoin	GLRKRLRKFRNKIKEKKCVRQNNKRVCK	synthetic	3527.33	3528.40	46	+14
sC18*-Tylotoin	GLRKRLRKFRNKKCVRQNNKRVCK	synthetic	3028.71	3029.39	56	+13

The peptides used in this part were synthesized by automated solid phase peptide synthesis following Fmoc/*t*-Bu-strategy. Peptide sequences and analytical characteristics are presented in Table 10. Additionally, all peptides were *N*-terminally labeled with the fluorophore 5(6)-carboxyfluorescein for later fluorescence studies. Peptides were obtained in high purity as analyzed by analytical RP-HPLC and their identity was confirmed by electrospray ionization mass spectrometry. An exemplary HPLC chromatogram and ESI-MS spectrum of purified Tylotoin-sC18* is shown in Figure 32.

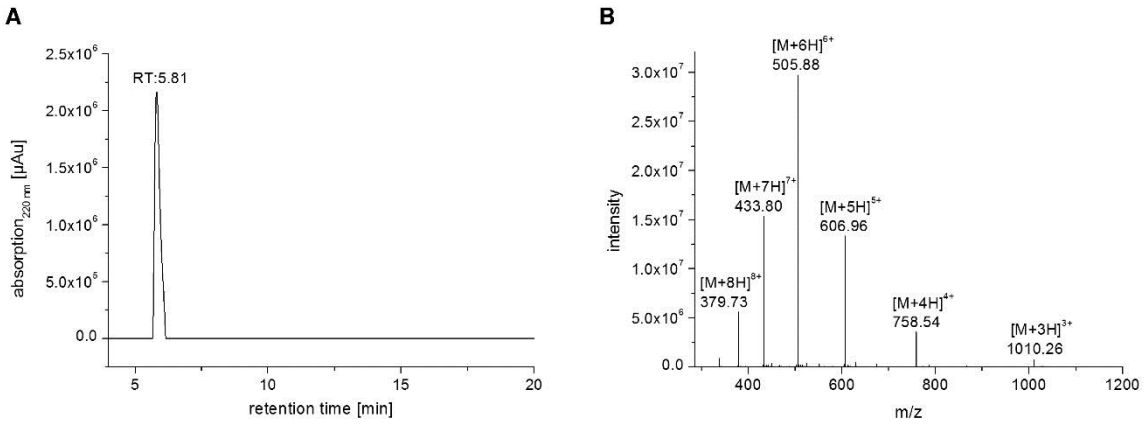

Figure 32. Chromatogram and ESI-MS of purified Tylotoin-sC18* obtained after preparative HPLC. The gradient was 5 – 55% acetonitrile in water (incl. 0.1% FA) over 15 min and the standard was subtracted. UV-chromatogram of Tylotoin-sC18* **(A)**. The peptide elutes at a retention time of 5.81 min. The corresponding mass-to-charge ratios are depicted in ESI-MS spectrum **(B)**. calculated molecular weight 3028.71 Da, charged molecular ions found; ($[M+3H]^{3+}$ = 1010.26; $[M+4H]^{4+}$ = 758.54; $[M+5H]^{5+}$ = 606.96; $[M+6H]^{6+}$ = 505.88; $[M+7H]^{7+}$ = 444.80; $[M+8H]^{8+}$ = 379.73).

The UV-chromatogram (Figure 32A) shows a main peak at a retention time of 5.81 min and the respective charged molecular ions are depicted in the ESI-MS spectrum (Figure 32B). The ESI-MS spectrum shows the 3-fold to 8-fold charged molecular ions corresponding to the peptide mass of Tylotoin-sC18* ($MW_{calc.}$ = 3028.71 Da). Thus, the mass-to-charge ratio (m/z) was found to be nearly identical to the theoretical m/z and the peptide was obtained in high purity as indicated in UV-chromatogram.

Structural characteristics

First, to get some insights into the structural arrangements of the chimeric peptide conjugates and the parent peptides, the secondary structure was determined using circular dichroism spectroscopy (Figure 33).

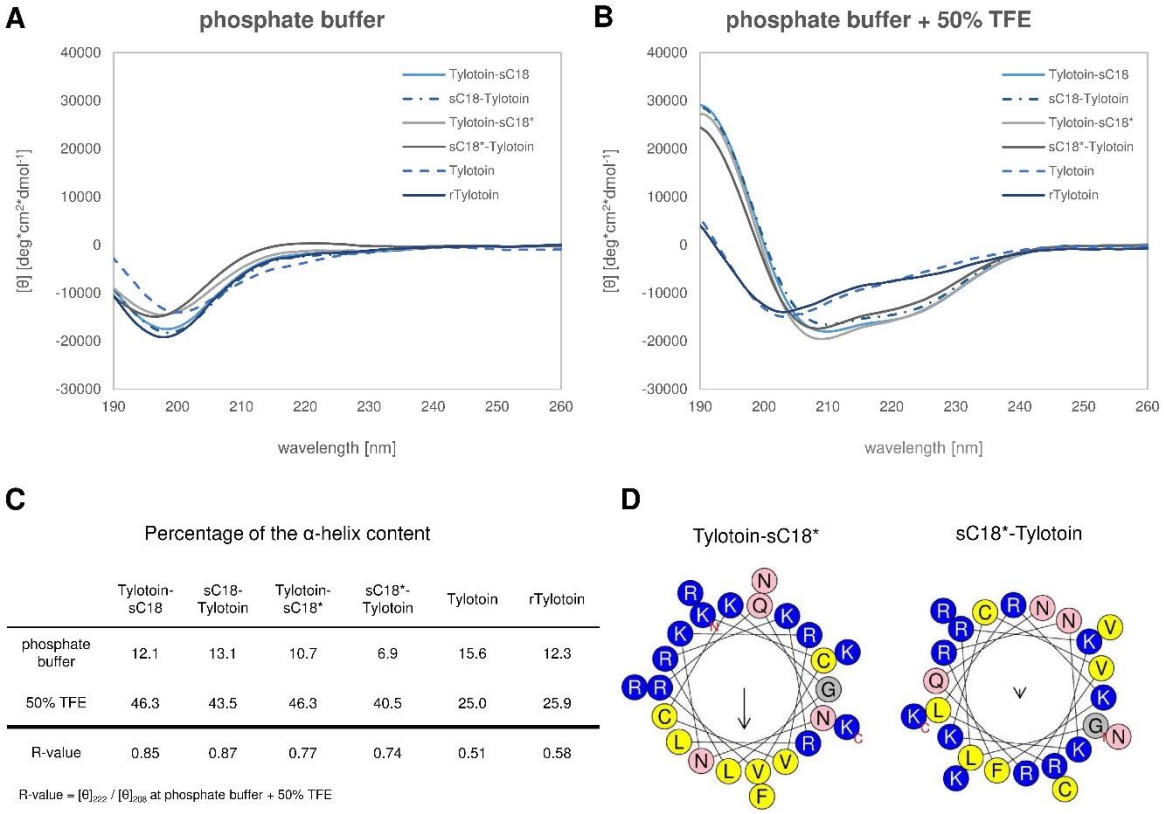

	Tylotoin-sC18	sC18-Tylotoin	Tylotoin-sC18*	sC18*-Tylotoin	Tylotoin	rTylotoin
phosphate buffer	12.1	13.1	10.7	6.9	15.6	12.3
50% TFE	46.3	43.5	46.3	40.5	25.0	25.9
R-value	0.85	0.87	0.77	0.74	0.51	0.58

R-value = $[\theta]_{222}$ / $[\theta]_{208}$ at phosphate buffer + 50% TFE

Figure 33. Structural characteristics of investigated peptides. CD spectra were acquired at a peptide concentration of 20 µM in 10 mM phosphate buffer, pH 7.0 **(A)** and in the additional presence of 50% TFE **(B)**. The percentage of the α-helix content was calculated from the ellipticity value at 222 nm using the following formula: (% α-helix = $(([\boldsymbol{\Theta_{222}}] - \mathbf{3000})/(-\mathbf{36000} - \mathbf{3000})) \times \mathbf{100}$) [34, 146]. R-values represent the ratio between the molar ellipticity values at 222 and 208 nm [117] and R = 1 defined as hallmark for a perfectly built α-helix [98]. **(C)** Helical wheel projections of Tyolotin-sC18* and sC18*-Tylotoin predicted by HeliQuest **(D)**.

The peptides were dissolved in 10 mM phosphate buffer as well as in phosphate buffer supplemented with 50% trifluoroethanol (TFE) to promote a helical assembly [56] and to stabilize the secondary structure [153].

All peptide conjugates as well as Tylotoin and a random sequence of Tylotoin alone display a spectrum typical of an unordered conformation in 10 mM phosphate buffer, pH 7.0 (Figure 33A), with minima around 197 nm – 200 nm. With the addition of TFE, the CD spectra revealed that all chimeric peptide conjugates become structured in α-helix conformations, whereas Tylotoin and rTylotoin are still in an unstructured form, respectively (Figure 33B). Previously, it was already shown that both sC18 [130] and sC18* [77] adopt an α-helical structure in the helix-inducing environment of TFE and thus, it was assumed that the attachment of the cell-penetrating peptide to Tylotoin supports the transition to helical structures. This was further supported after calculating the percentage of the α-helical content as well as the ratio between the molar ellipticity at 222 nm and 208 nm (R-value), where it is known that α-helical peptides have R-values of approximately 1 [117]. As seen from Figure 33C, both the α-helical content and the R-values were significantly increased

for the chimeric peptide conjugates in the presence of 50% TFE when compared with Tylotoin/rTylotoin alone. Moreover, the percentage of the α-helical content is slightly greater when CPP is fused to the *C*-terminus of Tylotoin. Therefore, a closer look at the helical wheel plot was taken, representing three-dimensional projection of amino acids within the α-helical structure [160]. A representative helical wheel plot for Tylotoin-sC18* and sC18*-Tylotoin is depicted in Figure 33D, respectively. The helical wheel projection of Tylotoin-sC18* highlighted two separate faces, one hydrophilic and one hydrophobic (VVLF). In contrast, the helical wheel plot of sC18*-Tylotoin showed no obvious differentiation into distinct domains. Thus, it was hypothesized that fusion of CPP to the *C*-terminal part of Tylotoin leads to a better hydrophobic/hydrophilic balance allowing optimal interaction of the peptide conjugates with the amphiphilic nature of biological membranes.

4.2.2 Cytotoxicity against keratinocytes and cancer cells

Next, the influence of the synthesized peptides on cell viability towards mammalian cells was investigated using a human skin and a cancer cell line. As representative cell line for skin cells, the human immortalized keratinocytes HaCaT were used. Keratinocytes are known to be an essential key cellular component of the epidermis involved in skin wound healing [136, 166, 201, 208]. Therefore, in order to use the peptides as potential wound healing agents, it is mandatory that the peptides exhibited no cytotoxic effects against human skin keratinocytes. Additionally, HeLa cells as representative cancer cell line were used to evaluate possible cytotoxic effects against tumor cells.

Therefore, both cell lines were exposed to chimeric peptide conjugates at certain concentrations, ranging from 10 to 100 µM. As controls, both sC18 and sC18* as well as Tylotoin alone were incubated with HaCaT and HeLa cells.

After 24 h of incubation at 37 °C, the cell viability was measured using either a tetrazolium- or resazurin-based cell viability assay, respectively (Figure 34).

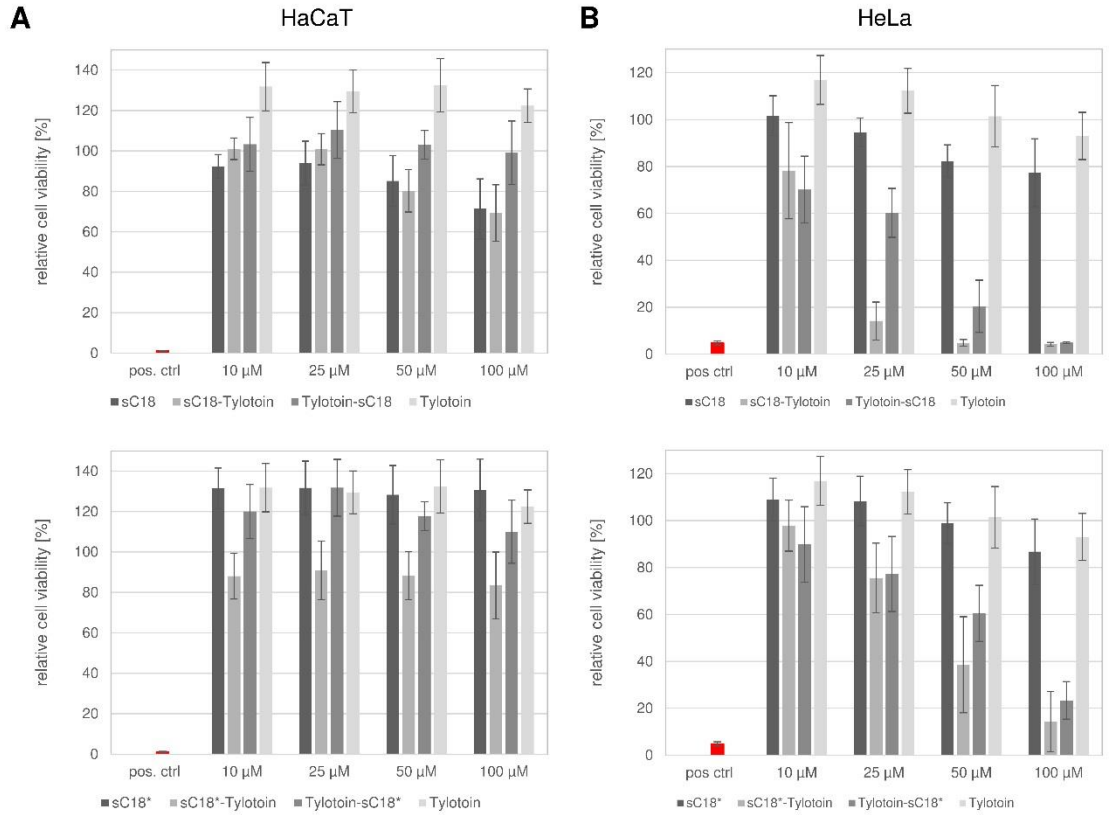

Figure 34. Cytotoxic profile of peptides against human keratinocytes (A) and cancer cells (B). Cells were incubated with indicated concentrations of peptides at 37 °C for 24 h. Cell viability of HaCaT cells was determined by MTT assay whereas the toxic effects against HeLa cells were analyzed by a resazurin-based cell viability assay relative to untreated cells. As positive control, cells were treated with 70% EtOH for 10 min. Experiments were conducted in triplicate with *n* = *3*. Error bars represent standard deviation.

As seen in Figure 34A, no cytotoxic activity at all was detected when HaCaT cells were incubated with Tylotoin within concentrations of up to 100 µM. Moreover, Tylotoin seemed to enhance the proliferation of HaCaT cells, which agrees with previously reported data [126]. The same effect was observed when keratinocytes were treated with sC18* alone and Tylotoin-sC18*. But within the given concentration range, a slight decrease in cell viability was detected for sC18*-Tylotoin. The incubation with sC18 and sC18-Tylotoin caused cytotoxic effects at higher concentration (> 50 µM), whereas the cell viability was not affected when HaCaT cells were incubated with Tylotoin-sC18.

Strikingly, the cell viability was much more negatively affected when cancer cells were treated with peptide conjugates for 24 h (Figure 34B). Interestingly, when compared to sC18* variants, chimeric peptide conjugates where sC18 is combined with Tylotoin caused a stronger decrease in cell viability in a concentration-dependent manner. As before, Tylotoin showed no relevant cytotoxic effects on the cells viability. Furthermore, the cytotoxic profile of sC18 and sC18* exhibiting no remarkable decrease in cell viability which agrees with former published results [68, 77, 130].

Even if the proliferative effect of HaCaT cells, as observed for Tylotoin, was less remarkable, the novel peptide conjugates provide a good template for additional studies to develop a new topical agent for wound healing, since the results clearly demonstrate no harmful effects on keratinocytes cell viability at lower concentrations. In contrast, the novel chimeric peptides revealed more distinct cytotoxic effects against the cancer cell line in a concentration-dependent manner, suggesting that these peptides might be exhibit in somehow selectivity towards cancer cells.

These features make the novel peptide conjugates highly attractive for further experimental studies.

4.2.3 Internalization into cells

In a next step, the cellular internalization efficiency of the new peptide conjugates compared to their linear versions was elucidated when incubating them with HaCaT and HeLa cells, to gain some insights into the capability of peptides cell entry.

Considering that the cytotoxic analysis revealed no harmful effects on cell viability, a non-cytotoxic concentration of 10 µM was selected for the following internalization studies.

First, both cell lines were incubated with 5(6)-carboxyfluorescein labeled sC18, the truncated version sC18* and Tylotoin alone. After 30 min of peptide incubation at 37 °C, the cells were treated with trypan blue solution to quench external fluorescence coming from surface-bound peptides and the cell nuclei were stained with the blue dye Hoechst 33342. The cellular uptake was then analyzed by confocal laser scanning microscopy (CLSM) and quantitatively by flow cytometry (Figure 35).

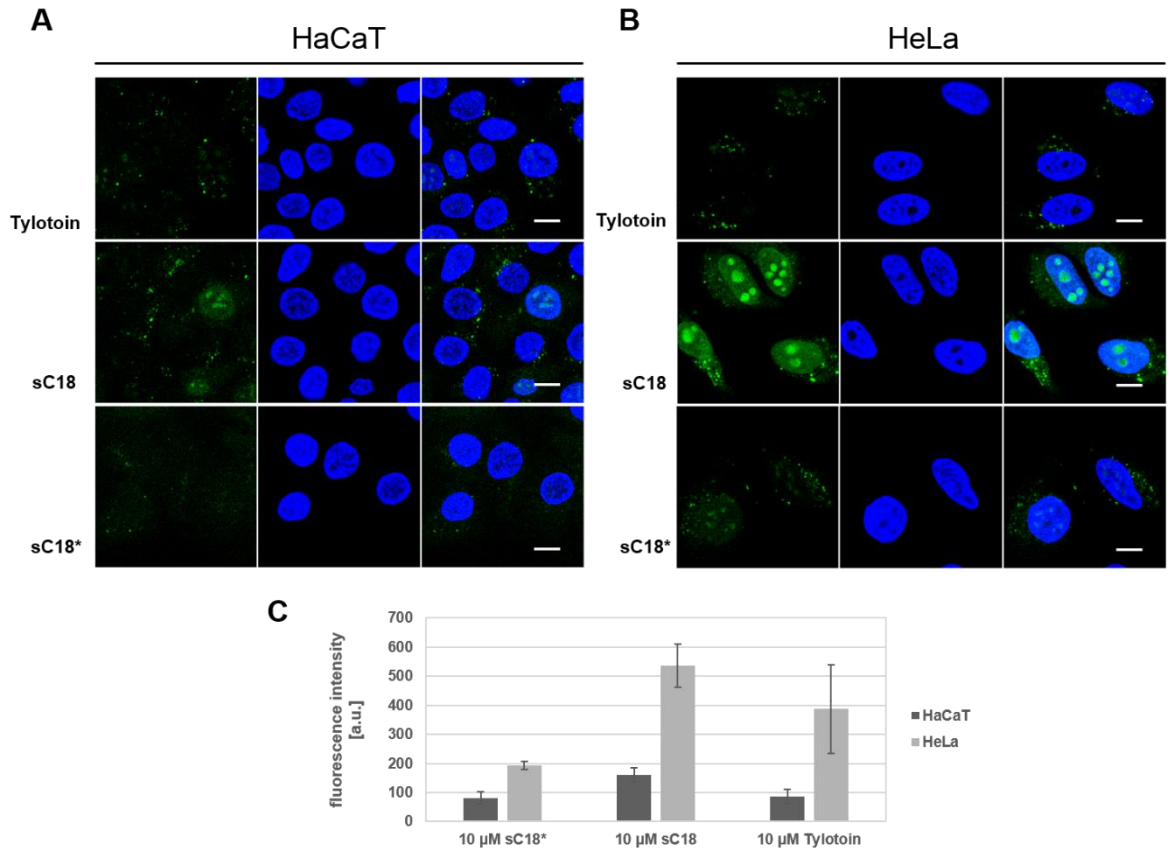

Figure 35. Cellular uptake of parent peptides into keratinocytes and cancer cells. Fluorescence microscopic images of human keratinocytes **(A)** and cancer cells **(B)** after 30 min incubation at 37 °C with 10 µM CF-labeled Tylotoin, sC18 and sC18*, respectively. External fluorescence was quenched by treatment with 150 µM trypan blue for 30 sec. Blue: Hoechst 33342 nuclear dye, Green: 5(6)-carboxyfluorescein-labeled peptides. Scale bars, 10 µm. Flow cytometric uptake studies of 10 µM CF-labeled peptides in HaCaT and HeLa cells at 37 °C for 30 min. Experiments were performed in triplicate with *n* = *2*. Error bars represent standard deviation **(C)**.

The fluorescence images of HaCaT cells treated with parent peptides are shown in Figure 35A. Obviously, all peptides are capable to internalize into keratinocytes, moreover an accumulation into cytosolic vesicles was detected and a distribution within the nucleus which was more pronounced for the sC18 peptide. In cancer cells, the cellular uptake was slightly higher as further confirmed by flow cytometric analysis (Figure 35B and C). Especially, the accumulation of sC18 into the cell nucleus, and more specifically into the nucleoli, was distinctly stronger. However, Gronewold *et al.* have not shown such a strong internalization pattern for the cellular uptake of sC18 but this is might be attributed to different microscopic settings [68]. Interestingly, the uptake studies of the truncated version of sC18 showed an overall weaker uptake efficiency. This might be due to the missing positively charged amino acid within the sequence, since it was already reported that a minimum charge density is required to observe cellular internalization [125, 210].

In this study, the uptake of Tylotoin into keratinocytes, moreover into the nucleoli, was reported for the first time. Nevertheless, for other amphibian skin peptides, e.g. Esc(1-21) [44] or temporin [43], internalization into the keratinocytes cytoplasm was already published.

Following, the cellular uptake of 10 µM and 1 µM CF-labeled chimeric Tylotoin conjugates within 30 min at 37 °C in HaCaT cells is shown in Figure 36.

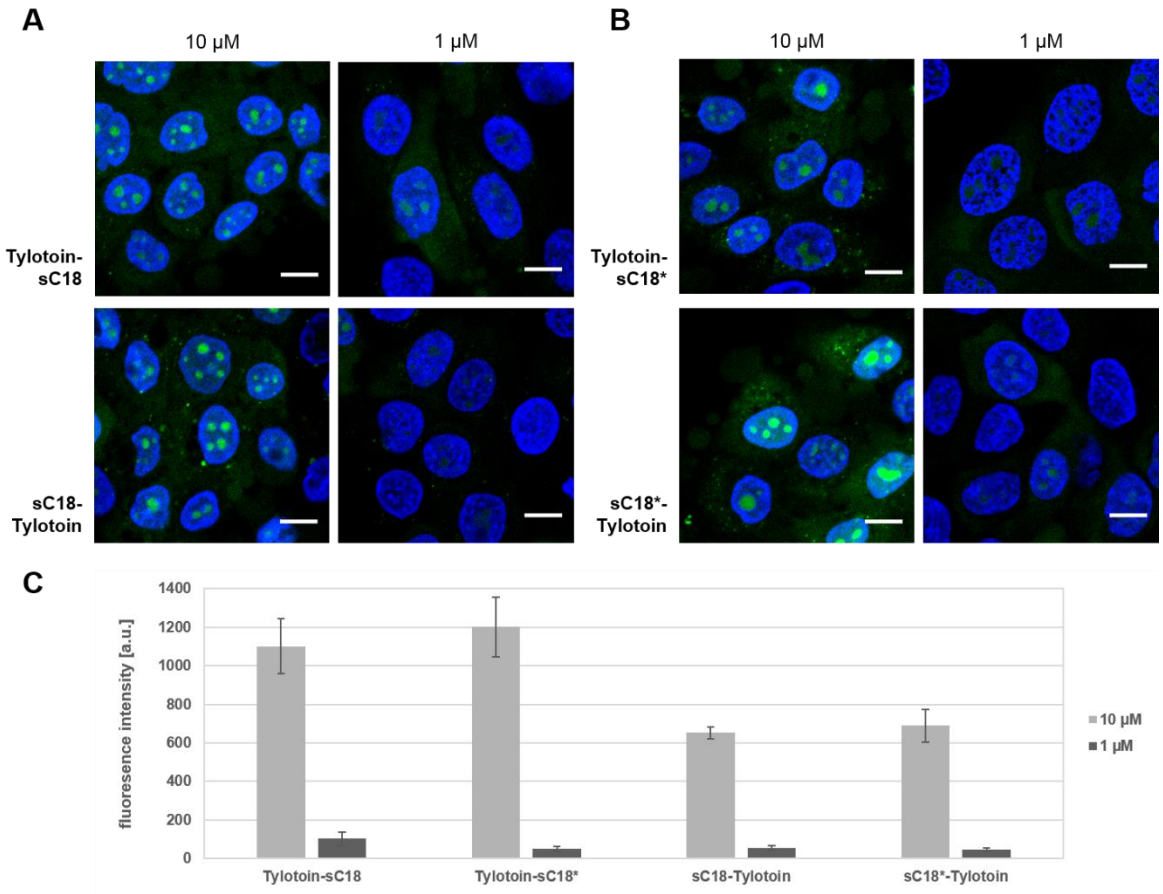

Figure 36. Internalization efficiency of Tylotoin peptide conjugates into HaCaT cells. Fluorescence microscopic images of human keratinocytes after 30 min incubation at 37 °C with 10 µM and 1 µM Tylotoin peptide conjugates **(A)**, **(B)**. External fluorescence was quenched by treatment with 150 µM trypan blue for 30 sec. Blue: Hoechst 33342 nuclear dye, Green: 5(6)-carboxyfluorescein-labeled peptides. Scale bars, 10 µm. Flow cytometric uptake analysis of 10 µM and 1 µM CF-labeled Tylotoin conjugates in HaCaT cells at 37 °C for 30 min. Experiments were performed in triplicate with $n = 3$. Error bars represent standard deviation **(C)**.

After incubating the cells with 10 µM peptide solutions, keratinocytes showed cytosolic as well as vesicular distribution patterns. Moreover, at higher concentrations, a significant accumulation of all chimeric peptides in the cell nucleoli occurred. These observations were even more pronounced when CPP is fused to the *N*-terminus of Tylotoin. Decreasing the peptide concentration to 1 µM, the novel designed peptides almost failed to internalize which correlates well with the flow cytometric uptake studies (Figure 36C) at this concentration. From the observations at 1 µM peptide concentrations, one might conclude that theses peptides internalize by direct penetration, distributing throughout the cytosol and in the cell nuclei, and then accumulate in vesicular pattern.

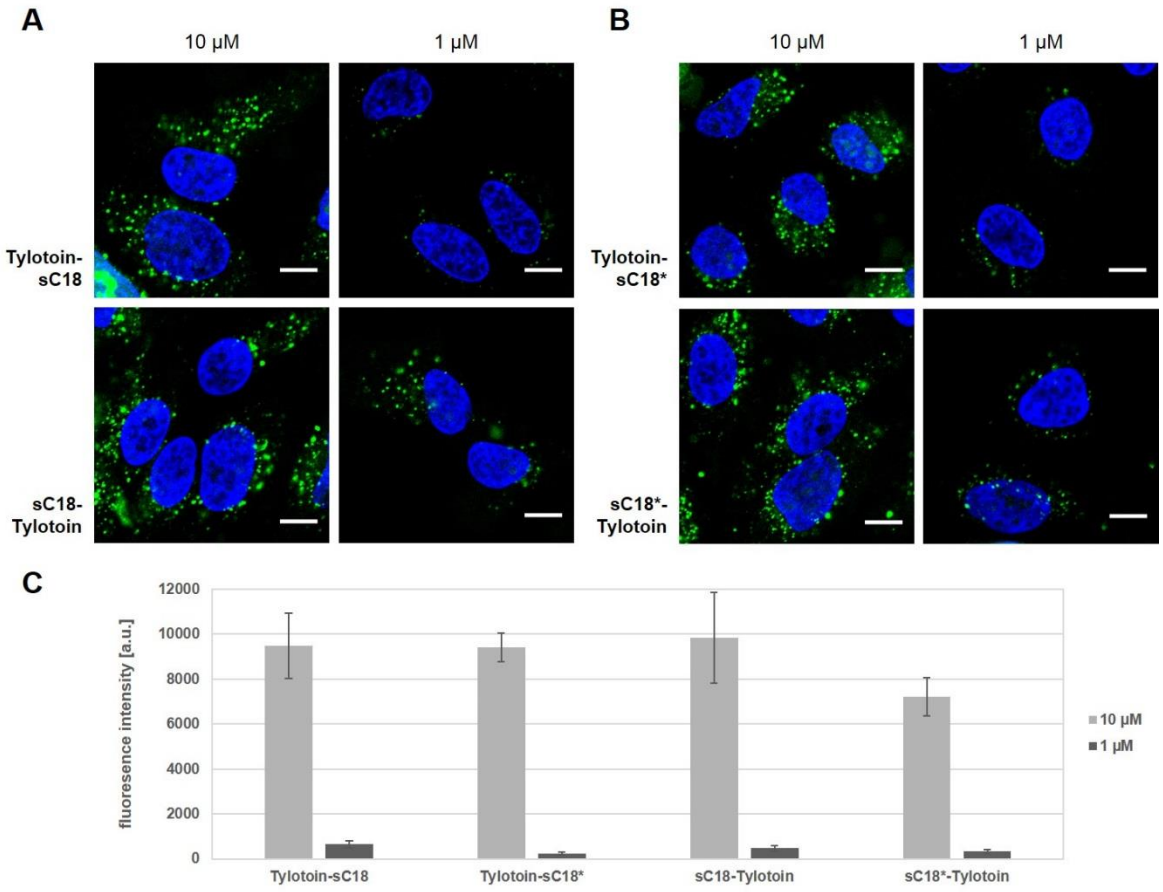

Figure 37. Internalization efficiency of Tylotoin peptide conjugates into cancer cells. Fluorescence microscopic images of cancer cell line HeLa after 30 min incubation at 37 °C with 10 µM and 1 µM Tylotoin conjugates **(A)**, **(B)**. External fluorescence was quenched by treatment with 150 µM trypan blue for 30 sec. Blue: Hoechst 33342 nuclear dye, Green: 5(6)-carboxyfluorescein-labeled peptides. Scale bars, 10 µm. Flow cytometric uptake analysis of 10 µM and 1 µM CF-labeled Tylotoin conjugates in Hela cells at 37 °C for 30 min. Experiments were performed in triplicate with *n* = *3*. Error bars represent standard deviation **(C)**.

The cellular uptake efficiency of novel designed peptide conjugates in HeLa cells was then investigated, again with peptide concentrations of 10 and 1 µM (Figure 37). When compared with HaCaT cells, a much stronger vesicular accumulation was detected at both concentrations as seen in Figure 37A and B. Whereas, the cytosolic distribution as well as the accumulation within the cell nucleus seemed not as distinct. Nevertheless, the intrinsic fluorescence of peptide conjugates measured by flow cytometry revealed a significant greater uptake at higher concentrations and moreover, an overall remarkable higher uptake in cancer cells than in skin cells (with up to 10-fold higher uptake rates). Hence, these data might indicate that all peptide conjugates are localized in vesicular structures, possibly in endo- or lysosomes, which are then released into the cytosol and nucleus after an initial endo- and lysosome disruption.

Taken together, the data obtained from HaCaT and HeLa cells, the uptake efficiency and the extent of the uptake pattern might be cell line-dependent, suggesting different affinities to uptake mechanisms which might be possible, since it has been reported that CPPs utilize

two or more pathways depending on the experimental conditions [69, 111]. But nevertheless, the combination of both peptides improved the cellular internalization towards the parent peptides and so far, no significant distinctions between the structural orientation of the peptides could be observed.

To get a deeper insight into the cellular uptake pattern, the internalization of the novel designed peptides over a longer time frame was analyzed by fluorescence microscopy. Therefore, both cell lines were incubated with 10 µM CF-labeled peptides in the time interval of 30 and 120 min at 37 °C.

The microscopic images of the cellular uptake of chimeric conjugates within 30 and 120 min into HaCaT cells are depicted in Figure 38.

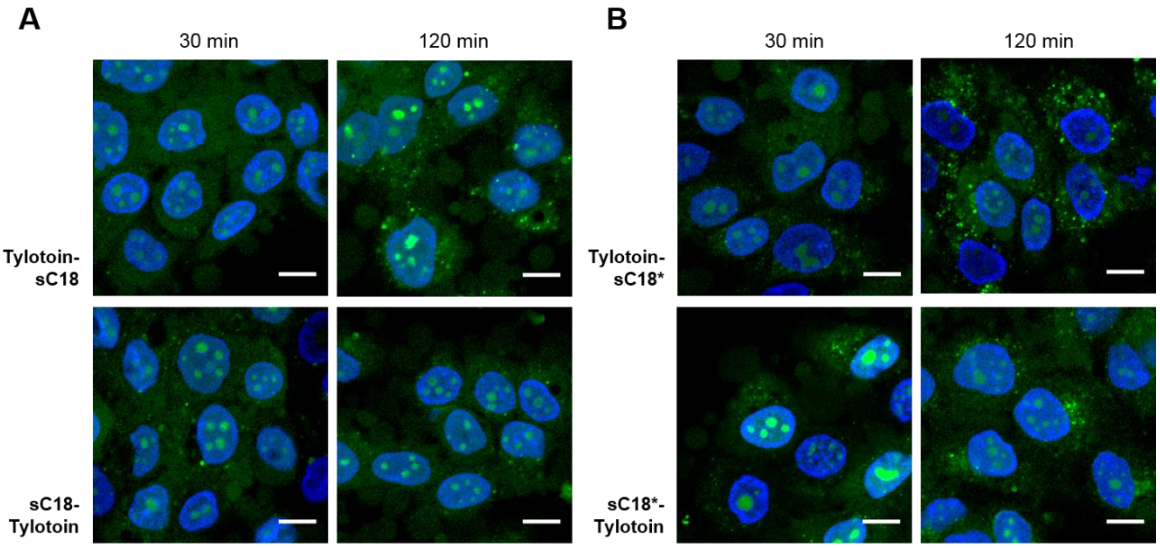

Figure 38. Time-dependent uptake of Tylotoin peptide conjugates into HaCaT cells. Fluorescence microscopic images of keratinocytes after incubation period of 30 min and 120 min at 37 °C with 10 µM sC18 variants **(A)** and sC18* variants **(B)**. External fluorescence was quenched by treatment with 150 µM trypan blue for 30 sec. Blue: Hoechst 33342 nuclear dye, Green: 5(6)-carboxyfluorescein-labeled peptides. Scale bars, 10 µm.

Besides cytosolic and nuclear peptide distribution, after an incubation time of 120 min, an additional punctuate pattern within the cells could be observed which was more obvious for Tylotoin-sC18 and Tylotoin-sC18*. However, the overall amount of internalized peptide variants seemed to stay equal over the evaluated time course.

The time interval study of the novel designed peptides uptake into HeLa cells is depicted in Figure 39.

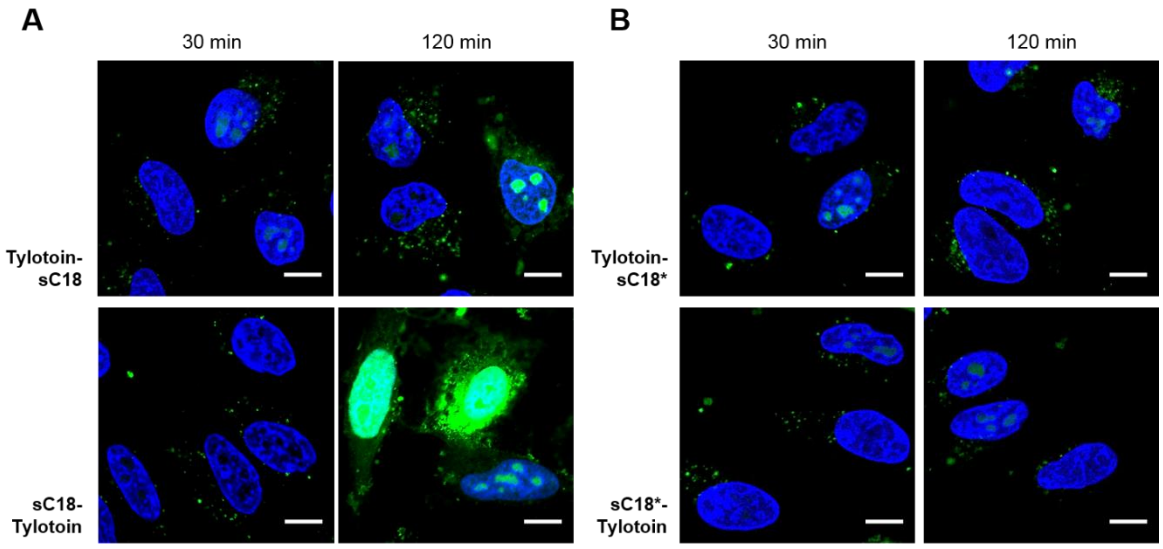

Figure 39. Time-dependent uptake of Tylotoin peptide conjugates into HeLa cells. Fluorescence microscopic images of cancer cells after incubation period of 30 min and 120 min at 37 °C with 10 µM sC18 variants **(A)** and sC18* variants **(B)**. External fluorescence was quenched by treatment with 150 µM trypan blue for 30 sec. Blue: Hoechst 33342 nuclear dye, Green: 5(6)-carboxyfluorescein-labeled peptides. Scale bars, 10 µm.

Here, it must be noted that the lower gain value used for the enhancement of the green signal (5.20 instead of 6.10, see Figure 37A and B) because otherwise, these images would have been overexposed. Nonetheless, after 120 min of peptide incubation, sC18 variants were stronger distributed within the cytoplasm and nucleus, more specifically into the nucleoli, which might be attributed to the slight decrease in cell viability at this peptide concentration. However, the amount of internalized sC18* variants during the time interval and the subcellular distribution seemed to remain more or less the same.

So far, these data correlate well with the already mentioned observations. After a longer incubation period, the chimeric peptides were located within vesicular structures and concentrated mainly at the nuclear periphery. Moreover, the novel designed peptide conjugates could accumulate more efficiently in cancer cells as seen from flow cytometric analysis before. The preferential accumulation of peptides in cancer cells might be accompanied by slightly higher cytotoxicity towards cancer cells than to normal skin cells.

Since all novel designed peptides showed no significant differences in uptake efficiency within a cell line (Figure 36C and Figure 37C) regardless whether the CPP is fused *N*- or *C*-terminally to Tylotoin, it was referred to toxicity studies and structural characteristics to select the most suitable peptide conjugate. Owing to the proliferative effect observed in HaCaT cells and the non-cytotoxicity in HeLa cells at concentrations used for experiments, Tylotoin-sC18* was selected for further studies. Moreover, the helical wheel projection revealed two distinct phases when sC18* is combined to the *C*-terminus of Tylotoin resulting in a balanced ratio between hydrophilicity and hydrophobicity which is important for the initial step of cell entry [46, 77].

Effect of endocytosis inhibition

Hence, with this potent peptide conjugate in hand, the cellular uptake mechanism of Tylotoin-sC18* was further investigated in greater detail. It was examined whether the internalization of the chimeric peptide is dependent on endocytotic processes. Thus, the experimental set-up was conducted either at 4 °C to inhibit the energy-dependent pathway [102] or in the presence of dynasore, where the endocytosis is totally suppressed [141, 176].

First, keratinocytes and cancer cells were incubated with 10 µM CF-labeled Tylotoin-sC18* for 30 min at 4 °C. The findings observed by fluorescence microscopy are presented in the upper panels of Figure 40A and B, respectively.

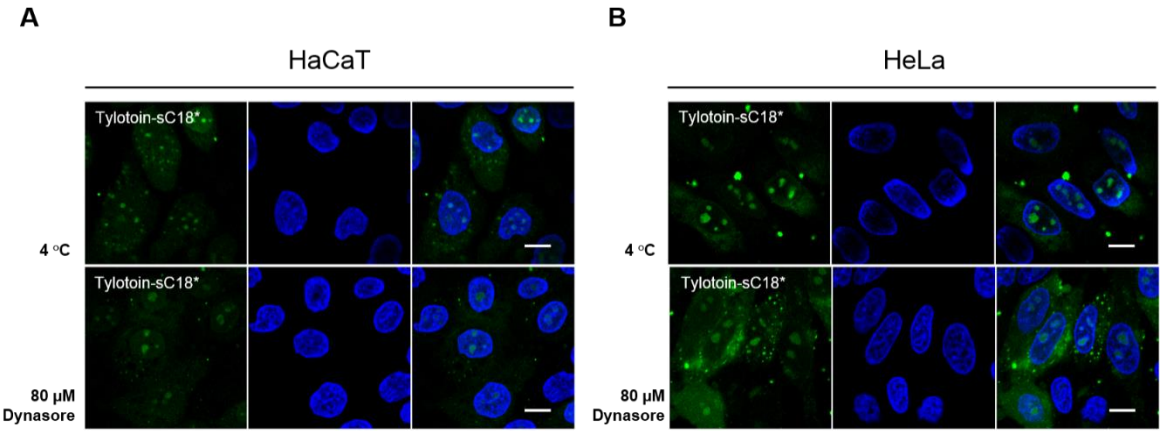

Figure 40. Effect of endocytosis inhibition on cellular uptake of Tylotoin-sC18* in keratinocytes (A) and cancer cells (B). Cells were incubated with 10 µM CF-labeled Tylotoin-sC18* for 30 min at 4 °C (upper panel) or cells were pretreated with 80 µM dynasore and subsequently with 10 µM CF-labeled peptide for 30 min at 37 °C. External fluorescence was quenched by treatment with 150 µM trypan blue for 30 sec. Green: 5(6)-carboxyfluorescein-labeled peptides, Blue: Hoechst 33342 nuclear dye. Scale bars, 10 µm.

The uptake of the peptide conjugate was slightly decreased in both cell lines relative to peptides incubation at 37 °C. However, the peptide is evenly distributed throughout the cytosol and in case of HeLa cells, the punctuate uptake pattern was not as strong as at 37 °C. Moreover, Tylotoin-sC18* is still localized within the nucleoli, approving the assumption that the peptide, to a certain extent, is also able to enter the cells by direct penetration.

Next, the cellular uptake studies were also performed in the presence of dynasore, a cell-permeable dynamin inhibitor [110]. Therefore, both cell lines were preincubated with 80 µM dynasore for 1 h and subsequently CF-labeled Tylotoin-sC18* was added for another 30 min at 37 °C. The microscopic images are depicted in the lower panels of Figure 40A and B, respectively. As expected, the internalization of chimeric peptide was not suppressed in dynasore-treated skin and cancer cells, respectively. Considering that dynasore prevents besides dynamin, which is essential for membrane fission during clathrin- and caveolin-

mediated endocytosis, also the vesicle formation and fusion steps of macropinocytosis [141, 176], it can be presumed that Tylotoin-sC18* is indeed capable to internalize by direct translocation.

Intracellular destination

Since the punctuate uptake pattern even when endocytosis is totally suppressed was still observed, yet another question of interest was to determine the intracellular fate of Tylotoin-sC18* after the peptide incubation at 37 °C.

Hence, after treating the cell lines with 10 µM CF-labeled Tylotoin-sC18* for either 30 or 120 min, respectively, the peptide solutions were removed, extracellular fluorescence was quenched and cells were further incubated for 6 h in peptide-free medium. The microscopic images are shown in Figure 41.

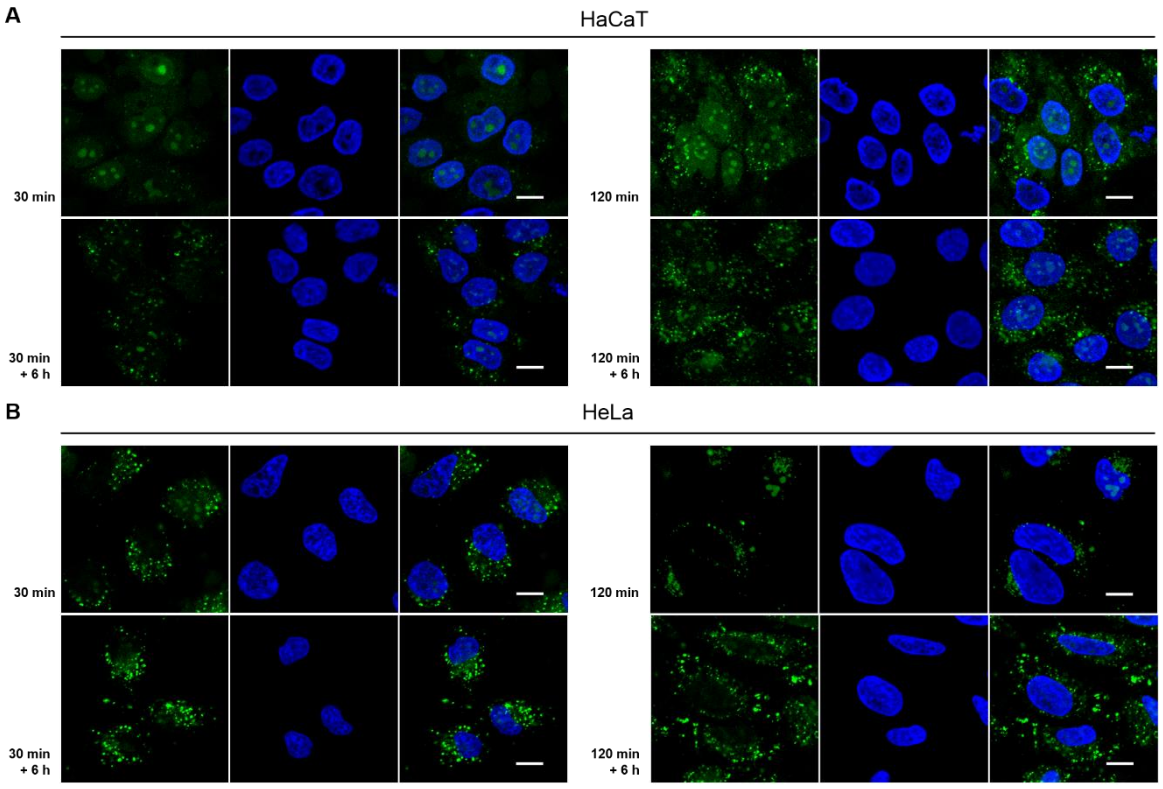

Figure 41. Intracellular fate of already internalized Tylotoin-sC18* after further 6 h of incubation in peptide-free media. Fluorescence images of HaCaT **(A)** and HeLa cells **(B)** treated with 10 µM CF-Tylotoin-sC18* at 37 °C for 30 and 120 min, respectively and after another 6 h of incubation in peptide-free medium. External fluorescence was quenched by treatment with 150 µM trypan blue for 30 sec. Green: 5(6)-carboxyfluorescein-labeled peptides, Blue: Hoechst 33342 nuclear dye. Scale bars, 10 µm.

After incubating HaCaT cells with 10 µM peptide conjugate for 30 min and further incubation in peptide-free medium, a more obvious accumulation into cytosolic vesicles was observed. In contrast, the cellular uptake of Tylotoin-sC18* after 120 min and the intracellular fate after another 6 h of incubation showed similar distribution patterns within skin cells (Figure 41A).

As seen from Figure 41B, the amount of internalized Tylotoin-sC18* in HeLa cells and the localization within the cells remained more or less equal regardless of incubation time.

Hence, these findings support the idea that in skin cells, the chimeric peptide conjugate is taken up by direct translocation after 30 min of incubation and over a longer time period, the peptides seemed to aggregate or might target specific cellular organelles since vesicular structures could still be observed. In HeLa cells, a punctuate uptake pattern was observed, which speaks in favor of an endocytotic uptake pathway, suggesting that the peptide is entrapped within endosomal vesicles and is not able to escape from endosomes. However, considering the only diminished cellular uptake at either 4 °C or in the presence of the endocytosis inhibitor and the fact that the peptide accumulated within the cell nucleoli, it is assumed that Tylotoin-sC18* is capable to enter the cells also by direct translocation.

Subcellular localization

Nowadays, specific organelle and tissue targeting is a major goal to ensure selective delivery of various therapeutic agents to reach its site of action within the cell [29, 158]. Thus, a large body of literature exists that demonstrates the successful application of CPPs to transport covalently or non-covalently linked therapeutic active biomolecules across the cell membrane and thus, enabling them to reach their specific cellular target [29, 68, 78, 158].

Owing to the fact that the peptides still accumulated within vesicular structures, it should be figured out whether Tylotoin-sC18* traffics specific intracellular organelles, like the endoplasmic reticulum (ER), lysosomes or mitochondria. Therefore, the localization of the peptide conjugate was investigated in the presence of specific cell organelle trackers.

For this purpose, both keratinocytes and cancer cells were incubated together with 10 µM CF-labeled peptides and either 1 µM Mito-Tracker or 75 nM Lyso-Tracker for 120 min at 37 °C, respectively. To verify the ability of Tylotoin-sC18* to target the ER, the red fluorescent dye ER-Tracker, which selectively localizes into endoplasmic reticula, was added 15 min prior to the end of peptide incubation. Then, microscopic analysis of possible co-localization was performed by confocal laser scanning microscopy.

The fluorescence images shown in Figure 42 represent the organelle localization stained with red fluorescent dye, the peptide labeled with 5(6)-carboxyfluorescein (green) and in blue the nuclear marker.

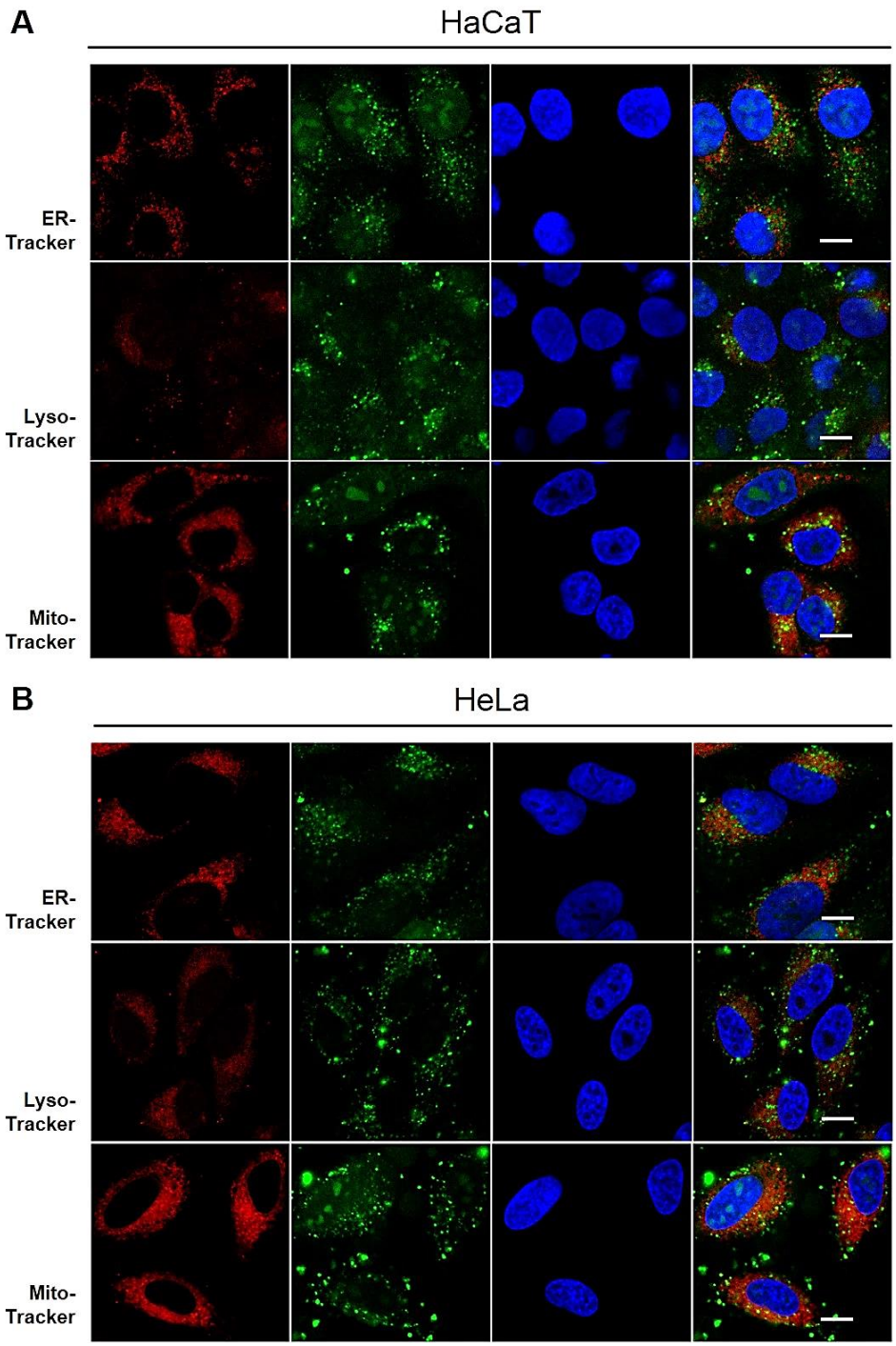

Figure 42. Cell organelle targeting study of Tylotoin-sC18* within keratinocytes (A) and cancer cells (B). Fluorescence images of cells stained with1 µM ER-Tracker for 15 min, 75 nM Lyso-Tracker and Mito-Tracker were incubated together with 10 µM CF-Tylotoin-sC18* for 120 min at 37 °C, respectively. External fluorescence was quenched by treatment with 150 µM trypan blue for 30 sec. Red: stained organelles, Green: 5(6)-carboxyfluorescein-labeled peptide, Blue: Hoechst 33342 nuclear dye, Scale bars, 10 µm.

First, it should be noted that the staining of the organelles was successful and worked very well, as seen in the red channel in Figure 42A and B. Furthermore, when using the different stains, the CF-labeled peptide showed similar intracellular distribution and the morphology of the nuclei looked quite well corroborating that the organelle labeling did not affect the cellular uptake.

Moreover, one could hardly detect any co-localization at all, either in HaCaT or in Hela cells, since the merged pictures revealed no obvious overlay of the red and green signal coming from the organelle staining and the labeled chimeric peptide, respectively.

Taking these observations into account, the novel designed peptide did not target the specific cellular organelles investigated. Consequently, the findings of this experiment support the hypothesis that the peptide aggregates over the time in keratinocytes and is, in case of the cancer cell line, still to some extent localized within vesicular structures. This leads to the assumption that the peptide might be entrapped within endosomes and has not yet been transported to lysosomes for degradation, since no co-localization with the Lyso-Tracker was observed. In a recent study, Qian *et al.* provide another explanation, which supports the idea of peptide aggregation [143]. Thus, Qian and coworkers suggested a novel mechanism for cell-penetrating peptides and their endosomal release process. Using model membranes and mammalian cells, they proposed that CPPs bind directly to the endosomal membrane, inducing membrane curvature and thus leads to budding of small vesicles which finally collapse into peptide/lipid aggregates [143].

Therefore, it is possible that Tylotoin-sC18* might escaped from endosomes and reached the cytosol, apparently through budding and subsequent rupture of small vesicles.

4.2.4 Peptide-lipid membrane interaction

In a next level, it was further focused on the initial stage of peptides cell entry and thus, one took advantage of artificial model membranes, more precisely giant unilamellar vesicles (GUVs).

Since Tylotoin-sC18* is rich in positively charged residues resulting in a net charge of +13 at physiological pH and due to the fact that electrostatic interactions between positively charged CPPs and the negative charges within the cell membrane are of particular importance during the first stage of peptides cell entry [20, 85, 86], both zwitterionic and anionic lipid model systems were employed to ensure better comparability.

Therefore, giant unilamellar vesicles either composed of zwitterionic lipids (DOPC and DOPE) or with additional incorporation of DOPG as negatively charged phospholipid were prepared and subsequently, the interaction and binding affinity of Tylotoin-sC18* towards both membrane compositions were investigated using confocal laser scanning microscopy.

For that, 20 µM of CF-labeled Tylotoin-sC18* as well as CF-Tylotoin and CF-sC18* serving as controls were incubated with neutral GUVs (DOPC/DOPE, 50:50) (Figure 43A), and anionic GUVs (DOPC/DOPE/DOPG, 40:30:30) (Figure 43B) for 90 min. For visualization, GUV membranes were additionally doped with 0.2 mol% Atto550 labeled DOPE (red) and

to monitor the GUV membrane integrity, vesicles were loaded with the blue fluorophore Oyster 405.

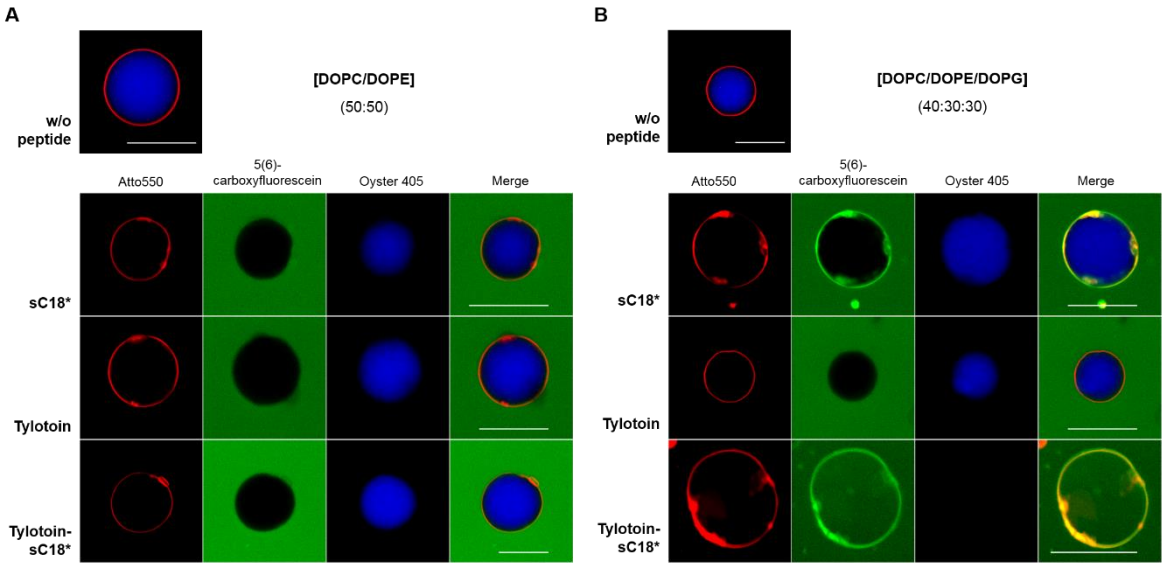

Figure 43. Interaction of Tylotoin-sC18* and its precursor peptides with model membranes. CF-labeled peptides (20 µM) were incubated with neutral **(A)** and negatively charged GUVs **(B)** loaded with Oyster 405 (blue dye) for 90 min and analyzed by CLSM. To visualize their membranes, vesicles were prior doped with 0.2 mol% Atto550-labeled DOPE (red). Scale bars, 30 µm.

As shown in Figure 43A, no significant accumulation of peptides on membranes of neutral GUVs was observed, since no overlay with the red-labeled vesicle membrane could be detected. Furthermore, the influence of peptides on membrane integrity was examined by studying induced leakage of a GUV-encapsulated blue fluorescent dye. But again, no noticeable differences in the Oyster 405 signal (blue) before and after peptide addition could be revealed and thus, no obvious dye release. Owing to the fact that the presence of anionic lipids is crucial to trigger peptide-membrane interactions of cationic peptides [35, 181], these findings are in accordance with the literature.

In contrast, when anionic GUVs were incubated with 20 µM of CF-labeled peptide solutions, a strong peptide signal on the membranes within 90 min could be detected, except for CF-Tylotoin (Figure 43B). Here, no obvious membrane interaction could be observed at this concentration for Tylotoin alone. However, the strong membrane interaction observed for CF-sC18* and CF-Tylotoin-sC18* demonstrated the importance of negatively charged lipids to accumulate to these vesicle membranes. These results are in line with previous reports proving that the presence of negatively charged counter-anions, such as phosphatidylglycerol (DOPG) or pyrenebutyrate (PyB), is essential to induce the peptide-membrane interactions of arginine-rich peptides [35, 91, 181]. Moreover, previous studies have demonstrated that the cellular membrane of cancer cells is primary anionic [85, 120], which is interesting considering that our novel peptide conjugate showed an overall stronger

accumulation on anionic GUV membranes compared to neutral ones, suggesting preferential accumulation towards cancer cells as already mentioned previously from internalization studies.

Furthermore, the interaction of Tylotoin-sC18* with the anionic lipid membrane resulted in a significant dye release, indicating that the membrane becomes prone to leak as well as in peptide influx as seen from the green signal within the vesicle, presumably leading to pore forming events. This observation is in accordance with Cahill, K., who reported that the higher the number of positive charges, the higher is the propensity of the peptide to induce pore formation in membranes [25]. Moreover, the results observed for CF-labeled sC18* are in close agreement with those obtained by Horn *et al.* [77] as well. However, since the vesicles were still good in shape after the treatment with the peptide conjugate, the pore forming events are not accompanied by membrane disruption. Presumably, Tylotoin-sC18* is able to translocate the lipid bilayer quickly through transient pore-like structures. This assumption is similar to that reported by Herce *et al.*, who revealed by molecular-dynamics simulations that the Arg-rich Tat peptide crosses phospholipid bilayers by destabilizing the membrane and inducing transient pores, which close after a few peptides translocate [75]. A further possible explanation for the dye release and the peptide influx without destroying the vesicle membranes may involve the mechanism of loosening lipid packing, which might enhance the hydrophobic interaction of the peptide backbone with lipid acyl chains, thus facilitating the membrane translocation of Arg-rich peptides. A recent study by Murayama *et al.* supports this interpretation [127]. They reported on the formation of so called lipid packing defects, caused by membrane bending [190], as key factor that governs the translocation of Arg-rich CPPs across the membrane (Figure 44) [127].

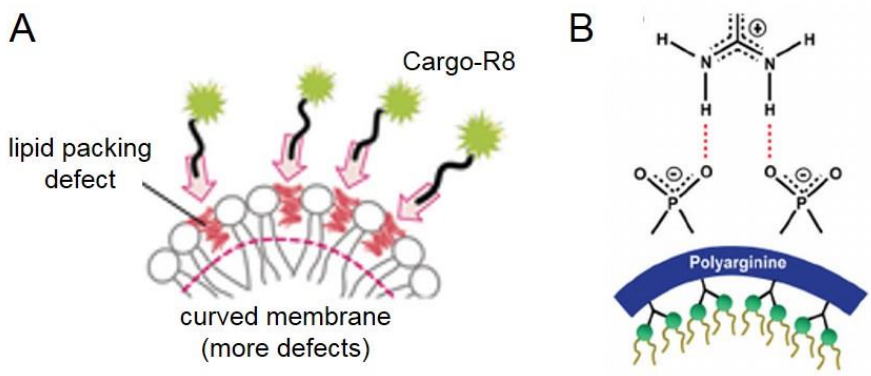

Figure 44. Direct translocation of R8 through the lipid bilayer. This process is facilitated by curvature-induced defects in lipid packing **(A)**. These defects in lipid packing arise from membrane bending caused by the interaction of guanidium functions and the phosphate groups of membrane lipids **(B)**. (modified after Mishra *et al.*, 2011 [123] and Murayama *et al.*, 2017 [127])

Thereby, the formation of bidentate hydrogen bonds between the guanidium moieties of Arg and the phosphate groups of membrane lipids induces positive membrane curvature (Figure

44B), which resulted in membrane structural defects, enabling the direct translocation of oligo-arginine (R8) across the plasma membrane (Figure 44A) [127].

Moreover, since model membrane systems are not affected by endocytotic processes, these findings further support the hypothesis that Tylotoin-sC18* is indeed able to directly penetrate the cell membrane through membrane destabilization effects.

4.2.5 Efficacy of Tylotoin-sC18* on keratinocyte migration in a scratch-wound closure assay

Keratinocytes are the predominant cell type of the epidermis, the outermost layer of skin, and thus provide a physical barrier between the organism and the environment, protecting it from external agents and pathogens [136]. Upon injury of the skin, as the epidermal barrier is disrupted, migration and proliferation of keratinocytes represent a crucial step in the re-epithelization phase of the wound healing process [119, 136, 166, 201, 208].

Here, the ability of Tylotoin-sC18* to induce migration and proliferation of keratinocytes into a wound area was investigated using an *in vitro* wound closure assay. Therefore, confluent monolayers of HaCaT cells cultured in 12-well plates were mechanically scratched with a sterile pipette tip and then allowed to re-epithelialize for 30 h at 37 °C in the presence of Tylotoin-sC18*.

Since Mu *et al.* demonstrated that Tylotoin promotes migration of HaCaT cells in a concentration-dependent manner [126], the concentration of 13.5 µM for the peptide conjugate was selected. Furthermore, the human epidermal growth factor (hEGF) was used as positive control and untreated cells served as negative control. The cell migration was monitored by phase-contrast microscopy depicted in Figure 45.

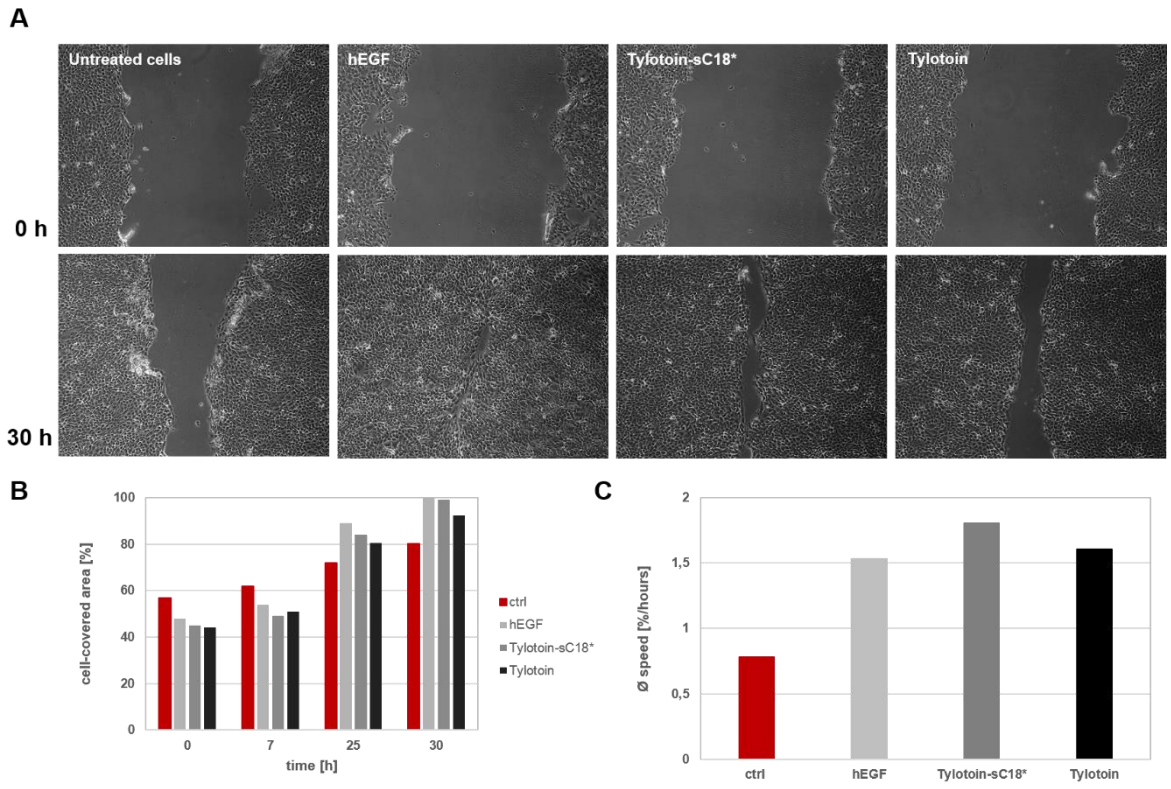

Figure 45. Tylotoin-sC18* promotes migration of HaCaT cells. Confluent cells were wounded by scratching with a pipette tip and then treated with 13.5 µM Tylotoin-sC18*, 13.5 µM Tylotoin and 100 ng/ml hEGF, respectively. Cells incubated with maintenance medium only served as control. Wound closure was monitored at 0, 7, 25 and 30 h after peptide addition by inverted light microscope **(A)**. The percentage of corresponding cell-covered area at each time point **(B)** and the average speed (% wound closure/hours) **(C)** were analyzed by Wimasis Image Analysis.

In Figure 45A, compared to migration in the untreated control group, the migration of keratinocytes into the wounded area was distinctly increased in the presence of Tylotoin-sC18* 30 h after scratching, similar with the human epidermal growth factor (hEGF). Moreover, the ability of Tylotoin-sC18* to enhance migration of keratinocytes seems to be improved compared to Tylotoin alone, since the average speed of the cell-covered area per hour was accelerated for Tylotoin-sC18* (Figure 45C). These findings indicated that the novel designed peptide conjugate had comparable migration efficiency with Tylotoin and hEGF, suggesting that the CPP connected to Tylotoin did not cause any loss in its activity. Moreover, the combination of both peptides might further improve the wound healing promoting ability of Tylotoin.

However, since wound closure results from both cell migration and proliferation, the wound healing assay was also performed in the presence of mitomycin C, which is known to inhibit mitosis of the cells and thus allows to distinguish migration from proliferation [45, 95].

Therefore, confluent monolayers of keratinocytes were preincubated with 20 µM mitomycin C for 90 min to prevent cell proliferation. Subsequently, the migratory effect of Tylotoin-sC18* compared with untreated cells was monitored in the wound healing assay depicted in Figure 46.

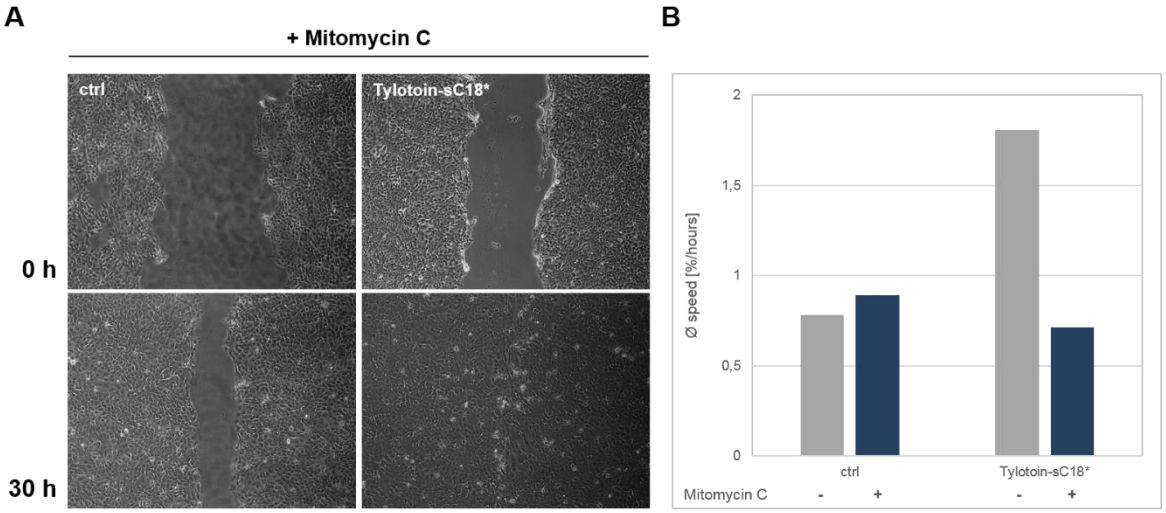

Figure 46. Influence of mitomycin C on Tylotoin-sC18*-induced wound closure. Confluent monolayer of immortalized HaCaT cells were treated with 20 µM mitomycin C for 90 min prior to scrape formation to avoid cell proliferation. Wound closure in the presence of 13.5 µM peptide or even maintenance medium was monitored after 0, 7, 25 and 30 h by inverted light microscope, respectively **(A)**. The corresponding mean speed (% wound closure/hours) of wound healing was calculated by Wimasis Image Analysis **(B)**.

Data shown in Figure 46A conclude that the wound healing rate of Tylotoin-sC18* is higher than in the control group, since a larger number of cells migrated into the wounded gap in the presence of chimeric conjugate, which resulted in complete wound closure. But taking a closer look on average speed, expressed as cell-covered area per hour, it was found that the presence of mitomycin C remarkably suppresses the cell migration ability of Tylotoin-sC18* (Figure 46B).

These results might illustrate that besides migration also proliferation of HaCaT cells contributes to the wound healing effect induced by Tylotoin-sC18* as well.

4.2.6 Mechanism of peptide-induced cell migration

As several cytokines and growth factors have been shown to influence the process of re-epithelialization [27, 119], the epidermal growth factor receptor (EGFR) was selected to further investigate the pathway by which Tylotoin-sC18* induces migration and proliferation of keratinocytes. So far, authors of several studies have demonstrated the importance of human EGFR to enhance both keratinocytes migration and proliferation [9, 31, 34, 131]. Moreover, it was already shown for e.g. LL-37 [182], Esculentin-1a(1-21) [44], a derivative of a frog skin AMP, and DRGN-1 [34], an AMP obtained from plasma of Komodo dragon, to act in a EGF-receptor dependent manner.

Thus, to examine whether Tylotoin-sC18* is also capable to activate the EGFR pathway, the potential phosphorylation of the EGF-receptor was analyzed by Western blotting using an anti-phospho EGFR antibody.

Since Tokumaru *et al.* revealed that LL-37 phosphorylated EGFR within 10 min enduring for 15 min [182], subconfluent HaCaT cells were stimulated with 13.5 µM Tylotoin-sC18* for three indicated time points, 5, 15 and 25 min, respectively. The human epidermal growth factor served as positive control and the EGFR inhibitor tyrphostin AG1478 was added 10 min prior to EGF treatment to confirm the contribution of EGFR signaling in EGF induced migration of keratinocytes.

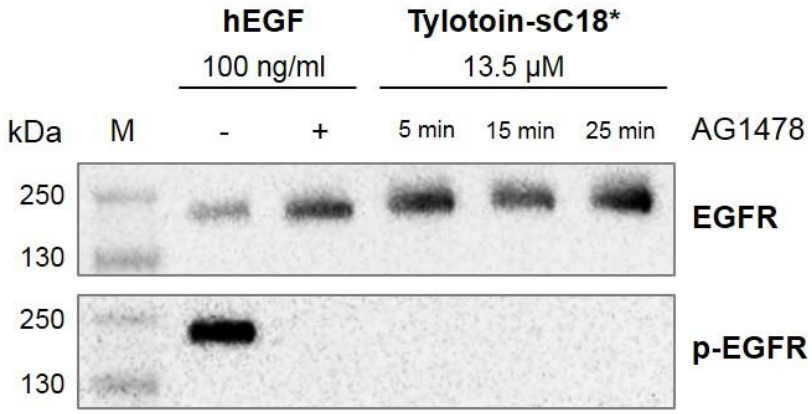

Figure 47. Effects of Tylotoin-sC18* on EGFR activation in HaCaT cells. Subconfluent keratinocytes were starved in serum-free medium for 16 h and subsequently stimulated with 13.5 µM Tylotoin-sC18*. The cells were harvested into lysis buffer at the indicated time points. hEGF (100 ng/ml) served as positive control. For EGFR inhibition, cells were pretreated with 0.2 µM AG1478 for 10 min and subsequently treated with hEGF for 5 min. EGFR indicates total EGFR protein.

As illustrated in Figure 47, EGF treatment led to phosphorylation of the EGF-receptor at 5 min. Moreover, the activation of EGFR was significantly impaired by inhibiting EGFR-mediated signaling through AG1478, confirming the importance of EGF during the process of re-epithelization. However, no activation of EGFR was observed at all when keratinocytes were stimulated with Tylotoin-sC18*, indicating that the peptide-induced migration and proliferation of keratinocytes does not occur via EGF/EGFR signaling pathway.

4.2.7 Antimicrobial activity

Since the complex process of wound healing is often affected by bacterial infections, which is also a key reason why wound repair may decelerate, and thus leading to increased risks of patient morbidity and mortality, there is an urgent need to discover new treatments for microbial infected wounds [93, 101]. Furthermore, due to the currently increasing number of multidrug-resistant bacteria, other antimicrobial agents like AMPs may provide an attractive alternative to conventional antibiotics [116].

Recently, it was shown by our group that the cell-penetrating peptide sC18 revealed still moderate antimicrobial activities, which could be further increased by conjugation with imidazolium salts [148] as well as the exchange of specific amino acids with phenylalanine leading to enhanced antimicrobial activities [150]. Furthermore, Mu and coworkers have

highlighted the important role of the antimicrobial peptide Tylotoin during wound healing events, as mentioned earlier [126]. Moreover, there is even more evidence for AMPs to be important modulators in wound healing often accompanied by multiple beneficial features e.g. antimicrobial activities against a broad spectrum of bacteria or the positive effects on cellular behaviors during wound repair [61, 116].

Therefore, it was particularly interesting whether the combination of both, Tylotoin and sC18*, would lead to an efficient peptide conjugate with antimicrobial activity.

Hence, the antimicrobial effect of Tylotoin-sC18* as well as Tylotoin and sC18* alone was tested within a concentration range of 2.5 to 25 µM against *M. luteus* as representative for gram-positive bacteria and *S. typhimurium* as representative of gram-negative bacteria using INT-assay.

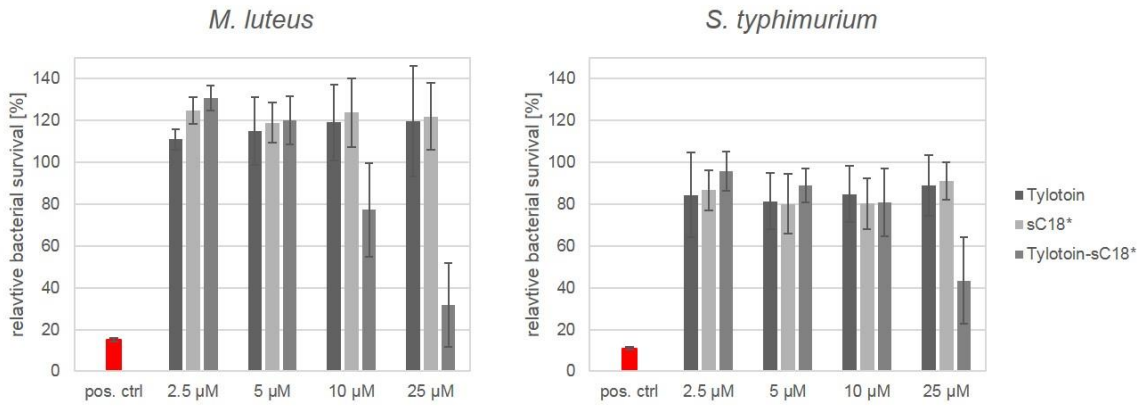

Figure 48. Antimicrobial effect of peptides against gram-positive and gram-negative bacteria. *M. luteus* and *S. typhimurium* were incubated with indicated concentrations of peptides at 37 °C. After 6 h of incubation, bacterial survival is expressed as percentage with respect to water-treated bacteria using INT assay. Treatment with 70% EtOH served as positive control. Experiments were achieved in triplicate with *n = 2*. Error bars represent standard deviation.

As illustrated in Figure 48, the parent peptides Tylotoin and sC18* revealed no toxic effect against the gram-positive bacteria within the defined concentration range. Moreover, due to conditions of stress caused through peptides, the growth of *M. luteus* was slightly increased. However, the novel peptide conjugate revealed the strongest activity against the gram-positive bacteria, thus relative bacterial survival was diminished by about 20% at 10 µM and decreased further to 30% of living bacteria at a peptide concentration of 25 µM. Similar results were obtained when gram-negative bacteria were incubated with peptides for 6 h as depicted in the right panel of Figure 48. Here again, Tylotoin-sC18* revealed antimicrobial effects at higher concentration against *S. typhimurium*, while Tylotoin and sC18* alone showed no antimicrobial activities.

Consequently, since parent peptides do not show any toxic effects at all, it can be assumed that the combination of both peptides leads to an efficient peptide conjugate with indeed significant antimicrobial activity in a concentration-dependent manner against both gram-

positive and gram-negative bacteria. Moreover, considering that anionic phospholipid headgroups are not only related to cancer cells but also a main constituent of bacteria lipid bilayer [135, 184], these findings provide further support for the hypothesis that peptides with positively charged amino acids accompanied by an amphipathic character are essential for the initial step of cell entry as well as for the interaction with bacterial membranes.

Finally, owing to multiple features obtained for Tylotoin-sC18*, including antimicrobial as well as wound healing activities, this novel designed peptide conjugate Tylotoin-sC18* may represent a promising agent for new therapeutic approaches in the treatment of infected wounds.

5. Conclusion and outlook

CPPs and the interaction with membrane components

Over the recent decade, cell-penetrating peptides have gained extensive interest due to their capability to penetrate the cell membrane and even more to deliver a wide range of various bioactive molecules inside the cells, which would otherwise be unable to cross the membrane barrier because of their size and hydrophilic nature [71, 84]. Thus, CPPs have emerged as very promising delivery vehicles in the field of therapeutic agents [16, 84].

So far, a large body of literature exists that reported on the development and modification of new CPPs to further improve their internalization efficacy, specificity and the cellular delivery of therapeutic agents [55, 207]. Despite that, the cellular mechanism behind is still a subject under debate and has to be urgently resolved [111]. For this purpose, great efforts have been put into the clarification of peptides mode of action. Thereby, the employment of artificial membrane systems has lately gained widespread popularity to comprehend the molecular requirements and mechanism of cell entry.

In this thesis, different biophysical techniques, which are accompanied by the use of model membrane systems, were successfully established with the final goal to gather important and useful information about cell-penetrating peptides initial step of cell entry. Thus, one focus laid on assessing the interaction between two variants of structural modified CPPs and different lipid membrane systems. Recently, we reported on structural modifications of the cationic CPP sC18 with the aim to enhance its efficiency as cell-penetrating peptide [68, 77, 78]. More precisely, on the one hand, the peptide backbone of the shortened variant of sC18 was cyclized resulting in cyclic structures varying in size and on the other hand, a branched dimeric version of sC18 and sC18* was employed.

Herein, by using large and giant unilamellar vesicles, the essential role of negatively charged lipids for cationic cell-penetrating peptides in cellular translocation was underlined, despite whether the peptides were branched or cyclic. Thus, as a first step, binding of the CPPs to anionic lipids would occur mainly by electrostatic interactions through the hydrophilic nature of the CPPs.

In case of dimeric peptide variants, the enhanced interaction with the anionic model membranes, mimicking cancer cells, was further accompanied by stronger membrane perturbation effects compared to monomeric control peptides. These observations were confirmed by the peptide-induced dye release experiments. In this set-up, a rapid and efficient CF release in a matter of a few minutes was detected, and might indicate pore forming events. Overall, the preferential accumulation with anionic lipids and the

membrane-active properties might be related to the high charge density of the dimeric peptides over their monomeric versions.

From this point, it is quite interesting that several studies reported on the enhanced anionic nature of cancer cell membranes [85, 86] when considering the stated selectivity of $(sC18)_2$ towards tumor cells [68, 78]. Consequently, the enhanced interactions with negatively charged membranes might be contributed to its effectiveness as a lytic anticancer peptide.

Moreover, cholesterol was turned out to play an important role in initial membrane binding and peptides membrane disrupting activity in large unilamellar vesicles mimicking lipid-raft domains. Abolishing the formation of liquid-ordered domains by cholesterol extraction using MβCD resulted in significantly diminished uptake efficiency of $(sC18)_2$ as observed for HEK- 293 and MCF-7 cells as representatives of healthy and cancer cells, respectively. In agreement with the literature, several publications underlined that cholesterol extraction led to a remarkable diminution in the internalization efficiency of the well-characterized Tat peptide [90] and penetratin [105], a result which was assumed to be related to the inhibition of raft-dependent endocytosis of these peptides [175]. Thus, it might indeed be possible that $(sC18)_2$ penetrates the cells, besides direct translocation, via raft-dependent endocytosis, since a crucial role in endocytosis is attributed to cholesterol [80].

However, judging from the aspect that one of the unresolved subjects in the application field of CPPs in therapeutics relates to the lack of selectivity towards targeted cells or intracellular compartments [85], these results might provide initial insights of molecular requirements important to improve their *in vivo* efficiency and target-specificity.

Focusing on cyclic peptide variants, the high content of negatively charged phospholipids within vesicle membranes has also increased their binding affinity as observed from microscopic and flow cytometric analysis. Together with previously mentioned observations, this further supports the idea that electrostatic interaction is indeed responsible for the initial binding of sC18 conjugates to plasma membranes.

Furthermore, the structural arrangement of peptides seems to play a role as well in peptide-membrane interactions [130, 171]. Thus, CD spectroscopy revealed that of course the small cycle cyc1 and its linear counterpart attained a transition to an α-helical formation when in contact with negatively charged LUVs. Despite the strong binding affinity of cyc3 to anionic lipids, no obvious secondary structure conformation could be obtained. These findings were additionally corroborated by solution phase NMR studies shown by Horn *et al.* [77]. Here, the structures of the linear peptide sC18* and the large-sized cycle cyc3 were examined in the presence of SDS micelles as a membrane-mimetic environment. The NMR spectroscopy of the linear counterpart revealed a short helical fragment between the

residues R3 - R7 at the *N*-terminus. On the contrary, cyc3 did not show any secondary structural motif even if the final structure is not completely unordered [77].

However, the ability of cyc3 to interact with both neutral and anionic LUVs might be attributed to the flexibility of the larger ring size enabling cyc3 to adopt the most suitable structure required for efficient interaction with the membrane bilayer. Therefore, a certain flexibility and thus the static arrangement of the guanidinium groups within the large cycle seems to positively affect peptide-membrane interaction, thus leading to cellular uptake.

Additionally, for these cyclic peptides, it was aimed to elucidate in more detail how cells plasma membrane compounds affect peptides cell entry in conditions lacking endocytosis. Herein, the findings suggest that some membrane proteins embedded within the vesicle membrane could specifically increase the peptide uptake across the cell membrane. However, further investigation is required.

Finally, the present data let one assume that the lipid composition of the target membrane plays a critical role in the initial stage of cell contact and thus peptides mode of action. The modified peptide variants of sC18 demonstrated improved binding and membrane activities over their linear counterpart sC18 and sC18*.

Beyond that, this study demonstrates the usefulness of plasma membrane vesicles as membrane models in biophysical studies of investigating peptide-membrane interactions in order to provide new and detailed molecular understanding of how CPPs interact with the cellular membrane of eukaryotic cells. Even though, these results cannot be directly translated into peptides mode of action, it can provide a good starting point to develop peptides with improved uptake efficiencies and moreover with specific cell or tissue selectivity.

Nevertheless, the next step would be to analyze the exact lipid composition of the plasma membrane of the cell lines used, since it has been assumed that the uptake mechanism of our peptide conjugates is dependent of a certain membrane composition and microdomain organization. This could be achieved by plasma membrane isolation of HEK-293 and MCF- 7 cells using sucrose density centrifugation accompanied by lipid detection via mass spectroscopy [195, 202]. Using this method, Wallbrecher *et al.* demonstrated lately that the plasma membrane of HEK-293 contains only minor amounts of sphingomyelin compared to HeLa cells. This probably resulted in a more resistant membrane for HeLa cells, a result interpreted as reason why nona-arginine (R9) entered HEK cells by direct penetration already at low concentrations [195].

Finally, once taken up into cells, the CPPs might interact and translocate across membranes of different compositions when entering or escaping the different intracellular

organelles. Therefore, the knowledge about lipids present in the membranes should be increased in order to understand the peptide-lipid relationship.

CPPs and wound repair

Wound repair is an evolutionarily conserved process among species [12, 178]. However, this complex process differs between mammalians and amphibians. Hence, lower vertebrates, e.g. axolotl or *Xenopus* are capable of scarless wound healing and to regenerate fully functional limbs [108, 205] in an incredible quick time when compared to wound healing in mammalians [126] making this field highly attractive to study.

Recently, Mu *et al.* highlighted Tylotoin, a short peptide identified from salamander skin, as a potent template for the development of novel wound healing agents due to its efficient wound healing abilities [126]. In this thesis, a wound healing promoting peptide and a cell-penetrating peptide were combined for the first time with the ultimate goal to improve the delivery of Tylotoin across the cell membrane. Moreover, the ability of sC18* to further improve the migration of keratinocytes was evaluated. Since keratinocytes are key cellular components of the epidermis, which are involved in wound healing, the investigation could further shed light on a potential wound healing efficacy.

The structural analysis using circular dichroism spectroscopy revealed that the presence of sC18 supported the transition to an α-helical conformation for the chimeric peptides in a membrane-mimetic environment. Moreover, the fusion of the CPP to the *C*-terminal part of Tylotoin leads to a better hydrophobic/hydrophilic balance allowing optimal interaction of the peptide conjugates with the amphiphilic nature of biological membranes.

Nevertheless, so far, nothing is known about the translocation mechanism of Tylotoin into mammalian cells. Therefore, the uptake of *N*-terminally 5(6)-carboxyfluorescein labeled peptide conjugates into skin cells and HeLa cells, as representative for cancer cells, was studied by confocal laser scanning microscopy and flow cytometry. The chimeric peptides were found to exhibit improved cellular internalization efficiencies compared to the parent peptides. In addition, the observed vesicular structures within the cytosol speak in favor for an uptake mechanism via endocytosis. However, in the presence of dynasore, an endocytosis inhibitor, and at lower temperature, the cellular uptake was diminished but to our surprise, the chimeric peptide Tylotoin-sC18* was still localized within the cytosol in punctuate pattern and moreover in the nucleoli leading to the assumption that the conjugate can penetrate the cells also via direct translocation.

Though, since these vesicular structures were still observed even when endocytosis is totally suppressed and the peptide signal did not match with any organelle tracker used,

these findings might arise the hypothesis that the peptides get intracellularly aggregated over time.

Form this point, it will be interesting to investigate the internalization pathway in more detail. One concept could be to model the endosomal escape using giant unilamellar vesicles [112, 143], since Qian *et al.* postulated a new mechanism of CPP uptake, shown in the following figure.

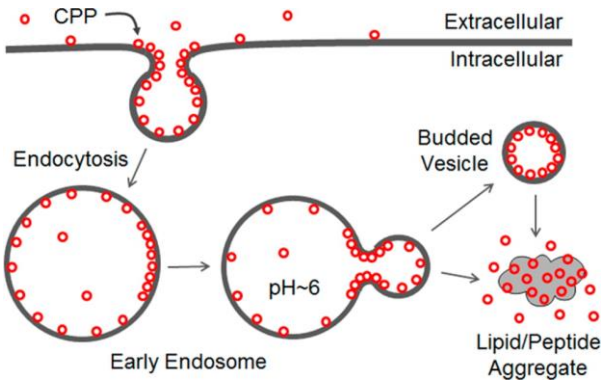

Figure 49. A novel mechanistic model for the endosomal escape process. (adapted from Qian *et al.*, 2016 [143])

This novel proposed mechanism based on the idea that the CPPs were taken up via endocytosis, CPPs subsequently bind to the lumen of the endosomal membrane, which finally leads to vesicle budding and/or peptide/lipid aggregates [143]. Therefore, giant unilamellar vesicles could be prepared mimicking the lipid composition of early and late endosomes to study the effect of different pH values e.g. to mimic the acidic environment in late endosome and thus the mode of action. Furthermore, it will be interesting to generate model membrane systems encapsulating the peptide in the lumen due to the fact that during endocytosis, peptides are trapped inside the endosomes.

Beyond that, it could be shown that the fusion of the cell-penetrating peptide to Tylotoin did not result in a loss of Tylotoins activity, on the contrary, Tylotoin-sC18* might further improve the wound healing promoting ability of Tylotoin as illustrated by the activity to promote *in vitro* wound closure by inducing migration and proliferation of keratinocytes. A next step would be the delivery of Tylotoin-sC18* across the skin. Besides *in vitro* cell culture models, several models for wound repair exist including *in vivo* human and animal skin models as well as *ex vivo* models, e.g. full-thickness skin models [1, 54, 164]. Since animal models, in particular rodents, do not accurately represent the structure of the human skin and owing to ethical and moral issues, the need for alternative skin models is essential [1, 187]. The use of artificial and reconstructed human skin equivalents is therefore receiving more attention [54]. Artificial *in vitro* skin models range from simple homogenous polymer materials, e.g. silicone membranes through to lipid-based models [1, 54]. Whereas reconstructed skin models are cell culture-based models containing layers of human cells

in culture laid down over a polymeric matrix [54]. Although *in vitro* models are sufficient to identify the key underlying mechanisms and to aim a better understanding of the process of wound repair, *in vivo* experiments are indispensable for effective drug development [11].

Concerning the molecular mechanism behind, several studies reported on the involvement of the epidermal growth factor receptor (EGFR) in the peptide-induced signaling pathway controlling keratinocytes migration [44, 138, 182]. However, Tylotoin-sC18* does not induce cell migration via the EGF/EGFR signaling pathway. Besides the epidermal growth factor, numerous other growth factors as well as cytokines participate in the wound healing process, e.g. transforming growth factors (TGF-βs), fibroblast and vascular endothelial growth factors, as well as several proinflammatory cytokines [19]. Since Mu *et al.* could already show that Tylotoin is able to induce TGF-β1 secretion *in vitro* and *in vivo* models, it should be interesting whether the conjugate Tylotoin-sC18* stimulates the release of TGF-β1 and transactivates components of downstream TGF-β signaling, such as Smad2 and Smad2, as well [126]. Also, the MAPK (mitogen-activated protein kinase) pathway is likely involved in the regulation of keratinocytes migration [12]. Therefore, several approaches could be further investigated with the final attempt to identify the molecular mechanism.

Nonetheless, Tylotoin-sC18* exhibited improved antimicrobial activity against representatives of gram-positive and -negative bacteria which is quite impressive since efficient wound healing is often hampered by bacterial infections [124]. Furthermore, the cellular uptake into the cancer cell line was much higher compared to skin cells, which might be contributed to the slightly higher toxicity of chimeric peptides against HeLa cells. Therefore, further studies will have to show whether these novel peptide conjugates may exhibit a certain selectivity towards cancer cells.

Finally, with this potent conjugate in hand showing antimicrobial and wound healing promoting activities and moreover being non-toxic towards keratinocytes, a novel promising agent might be identified for new therapeutic approaches in the treatment of infected wounds.

6. References

1. **Abd, E., Yousef, S. A., Pastore, M. N., Telaprolu, K., Mohammed, Y. H., Namjoshi, S., Grice, J. E., and Roberts, M. S. (2016)** Skin models for the testing of transdermal drugs. *Clin Pharmacol* 8, 163-176
2. **Agerberth, B., Gunne, H., Odeberg, J., Kogner, P., Boman, H. G., and Gudmundsson, G. H. (1995)** Fall-39, a Putative Human Peptide Antibiotic, Is Cysteine-Free and Expressed in Bone-Marrow and Testis. *Proceedings of the National Academy of Sciences of the United States of America* 92, 195-199
3. **Akashi, K., Miyata, H., Itoh, H., and Kinosita, K., Jr. (1996)** Preparation of giant liposomes in physiological conditions and their characterization under an optical microscope. *Biophysical journal* 71, 3242-3250
4. **Akbarzadeh, A., Rezaei-Sadabady, R., Davaran, S., Joo, S. W., Zarghami, N., Hanifehpour, Y., Samiei, M., Kouhi, M., and Nejati-Koshki, K. (2013)** Liposome: classification, preparation, and applications. *Nanoscale research letters* 8, 102
5. **Alberts, B., Johnson, A., Lewis, J., Walter, P., Raff, M., and Roberts, K.** (2002) *Molecular Biology of the Cell 4th Edition: International Student Edition*, Routledge
6. **Alves, I. D., Walrant, A., Bechara, C., and Sagan, S. (2012)** Is there anybody in there? On the mechanisms of wall crossing of cell penetrating peptides. *Current protein & peptide science* 13, 658-671
7. **Amand, H. L., Bostrom, C. L., Lincoln, P., Norden, B., and Esbjorner, E. K. (2011)** Binding of cell-penetrating penetratin peptides to plasma membrane vesicles correlates directly with cellular uptake. *Biochimica et biophysica acta* 1808, 1860-1867
8. **Amand, H. L., Rydberg, H. A., Fornander, L. H., Lincoln, P., Norden, B., and Esbjorner, E. K. (2012)** Cell surface binding and uptake of arginine- and lysine-rich penetratin peptides in absence and presence of proteoglycans. *Biochimica et biophysica acta* 1818, 2669-2678
9. **Ando, Y., and Jensen, P. J. (1993)** Epidermal growth factor and insulin-like growth factor I enhance keratinocyte migration. *The Journal of investigative dermatology* 100, 633-639
10. **Angelova, M. I., and Dimitrov, D. S. (1986)** Liposome Electroformation. *Faraday Discuss* 81, 303
11. **Ansell, D. M., Holden, K. A., and Hardman, M. J. (2012)** Animal models of wound repair: Are they cutting it? *Experimental dermatology* 21, 581-585
12. **Barrientos, S., Stojadinovic, O., Golinko, M. S., Brem, H., and Tomic-Canic, M. (2008)** Growth factors and cytokines in wound healing. *Wound repair and*

regeneration : official publication of the Wound Healing Society [and] the European Tissue Repair Society 16, 585-601

13. **Baum, C. L., and Arpey, C. J. (2005)** Normal cutaneous wound healing: clinical correlation with cellular and molecular events. *Dermatologic surgery : official publication for American Society for Dermatologic Surgery [et al.]* 31, 674-686; discussion 686
14. **Baumgart, T., Hammond, A. T., Sengupta, P., Hess, S. T., Holowka, D. A., Baird, B. A., and Webb, W. W. (2007)** Large-scale fluid/fluid phase separation of proteins and lipids in giant plasma membrane vesicles. *Proceedings of the National Academy of Sciences of the United States of America* 104, 3165-3170
15. **Baumgart, T., Hunt, G., Farkas, E. R., Webb, W. W., and Feigenson, G. W. (2007)** Fluorescence probe partitioning between Lo/Ld phases in lipid membranes. *Biochimica et biophysica acta* 1768, 2182-2194
16. **Bechara, C., and Sagan, S. (2013)** Cell-penetrating peptides: 20 years later, where do we stand? *FEBS letters* 587, 1693-1702
17. **Bechara, C., Pallerla, M., Burlina, F., Illien, F., Cribier, S., and Sagan, S. (2015)** Massive glycosaminoglycan-dependent entry of Trp-containing cell-penetrating peptides induced by exogenous sphingomyelinase or cholesterol depletion. *Cellular and molecular life sciences : CMLS* 72, 809-820
18. **Bergmann, R., Splith, K., Pietzsch, J., Bachmann, M., and Neundorf, I. (2017)** Biological characterization of novel nitroimidazole-peptide conjugates in vitro and in vivo. *Journal of peptide science : an official publication of the European Peptide Society* 23, 597-609
19. **Bielefeld, K. A., Amini-Nik, S., and Alman, B. A. (2013)** Cutaneous wound healing: recruiting developmental pathways for regeneration. *Cellular and molecular life sciences : CMLS* 70, 2059-2081
20. **Binder, H., and Lindblom, G. (2003)** Charge-dependent translocation of the Trojan peptide penetratin across lipid membranes. *Biophysical journal* 85, 982-995
21. **Bouwstra, J. A., and Honeywell-Nguyen, P. L. (2002)** Skin structure and mode of action of vesicles. *Advanced drug delivery reviews* 54 Suppl 1, S41-55
22. **Bouwstra, J. A., Honeywell-Nguyen, P. L., Gooris, G. S., and Ponec, M. (2003)** Structure of the skin barrier and its modulation by vesicular formulations. *Progress in lipid research* 42, 1-36
23. **Brender, J. R., McHenry, A. J., and Ramamoorthy, A. (2012)** Does cholesterol play a role in the bacterial selectivity of antimicrobial peptides? *Frontiers in immunology* 3, 195

24. **Bretscher, M. S. (1985)** The molecules of the cell membrane. *Scientific American* 253, 100-108
25. **Cahill, K. (2009)** Molecular electroporation and the transduction of oligoarginines. *Physical biology* 7, 16001
26. **Calder, P. C., and Yaqoob, P. (2007)** Lipid rafts--composition, characterization, and controversies. *The Journal of nutrition* 137, 545-547
27. **Carretero, M., Escamez, M. J., Garcia, M., Duarte, B., Holguin, A., Retamosa, L., Jorcano, J. L., Rio, M. D., and Larcher, F. (2008)** In vitro and in vivo wound healing-promoting activities of human cathelicidin LL-37. *The Journal of investigative dermatology* 128, 223-236
28. **Celentano, V., Diana, D., De Rosa, L., Romanelli, A., Fattorusso, R., and D'Andrea, L. D. (2012)** beta-Hairpin stabilization through an interstrand triazole bridge. *Chemical communications* 48, 762-764
29. **Cerrato, C. P., Kunnapuu, K., and Langel, U. (2017)** Cell-penetrating peptides with intracellular organelle targeting. *Expert opinion on drug delivery* 14, 245-255
30. **Chakrabarti, A., Witsenburg, J. J., Sinzinger, M. D., Richter, M., Wallbrecher, R., Cluitmans, J. C., Verdurmen, W. P., Tanis, S., Adjobo-Hermans, M. J., Rademann, J., and Brock, R. (2014)** Multivalent presentation of the cell-penetrating peptide nona-arginine on a linear scaffold strongly increases its membrane-perturbing capacity. *Biochimica et biophysica acta* 1838, 3097-3106
31. **Chen, J., Li, H., and Chen, J. (2017)** Human epidermal growth factor coupled to different structural classes of cell penetrating peptides: A comparative study. *International journal of biological macromolecules*
32. **Chen, K. L., and Bothun, G. D. (2014)** Nanoparticles meet cell membranes: probing nonspecific interactions using model membranes. *Environmental science & technology* 48, 873-880
33. **Chereddy, K. K., Her, C. H., Comune, M., Moia, C., Lopes, A., Porporato, P. E., Vanacker, J., Lam, M. C., Steinstraesser, L., Sonveaux, P., Zhu, H. J., Ferreira, L. S., Vandermeulen, G., and Preat, V. (2014)** PLGA nanoparticles loaded with host defense peptide LL37 promote wound healing. *Journal of Controlled Release* 194, 138-147
34. **Chung, E. M. C., Dean, S. N., Propst, C. N., Bishop, B. M., and van Hoek, M. L. (2017)** Komodo dragon-inspired synthetic peptide DRGN-1 promotes wound-healing of a mixed-biofilm infected wound. *NPJ biofilms and microbiomes* 3, 9
35. **Ciobanasu, C., Siebrasse, J. P., and Kubitscheck, U. (2010)** Cell-penetrating HIV1 TAT peptides can generate pores in model membranes. *Biophysical journal* 99, 153-162

36. **Copolovici, D. M., Langel, K., Eriste, E., and Langel, U. (2014)** Cell-penetrating peptides: design, synthesis, and applications. *ACS nano* 8, 1972-1994
37. **Czogalla, A., Grzybek, M., Jones, W., and Coskun, U. (2014)** Validity and applicability of membrane model systems for studying interactions of peripheral membrane proteins with lipids. *Biochimica et biophysica acta* 1841, 1049-1059
38. **D'Hondt, K., Heese-Peck, A., and Riezman, H. (2000)** Protein and lipid requirements for endocytosis. *Annual review of genetics* 34, 255-295
39. **Das, S., and Baker, A. B. (2016)** Biomaterials and Nanotherapeutics for Enhancing Skin Wound Healing. *Frontiers in bioengineering and biotechnology* 4, 82
40. **Derossi, D., Joliot, A. H., Chassaing, G., and Prochiantz, A. (1994)** The third helix of the Antennapedia homeodomain translocates through biological membranes. *The Journal of biological chemistry* 269, 10444-10450
41. **Desai, P., Patlolla, R. R., and Singh, M. (2010)** Interaction of nanoparticles and cell-penetrating peptides with skin for transdermal drug delivery. *Molecular membrane biology* 27, 247-259
42. **Deshayes, S., Plenat, T., Aldrian-Herrada, G., Divita, G., Le Grimellec, C., and Heitz, F. (2004)** Primary amphipathic cell-penetrating peptides: structural requirements and interactions with model membranes. *Biochemistry* 43, 7698-7706
43. **Di Grazia, A., Luca, V., Segev-Zarko, L. A., Shai, Y., and Mangoni, M. L. (2014)** Temporins A and B stimulate migration of HaCaT keratinocytes and kill intracellular Staphylococcus aureus. *Antimicrobial agents and chemotherapy* 58, 2520-2527
44. **Di Grazia, A., Cappiello, F., Imanishi, A., Mastrofrancesco, A., Picardo, M., Paus, R., and Mangoni, M. L. (2015)** The Frog Skin-Derived Antimicrobial Peptide Esculentin-1a(1-21)NH2 Promotes the Migration of Human HaCaT Keratinocytes in an EGF Receptor-Dependent Manner: A Novel Promoter of Human Skin Wound Healing? *PloS one* 10, e0128663
45. **Di, J., Huang, H., Qu, D., Tang, J., Cao, W., Lu, Z., Cheng, Q., Yang, J., Bai, J., Zhang, Y., and Zheng, J. (2015)** Rap2B promotes proliferation, migration, and invasion of human breast cancer through calcium-related ERK1/2 signaling pathway. *Scientific reports* 5, 12363
46. **Di Pisa, M., Chassaing, G., and Swiecicki, J. M. (2015)** Translocation mechanism(s) of cell-penetrating peptides: biophysical studies using artificial membrane bilayers. *Biochemistry* 54, 194-207
47. **Dinca, A., Chien, W. M., and Chin, M. T. (2016)** Intracellular Delivery of Proteins with Cell-Penetrating Peptides for Therapeutic Uses in Human Disease. *International journal of molecular sciences* 17, 263

48. **Domingues, T. M., Mattei, B., Seelig, J., Perez, K. R., Miranda, A., and Riske, K. A. (2013)** Interaction of the antimicrobial peptide gomesin with model membranes: a calorimetric study. *Langmuir : the ACS journal of surfaces and colloids* 29, 8609-8618

49. **Edidin, M. (2003)** The state of lipid rafts: from model membranes to cells. *Annual review of biophysics and biomolecular structure* 32, 257-283

50. **Eiriksdottir, E., Konate, K., Langel, U., Divita, G., and Deshayes, S. (2010)** Secondary structure of cell-penetrating peptides controls membrane interaction and insertion. *Biochimica et biophysica acta* 1798, 1119-1128

51. **Esbjörner, E. K., Gräslund, A., and Nordén, B.** (2006) Membrane Interactions of Cell-Penetrating Peptides. In *Handbook of Cell-Penetrating Peptides, Second Edition* pp. 109-137, CRC Press

52. **Farkhani, S. M., Valizadeh, A., Karami, H., Mohammadi, S., Sohrabi, N., and Badrzadeh, F. (2014)** Cell penetrating peptides: Efficient vectors for delivery of nanoparticles, nanocarriers, therapeutic and diagnostic molecules. *Peptides* 57, 78-94

53. **Favretto, M. E., Wallbrecher, R., Schmidt, S., van de Putte, R., and Brock, R. (2014)** Glycosaminoglycans in the cellular uptake of drug delivery vectors - bystanders or active players? *Journal of controlled release : official journal of the Controlled Release Society* 180, 81-90

54. **Flaten, G. E., Palac, Z., Engesland, A., Filipovic-Grcic, J., Vanic, Z., and Skalko-Basnet, N. (2015)** In vitro skin models as a tool in optimization of drug formulation. *Eur J Pharm Sci* 75, 10-24

55. **Fominaya, J., Bravo, J., and Rebollo, A. (2015)** Strategies to stabilize cell penetrating peptides for in vivo applications. *Therapeutic delivery* 6, 1171-1194

56. **Formaggio, F., and Toniolo, C. (2010)** Electronic and vibrational signatures of peptide helical structures: A tribute to Anton Mario Tamburro. *Chirality* 22 Suppl 1, E30-39

57. **Frankel, A. D., and Pabo, C. O. (1988)** Cellular Uptake of the Tat Protein from Human Immunodeficiency Virus. *Cell* 55, 1189-1193

58. **Fuchs, E., and Raghavan, S. (2002)** Getting under the skin of epidermal morphogenesis. *Nature reviews. Genetics* 3, 199-209

59. **Futaki, S., Suzuki, T., Ohashi, W., Yagami, T., Tanaka, S., Ueda, K., and Sugiura, Y. (2001)** Arginine-rich peptides. An abundant source of membrane-permeable peptides having potential as carriers for intracellular protein delivery. *The Journal of biological chemistry* 276, 5836-5840

60. **Galdiero, S., Falanga, A., Cantisani, M., Vitiello, M., Morelli, G., and Galdiero, M. (2013)** Peptide-lipid interactions: experiments and applications. *International journal of molecular sciences* 14, 18758-18789

61. **Ge, Y., MacDonald, D. L., Holroyd, K. J., Thornsberry, C., Wexler, H., and Zasloff, M. (1999)** In vitro antibacterial properties of pexiganan, an analog of magainin. *Antimicrobial agents and chemotherapy* 43, 782-788

62. **Geldmacher, Y., Splith, K., Kitanovic, I., Alborzinia, H., Can, S., Rubbiani, R., Nazif, M. A., Wefelmeier, P., Prokop, A., Ott, I., Wolfl, S., Neundorf, I., and Sheldrick, W. S. (2012)** Cellular impact and selectivity of half-sandwich organorhodium(III) anticancer complexes and their organoiridium(III) and trichloridorhodium(III) counterparts. *Journal of biological inorganic chemistry : JBIC : a publication of the Society of Biological Inorganic Chemistry* 17, 631-646

63. **Glukhov, E., Stark, M., Burrows, L. L., and Deber, C. M. (2005)** Basis for selectivity of cationic antimicrobial peptides for bacterial versus mammalian membranes. *The Journal of biological chemistry* 280, 33960-33967

64. **Gopal, R., Lee, J. K., Lee, J. H., Kim, Y. G., Oh, G. C., Seo, C. H., and Park, Y. (2013)** Effect of repetitive lysine-tryptophan motifs on the eukaryotic membrane. *International journal of molecular sciences* 14, 2190-2202

65. **Gorter, E., and Grendel, F. (1925)** On Bimolecular Layers of Lipoids on the Chromocytes of the Blood. *The Journal of experimental medicine* 41, 439-443

66. **Green, M., and Loewenstein, P. M. (1988)** Autonomous Functional Domains of Chemically Synthesized Human Immunodeficiency Virus Tat Trans-Activator Protein. *Cell* 55, 1179-1188

67. **Greenhalgh, D. G. (1996)** The role of growth factors in wound healing. *The Journal of trauma* 41, 159-167

68. **Gronewold, A., Horn, M., Randelovic, I., Tovari, J., Munoz Vazquez, S., Schomacker, K., and Neundorf, I. (2017)** Characterization of a Cell-Penetrating Peptide with Potential Anticancer Activity. *ChemMedChem* 12, 42-49

69. **Guo, Z., Peng, H., Kang, J., and Sun, D. (2016)** Cell-penetrating peptides: Possible transduction mechanisms and therapeutic applications. *Biomedical reports* 4, 528-534

70. **Guo, Z. R., Peng, H. Y., Kang, J. W., and Sun, D. X. (2016)** Cell-penetrating peptides: Possible transduction mechanisms and therapeutic applications. *Biomedical reports* 4, 528-534

71. **Gupta, B., Levchenko, T. S., and Torchilin, V. P. (2005)** Intracellular delivery of large molecules and small particles by cell-penetrating proteins and peptides. *Advanced drug delivery reviews* 57, 637-651

72. **Hao, M., Mukherjee, S., Sun, Y., and Maxfield, F. R. (2004)** Effects of cholesterol depletion and increased lipid unsaturation on the properties of endocytic membranes. *The Journal of biological chemistry* 279, 14171-14178

73. **Hardwicke, J., Schmaljohann, D., Boyce, D., and Thomas, D. (2008)** Epidermal growth factor therapy and wound healing--past, present and future perspectives. *The surgeon : journal of the Royal Colleges of Surgeons of Edinburgh and Ireland* 6, 172-177

74. **Heitz, F., Morris, M. C., and Divita, G. (2009)** Twenty years of cell-penetrating peptides: from molecular mechanisms to therapeutics. *British journal of pharmacology* 157, 195-206

75. **Herce, H. D., Garcia, A. E., Litt, J., Kane, R. S., Martin, P., Enrique, N., Rebolledo, A., and Milesi, V. (2009)** Arginine-rich peptides destabilize the plasma membrane, consistent with a pore formation translocation mechanism of cell-penetrating peptides. *Biophysical journal* 97, 1917-1925

76. **Horger, K. S., Estes, D. J., Capone, R., and Mayer, M. (2009)** Films of agarose enable rapid formation of giant liposomes in solutions of physiologic ionic strength. *Journal of the American Chemical Society* 131, 1810-1819

77. **Horn, M., Reichart, F., Natividad-Tietz, S., Diaz, D., and Neundorf, I. (2016)** Tuning the properties of a novel short cell-penetrating peptide by intramolecular cyclization with a triazole bridge. *Chemical communications* 52, 2261-2264

78. **Hoyer, J., Schatzschneider, U., Schulz-Siegmund, M., and Neundorf, I. (2012)** Dimerization of a cell-penetrating peptide leads to enhanced cellular uptake and drug delivery. *Beilstein journal of organic chemistry* 8, 1788-1797

79. **Hu, W., Splith, K., Neundorf, I., Merz, K., and Schatzschneider, U. (2012)** Influence of the metal center and linker on the intracellular distribution and biological activity of organometal-peptide conjugates. *Journal of biological inorganic chemistry : JBIC : a publication of the Society of Biological Inorganic Chemistry* 17, 175-185

80. **Imelli, N., Meier, O., Boucke, K., Hemmi, S., and Greber, U. F. (2004)** Cholesterol is required for endocytosis and endosomal escape of adenovirus type 2. *Journal of virology* 78, 3089-3098

81. **Iozzo, R. V., and Schaefer, L. (2015)** Proteoglycan form and function: A comprehensive nomenclature of proteoglycans. *Matrix biology : journal of the International Society for Matrix Biology* 42, 11-55

82. **Islam, M. Z., Alam, J. M., Tamba, Y., Karal, M. A., and Yamazaki, M. (2014)** The single GUV method for revealing the functions of antimicrobial, pore-forming toxin, and cell-penetrating peptides or proteins. *Physical chemistry chemical physics : PCCP* 16, 15752-15767

83. **Islam, M. Z., Ariyama, H., Alam, J. M., and Yamazaki, M. (2014)** Entry of cell-penetrating peptide transportan 10 into a single vesicle by translocating across lipid membrane and its induced pores. *Biochemistry* 53, 386-396
84. **Järver, P., Mager, I., and Langel, U. (2010)** In vivo biodistribution and efficacy of peptide mediated delivery. *Trends in pharmacological sciences* 31, 528-535
85. **Jobin, M. L., Bonnafous, P., Temsamani, H., Dole, F., Grelard, A., Dufourc, E. J., and Alves, I. D. (2013)** The enhanced membrane interaction and perturbation of a cell penetrating peptide in the presence of anionic lipids: toward an understanding of its selectivity for cancer cells. *Biochimica et biophysica acta* 1828, 1457-1470
86. **Jobin, M. L., and Alves, I. D. (2014)** On the importance of electrostatic interactions between cell penetrating peptides and membranes: a pathway toward tumor cell selectivity? *Biochimie* 107 Pt A, 154-159
87. **Jobin, M. L., Blanchet, M., Henry, S., Chaignepain, S., Manigand, C., Castano, S., Lecomte, S., Burlina, F., Sagan, S., and Alves, I. D. (2015)** The role of tryptophans on the cellular uptake and membrane interaction of arginine-rich cell penetrating peptides. *Biochimica et biophysica acta* 1848, 593-602
88. **Kaiser, E., Colescott, R. L., Bossinger, C. D., and Cook, P. I. (1970)** Color test for detection of free terminal amino groups in the solid-phase synthesis of peptides. *Analytical biochemistry* 34, 595-598
89. **Kamoun, E. A., Kenawy, E. S., and Chen, X. (2017)** A review on polymeric hydrogel membranes for wound dressing applications: PVA-based hydrogel dressings. *Journal of advanced research* 8, 217-233
90. **Kaplan, I. M., Wadia, J. S., and Dowdy, S. F. (2005)** Cationic TAT peptide transduction domain enters cells by macropinocytosis. *Journal of controlled release : official journal of the Controlled Release Society* 102, 247-253
91. **Katayama, S., Nakase, I., Yano, Y., Murayama, T., Nakata, Y., Matsuzaki, K., and Futaki, S. (2013)** Effects of pyrenebutyrate on the translocation of arginine-rich cell-penetrating peptides through artificial membranes: recruiting peptides to the membranes, dissipating liquid-ordered phases, and inducing curvature. *Biochimica et biophysica acta* 1828, 2134-2142
92. **Kelly, S. M., and Price, N. C. (2000)** The Use of Circular Dichroism in the Investigation of Protein Structure and Function. *Current protein & peptide science* 1, 349-384
93. **Kim, D. J., Lee, Y. W., Park, M. K., Shin, J. R., Lim, K. J., Cho, J. H., and Kim, S. C. (2014)** Efficacy of the designer antimicrobial peptide SHAP1 in wound healing and wound infection. *Amino acids* 46, 2333-2343

94. **Kirsner, R. S., and Eaglstein, W. H. (1993)** The wound healing process. *Dermatologic clinics* 11, 629-640

95. **Kolditz, F., Krausze, J., Heinz, D. W., Niemann, H. H., and Muller-Goymann, C. C. (2014)** Wound healing potential of a dimeric InlB variant analyzed by in vitro experiments on re-epithelialization of human skin models. *European journal of pharmaceutics and biopharmaceutics : official journal of Arbeitsgemeinschaft fur Pharmazeutische Verfahrenstechnik e.V* 86, 277-283

96. **Kondo, T., and Ishida, Y. (2010)** Molecular pathology of wound healing. *Forensic science international* 203, 93-98

97. **Koren, E., and Torchilin, V. P. (2012)** Cell-penetrating peptides: breaking through to the other side. *Trends Mol Med* 18, 385-393

98. **Lakshminarayanan, R., Fan, D., Du, C., and Moradian-Oldak, J. (2007)** The role of secondary structure in the entropically driven amelogenin self-assembly. *Biophysical journal* 93, 3664-3674

99. **Lamaze, C., and Schmid, S. L. (1995)** The emergence of clathrin-independent pinocytic pathways. *Current opinion in cell biology* 7, 573-580

100. **Lamb, H. M., and Wiseman, L. R. (1998)** Pexiganan acetate. *Drugs* 56, 1047-1052; discussion 1053-1044

101. **Landis, S. J. (2008)** Chronic wound infection and antimicrobial use. *Advances in skin & wound care* 21, 531-540; quiz 541-532

102. **Langel, U. (2002)** Cell-Penetrating Peptides : Processes and Applications. Pharmacology and Toxicology: Basic and Clinical Aspects.

103. **Lasic, D. D. (1988)** The mechanism of vesicle formation. *The Biochemical journal* 256, 1-11

104. **Lattig-Tunnemann, G., Prinz, M., Hoffmann, D., Behlke, J., Palm-Apergi, C., Morano, I., Herce, H. D., and Cardoso, M. C. (2011)** Backbone rigidity and static presentation of guanidinium groups increases cellular uptake of arginine-rich cell-penetrating peptides. *Nature communications* 2, 453

105. **Letoha, T., Gaal, S., Somlai, C., Venkei, Z., Glavinas, H., Kusz, E., Duda, E., Czajlik, A., Petak, F., and Penke, B. (2005)** Investigation of penetratin peptides. Part 2. In vitro uptake of penetratin and two of its derivatives. *Journal of peptide science : an official publication of the European Peptide Society* 11, 805-811

106. **Levental, I., Grzybek, M., and Simons, K. (2011)** Raft domains of variable properties and compositions in plasma membrane vesicles. *Proceedings of the National Academy of Sciences of the United States of America* 108, 11411-11416

107. **Leventis, P. A., and Grinstein, S. (2010)** The distribution and function of phosphatidylserine in cellular membranes. *Annual review of biophysics* 39, 407-427

108. **Levesque, M., Villiard, E., and Roy, S. (2010)** Skin wound healing in axolotls: a scarless process. *Journal of experimental zoology. Part B, Molecular and developmental evolution* 314, 684-697

109. **Li, J., Chen, J., and Kirsner, R. (2007)** Pathophysiology of acute wound healing. *Clinics in dermatology* 25, 9-18

110. **Macia, E., Ehrlich, M., Massol, R., Boucrot, E., Brunner, C., and Kirchhausen, T. (2006)** Dynasore, a cell-permeable inhibitor of dynamin. *Developmental cell* 10, 839-850

111. **Madani, F., Lindberg, S., Langel, U., Futaki, S., and Graslund, A. (2011)** Mechanisms of cellular uptake of cell-penetrating peptides. *Journal of biophysics* 2011, 1-10

112. **Madani, F., Peralvarez-Marin, A., and Graslund, A. (2011)** Liposome Model Systems to Study the Endosomal Escape of Cell-Penetrating Peptides: Transport across Phospholipid Membranes Induced by a Proton Gradient. *Journal of drug delivery* 2011, 897592

113. **Madani, F., and Graslund, A. (2015)** Investigating Membrane Interactions and Structures of CPPs. *Methods in molecular biology* 1324, 73-87

114. **Magzoub, M., Kilk, K., Eriksson, L. E., Langel, U., and Graslund, A. (2001)** Interaction and structure induction of cell-penetrating peptides in the presence of phospholipid vesicles. *Biochimica et biophysica acta* 1512, 77-89

115. **Mandal, D., Nasrolahi Shirazi, A., and Parang, K. (2011)** Cell-penetrating homochiral cyclic peptides as nuclear-targeting molecular transporters. *Angewandte Chemie* 50, 9633-9637

116. **Mangoni, M. L., McDermott, A. M., and Zasloff, M. (2016)** Antimicrobial peptides and wound healing: biological and therapeutic considerations. *Experimental dermatology* 25, 167-173

117. **Manning, M. C., and Woody, R. W. (1991)** Theoretical CD studies of polypeptide helices: examination of important electronic and geometric factors. *Biopolymers* 31, 569-586

118. **Mariño, G., and Kroemer, G. (2013)** Mechanisms of apoptotic phosphatidylserine exposure. *Cell research* 23, 1247-1248

119. **Martin, P. (1997)** Wound healing--aiming for perfect skin regeneration. *Science* 276, 75-81

120. **Martin, S. J., Reutelingsperger, C. P., McGahon, A. J., Rader, J. A., van Schie, R. C., LaFace, D. M., and Green, D. R. (1995)** Early redistribution of plasma membrane phosphatidylserine is a general feature of apoptosis regardless of the

initiating stimulus: inhibition by overexpression of Bcl-2 and Abl. *The Journal of experimental medicine* 182, 1545-1556

121. **Mickan, A., Sarko, D., Haberkorn, U., and Mier, W. (2014)** Rational design of CPP-based drug delivery systems: considerations from pharmacokinetics. *Current pharmaceutical biotechnology* 15, 200-209
122. **Milletti, F. (2012)** Cell-penetrating peptides: classes, origin, and current landscape. *Drug discovery today* 17, 850-860
123. **Mishra, A., Lai, G. H., Schmidt, N. W., Sun, V. Z., Rodriguez, A. R., Tong, R., Tang, L., Cheng, J., Deming, T. J., Kamei, D. T., and Wong, G. C. (2011)** Translocation of HIV TAT peptide and analogues induced by multiplexed membrane and cytoskeletal interactions. *Proceedings of the National Academy of Sciences of the United States of America* 108, 16883-16888
124. **Misic, A. M., Gardner, S. E., and Grice, E. A. (2014)** The Wound Microbiome: Modern Approaches to Examining the Role of Microorganisms in Impaired Chronic Wound Healing. *Advances in wound care* 3, 502-510
125. **Mitchell, D. J., Kim, D. T., Steinman, L., Fathman, C. G., and Rothbard, J. B. (2000)** Polyarginine enters cells more efficiently than other polycationic homopolymers. *The journal of peptide research : official journal of the American Peptide Society* 56, 318-325
126. **Mu, L., Tang, J., Liu, H., Shen, C., Rong, M., Zhang, Z., and Lai, R. (2014)** A potential wound-healing-promoting peptide from salamander skin. *FASEB journal : official publication of the Federation of American Societies for Experimental Biology* 28, 3919-3929
127. **Murayama, T., Masuda, T., Afonin, S., Kawano, K., Takatani-Nakase, T., Ida, H., Takahashi, Y., Fukuma, T., Ulrich, A. S., and Futaki, S. (2017)** Loosening of Lipid Packing Promotes Oligoarginine Entry into Cells. *Angewandte Chemie* 56, 7644-7647
128. **Nakase, I., Takeuchi, T., Tanaka, G., and Futaki, S. (2008)** Methodological and cellular aspects that govern the internalization mechanisms of arginine-rich cell-penetrating peptides. *Advanced drug delivery reviews* 60, 598-607
129. **Natividad-Tietz, S.** (2016) Peptide-mediated oligonucleotide delivery into eukaryotic cells. University of Cologne
130. **Neundorf, I., Rennert, R., Hoyer, J., Schramm, F., Lobner, K., Kitanovic, I., and Wolfl, S. (2009)** Fusion of a Short HA2-Derived Peptide Sequence to Cell-Penetrating Peptides Improves Cytosolic Uptake, but Enhances Cytotoxic Activity. *Pharmaceuticals* 2, 49-65

131. **Niyonsaba, F., Ushio, H., Nakano, N., Ng, W., Sayama, K., Hashimoto, K., Nagaoka, I., Okumura, K., and Ogawa, H. (2007)** Antimicrobial peptides human beta-defensins stimulate epidermal keratinocyte migration, proliferation and production of proinflammatory cytokines and chemokines. *The Journal of investigative dermatology* 127, 594-604

132. **Oehlke, J., Scheller, A., Wiesner, B., Krause, E., Beyermann, M., Klauschenz, E., Melzig, M., and Bienert, M. (1998)** Cellular uptake of an alpha-helical amphipathic model peptide with the potential to deliver polar compounds into the cell interior non-endocytically. *Biochimica et biophysica acta* 1414, 127-139

133. **Oh, D., Nasrolahi Shirazi, A., Northup, K., Sullivan, B., Tiwari, R. K., Bisoffi, M., and Parang, K. (2014)** Enhanced cellular uptake of short polyarginine peptides through fatty acylation and cyclization. *Molecular pharmaceutics* 11, 2845-2854

134. **Pae, J., Saalik, P., Liivamagi, L., Lubenets, D., Arukuusk, P., Langel, U., and Pooga, M. (2014)** Translocation of cell-penetrating peptides across the plasma membrane is controlled by cholesterol and microenvironment created by membranous proteins. *Journal of controlled release : official journal of the Controlled Release Society* 192, 103-113

135. **Parn, K., Eriste, E., and Langel, U. (2015)** The Antimicrobial and Antiviral Applications of Cell-Penetrating Peptides. *Methods in molecular biology* 1324, 223-245

136. **Pastar, I., Stojadinovic, O., Yin, N. C., Ramirez, H., Nusbaum, A. G., Sawaya, A., Patel, S. B., Khalid, L., Isseroff, R. R., and Tomic-Canic, M. (2014)** Epithelialization in Wound Healing: A Comprehensive Review. *Advances in wound care* 3, 445-464

137. **Peetla, C., Stine, A., and Labhasetwar, V. (2009)** Biophysical interactions with model lipid membranes: applications in drug discovery and drug delivery. *Molecular pharmaceutics* 6, 1264-1276

138. **Pfalzgraff, A., Heinbockel, L., Su, Q., Gutsmann, T., Brandenburg, K., and Weindl, G. (2016)** Synthetic antimicrobial and LPS-neutralising peptides suppress inflammatory and immune responses in skin cells and promote keratinocyte migration. *Scientific reports* 6, 31577

139. **Pooga, M., Hallbrink, M., Zorko, M., and Langel, U. (1998)** Cell penetration by transportan. *FASEB journal : official publication of the Federation of American Societies for Experimental Biology* 12, 67-77

140. **Poon, G. M., and Gariepy, J. (2007)** Cell-surface proteoglycans as molecular portals for cationic peptide and polymer entry into cells. *Biochemical Society transactions* 35, 788-793

141. **Preta, G., Cronin, J. G., and Sheldon, I. M. (2015)** Dynasore - not just a dynamin inhibitor. *Cell communication and signaling : CCS* 13, 24

142. **Purna, S. K., and Babu, M. (2000)** Collagen based dressings--a review. *Burns : journal of the International Society for Burn Injuries* 26, 54-62

143. **Qian, Z., Martyna, A., Hard, R. L., Wang, J., Appiah-Kubi, G., Coss, C., Phelps, M. A., Rossman, J. S., and Pei, D. (2016)** Discovery and Mechanism of Highly Efficient Cyclic Cell-Penetrating Peptides. *Biochemistry* 55, 2601-2612

144. **Ramsey, J. D., and Flynn, N. H. (2015)** Cell-penetrating peptides transport therapeutics into cells. *Pharmacology & therapeutics* 154, 78-86

145. **Raucher, D., and Ryu, J. S. (2015)** Cell-penetrating peptides: strategies for anticancer treatment. *Trends Mol Med* 21, 560-570

146. **Raussens, V., Ruysschaert, J. M., and Goormaghtigh, E. (2003)** Protein concentration is not an absolute prerequisite for the determination of secondary structure from circular dichroism spectra: a new scaling method. *Analytical biochemistry* 319, 114-121

147. **Reeves, J. P., and Dowben, R. M. (1969)** Formation and properties of thin-walled phospholipid vesicles. *Journal of cellular physiology* 73, 49-60

148. **Reinhardt, A., Horn, M., Schmauck, J. P., Brohl, A., Giernoth, R., Oelkrug, C., Schubert, A., and Neundorf, I. (2014)** Novel imidazolium salt--peptide conjugates and their antimicrobial activity. *Bioconjugate chemistry* 25, 2166-2174

149. **Reinhardt, A., and Neundorf, I. (2016)** Design and Application of Antimicrobial Peptide Conjugates. *International journal of molecular sciences* 17

150. **Reinhardt, A.** (2017) Antimicrobial peptides as new potential antibiotics. University of Cologne

151. **Reissmann, S. (2014)** Cell penetration: scope and limitations by the application of cell-penetrating peptides. *Journal of peptide science : an official publication of the European Peptide Society* 20, 760-784

152. **Richter, S., Bouvet, V., Wuest, M., Bergmann, R., Steinbach, J., Pietzsch, J., Neundorf, I., and Wuest, F. (2012)** (18)F-Labeled phosphopeptide-cell-penetrating peptide dimers with enhanced cell uptake properties in human cancer cells. *Nuclear medicine and biology* 39, 1202-1212

153. **Roccatano, D., Colombo, G., Fioroni, M., and Mark, A. E. (2002)** Mechanism by which 2,2,2-trifluoroethanol/water mixtures stabilize secondary-structure formation in peptides: a molecular dynamics study. *Proceedings of the National Academy of Sciences of the United States of America* 99, 12179-12184

154. **Rothbard, J. B., Jessop, T. C., and Wender, P. A. (2005)** Adaptive translocation: the role of hydrogen bonding and membrane potential in the uptake of guanidinium-rich transporters into cells. *Advanced drug delivery reviews* 57, 495-504

155. **Ruczynski, J., Wierzbicki, P. M., Kogut-Wierzbicka, M., Mucha, P., Siedlecka-Kroplewska, K., and Rekowski, P. (2014)** Cell-penetrating peptides as a promising tool for delivery of various molecules into the cells. *Folia histochemica et cytobiologica* 52, 257-269

156. **Säälik, P., Niinep, A., Pae, J., Hansen, M., Lubenets, D., Langel, U., and Pooga, M. (2011)** Penetration without cells: membrane translocation of cell-penetrating peptides in the model giant plasma membrane vesicles. *Journal of controlled release : official journal of the Controlled Release Society* 153, 117-125

157. **Saar, K., Lindgren, M., Hansen, M., Eiriksdottir, E., Jiang, Y., Rosenthal-Aizman, K., Sassian, M., and Langel, U. (2005)** Cell-penetrating peptides: a comparative membrane toxicity study. *Analytical biochemistry* 345, 55-65

158. **Sakhrani, N. M., and Padh, H. (2013)** Organelle targeting: third level of drug targeting. *Drug design, development and therapy* 7, 585-599

159. **Sanderson, J. M. (2005)** Peptide-lipid interactions: insights and perspectives. *Organic & biomolecular chemistry* 3, 201-212

160. **Schiffer, M., and Edmundson, A. B. (1967)** Use of helical wheels to represent the structures of proteins and to identify segments with helical potential. *Biophysical journal* 7, 121-135

161. **Schramp, M., Hedman, A., Li, W., Tan, X., and Anderson, R.** (2012) PIP Kinases from the Cell Membrane to the Nucleus. In *Phosphoinositides I: Enzymes of Synthesis and Degradation* (Balla, T., Wymann, M., and York, J. D., eds) pp. 25-59, Springer Netherlands, Dordrecht

162. **Scott, R. E. (1976)** Plasma membrane vesiculation: a new technique for isolation of plasma membranes. *Science* 194, 743-745

163. **Sen, C. K., Gordillo, G. M., Roy, S., Kirsner, R., Lambert, L., Hunt, T. K., Gottrup, F., Gurtner, G. C., and Longaker, M. T. (2009)** Human skin wounds: a major and snowballing threat to public health and the economy. *Wound repair and regeneration : official publication of the Wound Healing Society [and] the European Tissue Repair Society* 17, 763-771

164. **Sessa, G., and Weissmann, G. (1968)** Phospholipid spherules (liposomes) as a model for biological membranes. *Journal of lipid research* 9, 310-318

165. **Sezgin, E., Levental, I., Mayor, S., and Eggeling, C. (2017)** The mystery of membrane organization: composition, regulation and roles of lipid rafts. *Nature reviews. Molecular cell biology* 18, 361-374

166. **Shaw, T. J., and Martin, P. (2009)** Wound repair at a glance. *Journal of cell science* 122, 3209-3213

167. **Simons, K., and Ikonen, E. (1997)** Functional rafts in cell membranes. *Nature* 387, 569-572

168. **Simons, K., and Vaz, W. L. (2004)** Model systems, lipid rafts, and cell membranes. *Annual review of biophysics and biomolecular structure* 33, 269-295

169. **Singer, A. J., and Clark, R. A. (1999)** Cutaneous wound healing. *The New England journal of medicine* 341, 738-746

170. **Singer, S. J., and Nicolson, G. L. (1972)** The fluid mosaic model of the structure of cell membranes. *Science* 175, 720-731

171. **Smith, B. A., Daniels, D. S., Coplin, A. E., Jordan, G. E., McGregor, L. M., and Schepartz, A. (2008)** Minimally cationic cell-permeable miniature proteins via alpha-helical arginine display. *Journal of the American Chemical Society* 130, 2948-2949

172. **Splith, K., Hu, W., Schatzschneider, U., Gust, R., Ott, I., Onambele, L. A., Prokop, A., and Neundorf, I. (2010)** Protease-activatable organometal-Peptide bioconjugates with enhanced cytotoxicity on cancer cells. *Bioconjugate chemistry* 21, 1288-1296

173. **Splith, K., Bergmann, R., Pietzsch, J., and Neundorf, I. (2012)** Specific targeting of hypoxic tumor tissue with nitroimidazole-peptide conjugates. *ChemMedChem* 7, 57-61

174. **Steinstraesser, L., Koehler, T., Jacobsen, F., Daigeler, A., Goertz, O., Langer, S., Kesting, M., Steinau, H., Eriksson, E., and Hirsch, T. (2008)** Host defense peptides in wound healing. *Molecular medicine* 14, 528-537

175. **Subtil, A., Gaidarov, I., Kobylarz, K., Lampson, M. A., Keen, J. H., and McGraw, T. E. (1999)** Acute cholesterol depletion inhibits clathrin-coated pit budding. *Proceedings of the National Academy of Sciences of the United States of America* 96, 6775-6780

176. **Sudo, K., Niikura, K., Iwaki, K., Kohyama, S., Fujiwara, K., and Doi, N. (2017)** Human-derived fusogenic peptides for the intracellular delivery of proteins. *Journal of controlled release : official journal of the Controlled Release Society* 255, 1-11

177. **Sun, Y., Kaksonen, M., Madden, D. T., Schekman, R., and Drubin, D. G. (2005)** Interaction of Sla2p's ANTH domain with PtdIns(4,5)P2 is important for actin-dependent endocytic internalization. *Molecular biology of the cell* 16, 717-730

178. **Takeo, M., Lee, W., and Ito, M. (2015)** Wound healing and skin regeneration. *Cold Spring Harbor perspectives in medicine* 5, a023267

179. **Tan, X., Thapa, N., Choi, S., and Anderson, R. A. (2015)** Emerging roles of PtdIns(4,5)P2--beyond the plasma membrane. *Journal of cell science* 128, 4047-4056

180. **Temmerman, K., and Nickel, W. (2009)** A novel flow cytometric assay to quantify interactions between proteins and membrane lipids. *Journal of lipid research* 50, 1245-1254

181. **Tiriveedhi, V., and Butko, P. (2007)** A fluorescence spectroscopy study on the interactions of the TAT-PTD peptide with model lipid membranes. *Biochemistry* 46, 3888-3895

182. **Tokumaru, S., Sayama, K., Shirakata, Y., Komatsuzawa, H., Ouhara, K., Hanakawa, Y., Yahata, Y., Dai, X., Tohyama, M., Nagai, H., Yang, L., Higashiyama, S., Yoshimura, A., Sugai, M., and Hashimoto, K. (2005)** Induction of keratinocyte migration via transactivation of the epidermal growth factor receptor by the antimicrobial peptide LL-37. *Journal of immunology* 175, 4662-4668

183. **Tossi, A., Scocchi, M., Skerlavaj, B., and Gennaro, R. (1994)** Identification and characterization of a primary antibacterial domain in CAP18, a lipopolysaccharide binding protein from rabbit leukocytes. *FEBS letters* 339, 108-112

184. **Tossi, A., Sandri, L., and Giangaspero, A. (2000)** Amphipathic, alpha-helical antimicrobial peptides. *Biopolymers* 55, 4-30

185. **Traboulsi, H., Larkin, H., Bonin, M. A., Volkov, L., Lavoie, C. L., and Marsault, E. (2015)** Macrocyclic cell penetrating peptides: a study of structure-penetration properties. *Bioconjugate chemistry* 26, 405-411

186. **Trabulo, S., Cardoso, A. L., Mano, M., and De Lima, M. C. (2010)** Cell-Penetrating Peptides-Mechanisms of Cellular Uptake and Generation of Delivery Systems. *Pharmaceuticals* 3, 961-993

187. **Ud-Din, S., and Bayat, A. (2017)** Non-animal models of wound healing in cutaneous repair: In silico, in vitro, ex vivo, and in vivo models of wounds and scars in human skin. *Wound repair and regeneration : official publication of the Wound Healing Society [and] the European Tissue Repair Society* 25, 164-176

188. **Utsugi, T., Schroit, A. J., Connor, J., Bucana, C. D., and Fidler, I. J. (1991)** Elevated expression of phosphatidylserine in the outer membrane leaflet of human tumor cells and recognition by activated human blood monocytes. *Cancer research* 51, 3062-3066

189. **van Swaay, D., and deMello, A. (2013)** Microfluidic methods for forming liposomes. *Lab on a chip* 13, 752-767

190. **Vanni, S., Vamparys, L., Gautier, R., Drin, G., Etchebest, C., Fuchs, P. F., and Antonny, B. (2013)** Amphipathic lipid packing sensor motifs: probing bilayer defects with hydrophobic residues. *Biophysical journal* 104, 575-584

191. **Velnar, T., Bailey, T., and Smrkolj, V. (2009)** The wound healing process: an overview of the cellular and molecular mechanisms. *The Journal of international medical research* 37, 1528-1542

192. **Vives, E., Brodin, P., and Lebleu, B. (1997)** A truncated HIV-1 Tat protein basic domain rapidly translocates through the plasma membrane and accumulates in the cell nucleus. *The Journal of biological chemistry* 272, 16010-16017

193. **Vlodavsky, I., Goldshmidt, O., Zcharia, E., Atzmon, R., Rangini-Guatta, Z., Elkin, M., Peretz, T., and Friedmann, Y. (2002)** Mammalian heparanase: involvement in cancer metastasis, angiogenesis and normal development. *Seminars in cancer biology* 12, 121-129

194. **Walde, P., Cosentino, K., Engel, H., and Stano, P. (2010)** Giant vesicles: preparations and applications. *Chembiochem : a European journal of chemical biology* 11, 848-865

195. **Wallbrecher, R., Ackels, T., Olea, R. A., Klein, M. J., Caillon, L., Schiller, J., Bovee-Geurts, P. H., van Kuppevelt, T. H., Ulrich, A. S., Spehr, M., Adjobo-Hermans, M. J. W., and Brock, R. (2017)** Membrane permeation of arginine-rich cell-penetrating peptides independent of transmembrane potential as a function of lipid composition and membrane fluidity. *Journal of controlled release : official journal of the Controlled Release Society* 256, 68-78

196. **Walrant, A., Bechara, C., Alves, I. D., and Sagan, S. (2012)** Molecular partners for interaction and cell internalization of cell-penetrating peptides: how identical are they? *Nanomedicine* 7, 133-143

197. **Watson, H. (2015)** Biological membranes. *Essays in biochemistry* 59, 43-69

198. **Wender, P. A., Mitchell, D. J., Pattabiraman, K., Pelkey, E. T., Steinman, L., and Rothbard, J. B. (2000)** The design, synthesis, and evaluation of molecules that enable or enhance cellular uptake: peptoid molecular transporters. *Proceedings of the National Academy of Sciences of the United States of America* 97, 13003-13008

199. **Wender, P. A., Galliher, W. C., Goun, E. A., Jones, L. R., and Pillow, T. H. (2008)** The design of guanidinium-rich transporters and their internalization mechanisms. *Advanced drug delivery reviews* 60, 452-472

200. **Wheaten, S. A., Ablan, F. D., Spaller, B. L., Trieu, J. M., and Almeida, P. F. (2013)** Translocation of cationic amphipathic peptides across the membranes of pure phospholipid giant vesicles. *Journal of the American Chemical Society* 135, 16517-16525

201. **Wojtowicz, A. M., Oliveira, S., Carlson, M. W., Zawadzka, A., Rousseau, C. F., and Baksh, D. (2014)** The importance of both fibroblasts and keratinocytes in a bilayered living cellular construct used in wound healing. *Wound repair and regeneration : official publication of the Wound Healing Society [and] the European Tissue Repair Society* 22, 246-255

202. **Yao, Y., Hong, S., Zhou, H., Yuan, T., Zeng, R., and Liao, K. (2009)** The differential protein and lipid compositions of noncaveolar lipid microdomains and caveolae. *Cell research* 19, 497-506

203. **Yeagle, P. L.** (2004) *The Structure of Biological Membranes, Second Edition*, CRC Press

204. **Yeagle, P. L.** (2011) Introduction to Lipid Bilayers. In *The Structure of Biological Membranes, Third Edition* pp. 1-6, CRC Press

205. **Yokoyama, H., Maruoka, T., Aruga, A., Amano, T., Ohgo, S., Shiroishi, T., and Tamura, K. (2011)** Prx-1 expression in Xenopus laevis scarless skin-wound healing and its resemblance to epimorphic regeneration. *The Journal of investigative dermatology* 131, 2477-2485

206. **Zahid, M., and Robbins, P. D. (2015)** Cell-type specific penetrating peptides: therapeutic promises and challenges. *Molecules* 20, 13055-13070

207. **Zhang, F., Yang, D., Jiang, S., Wu, L., Qin, L., He, H., and Zhang, P. (2017)** Current Strategies to Improve the Target of Cell Penetrating Peptides used for Antitumor Therapeutics. *Current pharmaceutical design*

208. **Zhou, T., Wang, N., Xue, Y., Ding, T., Liu, X., Mo, X., and Sun, J. (2016)** Electrospun tilapia collagen nanofibers accelerating wound healing via inducing keratinocytes proliferation and differentiation. *Colloids and surfaces. B, Biointerfaces* 143, 415-422

209. **Ziegler, A., Blatter, X. L., Seelig, A., and Seelig, J. (2003)** Protein transduction domains of HIV-1 and SIV TAT interact with charged lipid vesicles. Binding mechanism and thermodynamic analysis. *Biochemistry* 42, 9185-9194

210. **Ziegler, A. (2008)** Thermodynamic studies and binding mechanisms of cell-penetrating peptides with lipids and glycosaminoglycans. *Advanced drug delivery reviews* 60, 580-597

211. **Zorko, M., and Langel, U. (2005)** Cell-penetrating peptides: mechanism and kinetics of cargo delivery. *Advanced drug delivery reviews* 57, 529-545

7. Attachment

7.1 List of abbreviations

ACN	acetonitrile
AMPs	antimicrobial peptides
CD	circular dichroism
CF	5(6)-carboxyfluorescein
CH_2Cl_2	dichloromethane
$CHCl_3$	chloroform
Chol	cholesterol
CLSM	confocal laser scanning microscopy
CPP	cell-penetrating peptide
cyc	cyclic
DIC	*N,N*-diisopropylcarbodiimide
DiI	1,1'-dioctadecyl-3,3,3',3'-tetramethylindocarbocyanine perchlorate
DIPEA	*N,N*-diisopropylethylamine
DMEM	Dulbecco's Modified Eagle Medium
DMF	*N,N*-dimethylformamide
DOPC	1,2-dioleoyl-*sn*-glycero-3-phosphocholine
DOPE	1,2-dioleoyl-*sn*-glycero-3-phophoethanolamine
DOPG	1,2-dioleoyl-*sn*-glycero-3-[phospho-*rac*-(1-glycerol)]
DOPS	1,2-dioleoyl-*sn*-glycero-3-phospho-L-serine
DOTA	1,4,7,10-tetraazacyclotetradecane-1,4,7,10 tetraacetic acid
DTT	dithiothreitol
EDT	1,2-ethanedithiol
EGF	epidermal growth factor
eq.	equivalent
ER	endoplasmic reticulum
ESI-MS	electrospray ionization mass spectrometry

Et_2O	diethyl ether
EtOH	ethanol
FA	formic acid
FBS	fetal bovine serum
Fmoc	9-fluorenylmethyloxycarbonyl
GPMVs	giant plasma membrane vesicles
GUVs	giant unilamellar vesicles
HaCaT	Human adult low Calcium high Temperature keratinocytes
HATU	*O*-(7-azabenzotriazol-1-yl)-*N*,*N*,*N'*,*N'*-tetramethyluronium hexafluorophosphate
HEK-293	human embryonic kidney 293 cell line
HeLa	human cervical carcinoma cell line
HEPES	4-(2-hydroxyethyl)-1-piperazineethanesulfonic acid
Hoechst	bisBenzimide H 33342 trihydrochloride
HPLC	high performance liquid chromatography
INT	*p*-iodonitrotetrazolium-chloride
KCN	potassium cyanide
L_d	liquid-disordered phase
L_o	liquid-ordered phase
LUVs	large unilamellar vesicles
M. luteus	*Micrococcus luteus*
m/z	mass-to-charge ratio
MCF-7	human breast adenocarcinoma cell line
MeOH	methanol
MTT	3-(4,5-dimethylthiazol-2yl)2,5-diphenyltetrazolium bromide
MW	molecular weight
NEM	*N*-ethylmaleimide
NIA	2-(2-nitroimidazol-1-yl)acetic acid

NODAGA	4-(4,7-bis(2-tert-butoxy-2-oxoethyl)-1,4,7-triazonan-1-yl)-5-tert-butoxy-5-oxopentaoic acid
P/L	peptide/lipid ratio
PFA	paraformaldehyde
PI	phosphatidylinositol
$PI(4,5)P_2$	phosphatidylinositol-(4,5)-bisphosphate
PMSF	phenylmethylsulfonyl fluoride
PyB	pyrenebutyrate
RPMI 1640	Roswell Park Memorial Institute, cell culture medium
RT	room temperature
S. typhimurium	*Salmonella typhimurium*
SC	Stratum corneum
SDS	sodium dodecyl sulfate
SM	sphingomyelin
SPPS	solid phase peptide synthesis
t-Bu	*tert.* butyl
t-BuOH	*tert*. butyl alcohol
TFA	trifluoroacetic acid
TFE	trifluoroethanol
TGF-β	transforming growth factor
TIS/TIPS	triisopropylsilane
v/v	volume per volume
w/v	weight per volume

amino acids:

A	Ala	alanine
B	Pra	L-propargylglycine
C	Cys	cysteine
E	Glu	glutamic acid

F	Phe	phenylalanine
G	Gly	glycine
I	Ile	isoleucine
K	Lys	lysine
L	Leu	leucine
N	Asn	asparagine
Q	Gln	glutamine
R	Arg	arginine
V	Val	valine
X		L-(Ɛ-azido)-lysine
Y	Tyr	tyrosine
βA	βAla	β-alanine

7.2 List of figures

7.3 List of tables

7.4 Declaration

Ich versichere, dass ich die von mir vorgelegte Dissertation selbstständig angefertigt, die benutzten Quellen und Hilfsmittel vollständig angegeben und die Stellen der Arbeit – einschließlich Tabellen, Karten und Abbildungen –, die anderen Werken im Wortlaut oder dem Sinn nach entnommen sind, in jedem Einzelfall als Entlehnung kenntlich gemacht habe; dass diese Dissertation noch keiner anderen Fakultät oder Universität zur Prüfung vorgelegen hat; dass sie – abgesehen von unten angegebenen Teilpublikationen – noch nicht veröffentlicht worden ist, sowie, dass ich eine solche Veröffentlichung vor Abschluss des Promotionsverfahrens nicht vornehmen werde. Die Bestimmungen der Promotionsordnung sind mir bekannt.

Die von mir vorgelegte Dissertation ist von Frau Prof. Dr. Ines Neundorf betreut worden.

Teilpuplikationen:

- **Reinhardt, A., Horn, M., Schmauck, J. P., Brohl, A., Giernoth, R., Oelkrug, C., Schubert, A., and Neundorf, I. (2014)** Novel Imidazolium Salt-Peptide Conjugates and Their Antimicrobial Activity. *Bioconjug. Chem.* 25, 2166-2174.

- **Horn M., Reichart F., Natividad-Tietz S., Diaz D., and Neundorf, I. (2016)** Tuning the properties of a novel short cell-penetrating peptide by intramolecular cyclization with a triazole bridge. *Chem. Commun.* 52, 2261-2264.

- **Reichart, F., Horn, M., and Neundorf, I. (2016)** Cyclization of a cell-penetrating peptide via click-chemistry increases proteolytic resistance and improves drug delivery. *J. Pept. Sci.* 22, 421-426.

- **Gronewold, A., Horn, M., Ranđelović, I., Tóvári, J., Muñoz Vázquez, S., Schomäcker, K., and Neundorf, I. (2017)** Characterization of a Cell-Penetrating Peptide with Potential Anticancer Activity. *ChemMedChem.* 12, 42-49.

- **Gronewold, A., Horn, M., Ranđelović, I., Tóvári, J., Muñoz Vázquez, S., Schomäcker, K., and Neundorf, I. (2017)** Corrigendum: Characterization of a Cell-Penetrating Peptide with Potential Anticancer Activity. *ChemMedChem.* 12, 712.

Posterpräsentationen:

- **Horn, M., Reichart, F., and Neundorf, I. (2015**) Interaction of the cell penetrating peptide sC18 and its derivatives with model membranes. *12th German Peptide Symposium, Darmstadt, Deutschland.*

- **Horn, M., Reichart, F., and Neundorf, I. (2015)** Interaction of amphipathic cyclic peptides with model membranes. *International Symposium CPP, Paris, Frankreich.*

Ort, Datum

Mareike Horn